UNIVERSITÀ DI SIENA 1240

UNIONE EUROPEA
FSE REACT-EU

MUR

PON RICERCA E INNOVAZIONE

Percorso dottorale sviluppato con il sostegno finanziario del programma PON REACT-EU

Dipartimento di Scienze della Vita

Dottorato in Scienze della Vita – Life Sciences

XXXVII Ciclo

Coordinatrice: Prof.ssa Simona Maccherini

The beetle's gut microbiome and its power to ecologically decompose polystyrene waste

Settore scientifico disciplinare: *BIOS-03/A*

Candidato

Dott. Felice Zarra

Università degli Studi di Siena

Supervisore

Prof. Antonio Carapelli

Università degli Studi di Siena

Anno accademico di conseguimento del titolo di Dottore di ricerca

2023/24

TABLE OF CONTENTS

ABSTRACT 1

RIASSUNTO 2

GENERAL INTRODUCTION 3

Plastic pollution and waste management strategies 3

Biodegradation of polystyrene by plastivorous insects and their gut microbiota 7

Alphitobius diaperinus (Panzer, 1797) *13*

CHAPTER 1 16

1.1 INTRODUCTION 16

1.2 MATERIALS AND METHODS 18

1.2.1 Optimization of rearing conditions 18

1.2.2 Chemical analyses 20

1.2.2.1 Rearing setup 20

1.2.2.2 Micro-Fourier Transform Infrared Spectroscopy (micro-FTIR) 20

1.2.2.3 Gas Chromatography–Mass Spectrometry (GC–MS) 21

1.2.3 Metabarcoding analyses 22

1.2.3.1 Rearing setup 22

1.2.3.2 Sample preparation 23

1.2.3.3 Extraction and sequencing of bacterial DNA 24

1.2.3.4 Data analysis 25

1.3 RESULTS 27

1.3.1 Optimization of rearing conditions 27

1.3.2 Chemical analyses 28

1.3.2.1 Micro-Fourier Transform Infrared Spectroscopy (micro-FTIR) 28

1.3.2.2 Gas Chromatography–Mass Spectrometry (GC–MS) 30

1.3.3 Metabarcoding analyses 32

1.3.3.1 Analysis of gut microbiota across larval instars 32
1.3.3.2 Analysis of gut microbiota across gut sections 37
1.4 DISCUSSION 45
CHAPTER 2 52
2.1 INTRODUCTION 52
2.2 MATERIALS AND METHODS 54
2.2.1 Bacterial strain isolation and culturing conditions 54
2.2.2 Genomic DNA extraction and sequencing 54
2.2.3 Genome assembly and annotation 55
2.2.4 Identification of styrene degradation pathways 56
2.2.5 Phylogenetic analysis 56
2.2.6 Data availability 57
2.3 RESULTS 60
2.3.1 Genome features 60
2.3.2 Styrene degradation pathway 64
2.3.3 Phylogenetic analysis 67
2.4 DISCUSSION 70
CONCLUSIONS 73
ACKNOWLEDGEMENTS 76
REFERENCES 77

ABSTRACT

The intensive use of plastic, combined with ineffective waste management, has exacerbated the issue of plastic pollution. This phenomenon represents one of the most critical environmental emergencies of the past century, with well-documented negative effects on biodiversity and ecosystems. Recently, the scientific community has increasingly focused on biodegradation as a potential strategy for plastic disposal, particularly investigating the role of plastivorous insects and their gut microbiota. In this context, *Alphitobius diaperinus* (Coleoptera: Tenebrionidae) has emerged as a promising candidate for polystyrene (PS) degradation. The first chapter of this study explores three key aspects of PS biodegradation by this insect. First, rearing conditions were optimized to enhance larval degradation efficiency. Second, chemical analyses were conducted to characterize the structural modifications of PS after digestion and to confirm the presence of degradation byproducts, such as α-methylstyrene and cumyl alcohol, within the larvae's gut. These analyses were performed using two complementary techniques: micro-Fourier Transform Infrared Spectroscopy (micro-FTIR) and Gas Chromatography-Mass Spectrometry (GC-MS). Finally, gut microbiota composition was assessed through metabarcoding analysis using full-length PacBio HiFi sequencing of the 16S rDNA gene. Significant differences were observed between the microbiota of PS-fed larvae and that of the control group under different experimental conditions, highlighting the potential involvement of specific bacterial taxa in PS metabolism. The second chapter focuses on a bacterial strain isolated from the gut microbiota of PS-fed larvae through enrichment cultures in a medium where PS was the sole carbon source. This bacterium, identified as *Stenotrophomonas indicatrix* strain DAI2m/c, underwent whole-genome sequencing to identify enzymes-encoding genes involved in intracellular metabolic pathways responsible for styrene degradation. The study confirmed that the bacterial genome encodes all the enzymes required for one of the two recognized PS degradation pathways. The overall findings of this study provide new insights into the role of plastivorous insects, particularly their gut microbiota, in polystyrene degradation processes. Moreover, they open new perspectives for the development of innovative biotechnological solutions for sustainable plastic waste management.

RIASSUNTO

L'uso intensivo della plastica, combinato a una gestione inefficace dei rifiuti, ha aggravato il problema dell'inquinamento plastico. Questo fenomeno rappresenta una delle emergenze ambientali più gravi dell'ultimo secolo, con effetti negativi ben documentati sulla biodiversità e sugli ecosistemi. Recentemente, la comunità scientifica ha rivolto un'attenzione crescente alla biodegradazione come possibile strategia per lo smaltimento della plastica, con particolare interesse per il ruolo degli insetti plastivori e del loro microbiota intestinale. In questo contesto, *Alphitobius diaperinus* (Coleoptera: Tenebrionidae) è emerso come un candidato promettente per la degradazione del polistirene (PS). Il primo capitolo di questo studio esplora tre aspetti chiave della biodegradazione del PS da parte di questo insetto. In primo luogo, sono state ottimizzate le condizioni di allevamento per aumentare l'efficienza di degradazione da parte delle larve. In secondo luogo, sono state condotte analisi chimiche per caratterizzare le modificazioni strutturali del polimero di PS dopo la digestione e confermare la presenza di sottoprodotti di degradazione, come α-metilstirene e alcol cumilico, all'interno dell'intestino delle larve. Queste analisi sono state eseguite utilizzando due tecniche complementari: la microscopia infrarossa a trasformata di Fourier (micro-FTIR) e la gascromatografia-spettrometria di massa (GC-MS). Infine, la composizione del microbiota intestinale è stata analizzata mediante tecniche di metabarcoding, utilizzando il sequenziamento full-lenght PacBio HiFi del gene 16S rDNA. Sono state osservate differenze significative tra il microbiota delle larve alimentate con PS e quello del gruppo di controllo in diverse condizioni sperimentali, evidenziando il potenziale coinvolgimento di specifici taxa batterici nel metabolismo del PS. Il secondo capitolo si concentra su un ceppo batterico isolato dal microbiota intestinale delle larve alimentate con PS, tramite colture di arricchimento in un terreno in cui il PS rappresentava l'unica fonte di carbonio. Questo batterio, identificato come *Stenotrophomonas indicatrix* strain DAI2m/c, è stato sottoposto a sequenziamento dell'intero genoma per individuare i geni codificanti per enzimi coinvolti nei percorsi metabolici intracellulari responsabili della degradazione dello stirene. Lo studio ha confermato che il genoma del batterio codifica tutti gli enzimi necessari per uno dei due pathway di degradazione del PS riconosciuti. I risultati complessivi di questo studio forniscono nuove prospettive sul ruolo degli insetti plastivori, in particolare del loro microbiota intestinale, nei processi di degradazione del polistirene. Inoltre, aprono nuove possibilità per lo sviluppo di soluzioni biotecnologiche innovative per una gestione sostenibile dei rifiuti plastici.

GENERAL INTRODUCTION

Plastic pollution and waste management strategies

Plastic pollution is among the most pressing environmental challenges of the last century. Despite the well-documented toxic effects on global biodiversity (Bucci et al., 2020), plastic production continues to rise. In 2022, global plastic production reached approximately 400.3 million tons, marking a significant increase from around 370 million tons in 2018 (Fig. 1) (Plastics Europe, 2023). This persistent growth can be attributed to the exceptional properties of plastic materials, including their longevity, lightweight nature, water resistance, high elasticity, strength, durability, corrosion resistance, ease of transport, and low cost (Lamba et al., 2022). These characteristics make plastics indispensable across a wide range of industries. Among their many applications, packaging represents one of the most significant, accounting for approximately 40% of global plastic use. This includes packaging for food, pharmaceuticals, chemicals, cosmetics, and detergents, where plastics have enabled the development of cost-effective, hygienic, and energy-efficient solutions (Plastics Europe, 2023; Evode et al., 2021).

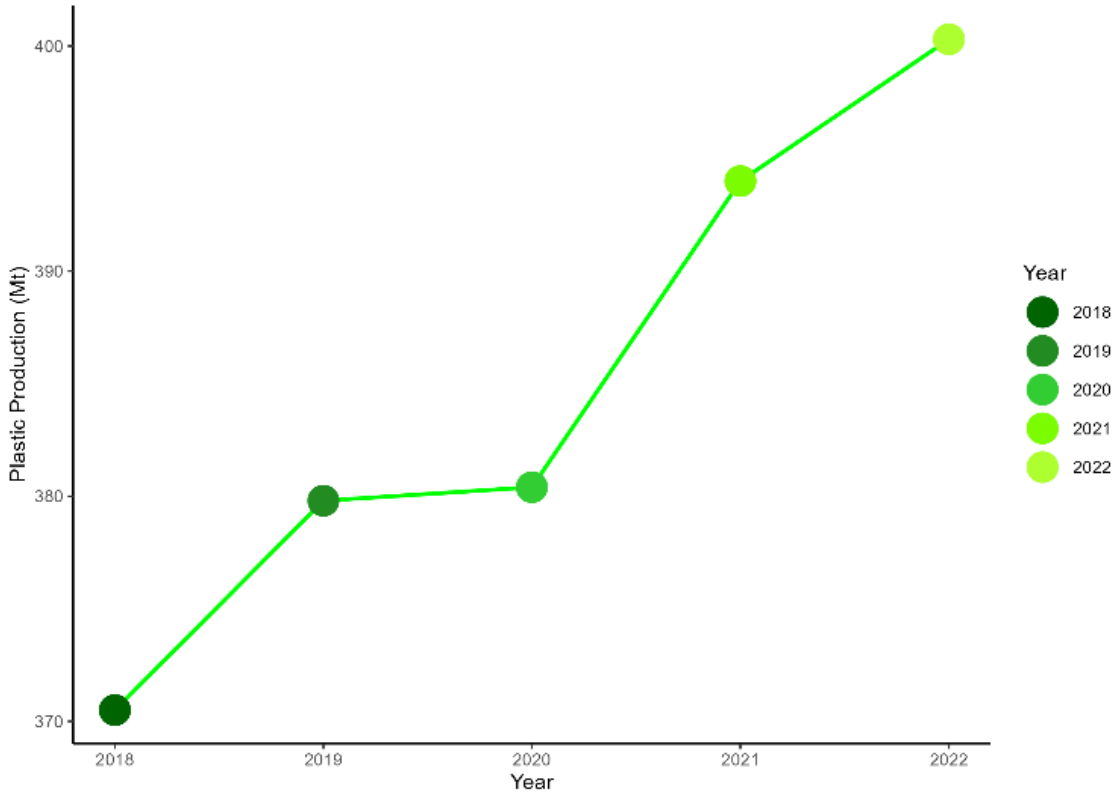

Fig. 1 - Trend of global plastic production from 2018 to 2022 (in million tonnes) (Plastics Europe, 2023).

Plastics are synthetic materials composed of long chains of polymeric molecules with a high molecular weight. Derived from petrochemicals, their primary components include hydrogen, carbon, and various organic or inorganic additives (Siddiqui et al., 2024; Sharma et al., 2023). Plastics can be categorized based on their thermal properties into thermoplastics and thermosetting polymers. Thermoplastics are a category of plastics that can be repeatedly softened by heat and hardened by cooling, allowing them to be reshaped multiple times. This group includes materials such as Polyethylene Terephthalate (PET), Polyethylene (PE), Low-Density Polyethylene (LDPE), High-Density Polyethylene (HDPE), Polystyrene (PS), Expanded polystyrene (EPS), Polyvinyl-chloride (PVC), Polycarbonate, Polypropylene (PP), Polylactic acid (PLA) and Polyhydroxyalkanoates (PHA). In contrast, thermosetting plastics undergo a permanent chemical change when heated. They consist of materials like Polyurethane (PUR), Phenolic resins, Epoxy resins, Silicone, Vinyl ester, Acrylic resins, Urea-formaldehyde (UF) resins (Asiandu et al., 2021). The global production of different plastic types in 2022 is illustrated in Fig. 2.

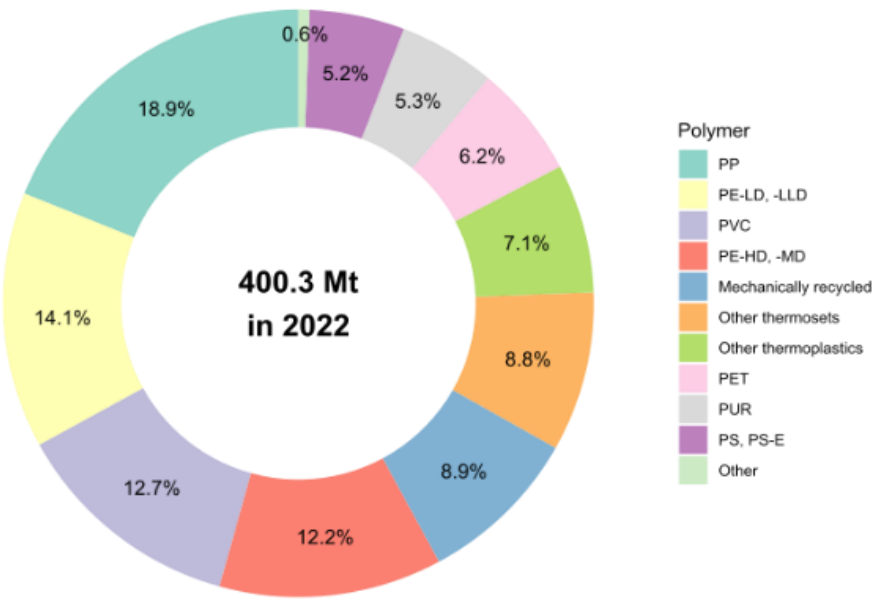

Fig. 2 - Percentage distribution of different plastic types produced globally in 2022 (Plastics Europe, 2023).

The widespread use of plastics across multiple sectors, especially for single-use products, has led to the generation of an enormous amount of Plastic Waste (PW) over the years. This PW has infiltrated all ecosystems of our planet, from terrestrial to aquatic environments, creating a

global environmental crisis (Li et al., 2021). In many regions, the inappropriate or absent PW management has further intensified the issue, allowing significant quantities of PW to enter the environment, where it can persist for hundreds of years due to its resistant chemical and physical properties (Huang et al., 2022; Pivato et al., 2022; Bucci et al., 2020). When PW is accumulated in the ecosystem or dumped in landfills, it undergoes gradual fragmentation through the action of biological, chemical, and physical processes, breaking down into smaller particles known as micro-nano plastics (MNPs). These include microplastics (MPs), ranging in size from 1 μm to 5 mm, and nanoplastics (NPs), which range from 1 to 100 nm (Germanov et al., 2018; Gallo et al., 2018). MNPs function as carriers or binders for various co-contaminants, including heavy metals, brominated flame retardants, plasticizers, and pharmaceutical toxins (Wojnowska-Baryła et al., 2022). It's well established that these MNPs may accumulate in biological tissues, leading to harmful consequences, including immunological response, neuroinflammation, oxidative stress, DNA damage, and metabolic disorders (Germanov et al., 2018; Gallo et al., 2018; Xu et al., 2024). The persistence of MNPs in the environment not only impacts organisms that directly ingest them but also poses risks to human health through bioaccumulation across food chains.

Currently, several strategies are used for the disposal of non-biodegradable plastic waste (NPW), though some of these methods are still being optimized or developed. These disposal methods can be categorized into conventional and advanced NPW treatment technologies (Zhang et al., 2021). Conventional methods include the use of incinerators and landfills. Traditional incineration of plastics requires significant energy and has a negative impact on biodiversity due to the production of harmful by-products, such as CO_2, acidic gases, organic compounds like dioxins and furans, heavy metals, and particulate matter, all of which pose serious health risks to living organisms (Siddiqui et al., 2024; Zhang et al., 2021). Landfills, on the other hand, are commonly used for plastic waste disposal, but the long-term degradation of waste in landfills produces not only MNPs, but also toxic leachates and gases as by-products of biological, chemical, and physical processes, further damaging the surrounding environment. Both incinerators and landfills have been linked to harmful environmental effects (Siddiqui et al., 2024; Zhang et al., 2021; Huang et al., 2022).

To address the challenges associated with conventional plastic disposal, efforts have shifted towards advanced recycling technologies (Fig. 3). The American Society for Testing and Materials (ASTM) classifies these processes into four categories based on their technological characteristics (Okan et al., 2019). Primary (ASTM I) and secondary recycling (ASTM II)

involve the mechanical reprocessing of plastic waste, with the first maintaining the original material properties and the latter producing lower-performance products. Tertiary recycling (ASTM III) recovers valuable chemical intermediates, such as gases and liquids, while quaternary recycling (ASTM IV) relies on incineration to generate energy. Despite these advancements, recycling remains limited by material degradation, high operational costs, pollution, and technological complexity (Okan et al., 2019).

Alternatively, advanced non-biodegradable plastic waste (NPW) treatment methods include degradation processes, which aim to break down plastics into simpler compounds such as carbon dioxide and water. These approaches can be broadly categorized into biodegradation and oxo-biodegradation (Zhang et al., 2021). Biodegradation stands out as a key process in sustainable plastic waste management. It involves microorganisms and invertebrates breaking down plastic polymers; however, it remains a slow process, primarily limited to specific plastic types, highlighting the necessity for deeper research to improve its applicability. Oxo-biodegradation, on the other hand, employs abiotic pretreatments like photodegradation and thermodegradation to improve plastic biodegradability, but it is associated with concerns regarding the possible generation of toxic by-products (Fig. 3) (Zhang et al., 2021).

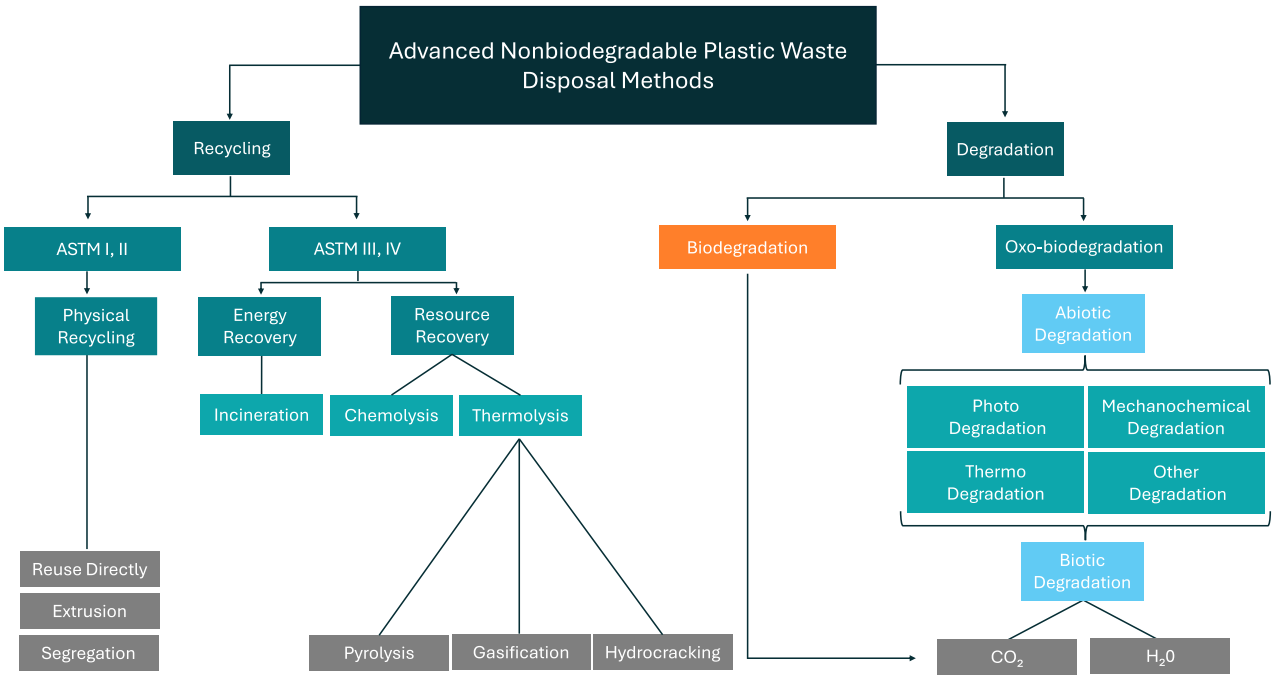

Fig. 3 - Classification of advanced non-biodegradable plastic waste disposal methods, including recycling, biodegradation, and oxo-biodegradation, with their respective subcategories. Adapted from the study of Zhang et al. (2021).

Both conventional and advanced NPW strategies present significant limitations. Among these approaches, biodegradation emerges as the most natural and environmentally sustainable solution for plastic waste disposal, emphasizing the importance of further investigation in this area. Various microorganisms and invertebrates, particularly plastivorous insects, have been investigated for their role in plastic degradation (Siddiqui et al., 2024). Building on this perspective, this study specifically explores the potential of a beetle species and its gut microbiota in polystyrene biodegradation.

Biodegradation of polystyrene by plastivorous insects and their gut microbiota

Polystyrene (PS), commonly known as Styrofoam, was first discovered in 1839 by Eduard Simon. It is a high molecular weight thermoplastic polymer with the chemical formula $(C_8H_8)_n$ and is synthesized from the styrene monomer (Fig. 4) (Ho et al., 2018).

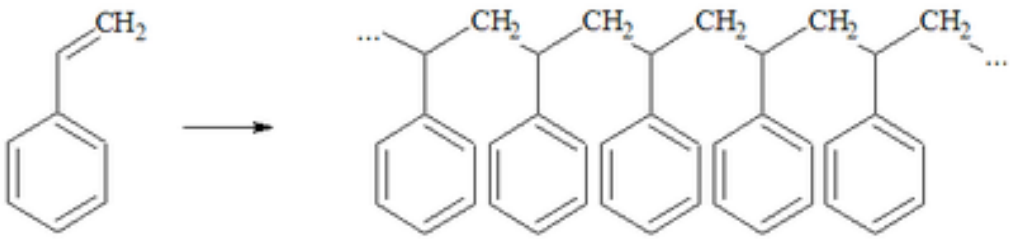

Fig. 4 - Chemical structure of polystyrene (PS). Retrieved from: https://chimicamo.org/chimica-organica/stirene/.

The primary forms of polystyrene used in industry include general-purpose polystyrene (GPPS), expanded polystyrene foam (EPS), extruded polystyrene foam (XPS), high-impact polystyrene (HIPS), and syndiotactic polystyrene (SPS) (Chaukura et al., 2016; Vo et al., 2011). GPPS is widely used in the production of items such as cookie trays, produce baskets, and pie containers. EPS foam is commonly employed in manufacturing cups, food containers, coolers like grape or fish boxes, and insulated panel systems. XPS serves as a thermal insulator in building and construction applications, while HIPS is used for products like yogurt containers, cold drink cups, lids, and reusable or single-service plates (Ho et al., 2018; Vo et al., 2011). SPS, on the other hand, is utilized in automotive power distribution centers, electrical

connectors, and consumer products like baking tins, owing to its high dimensional stability and resistance to warping (Schellenberg & Leder, 2006). PS is widely used thanks to its advantageous mechanical and chemical properties, including high molecular weight, strength, durability, shock absorption, insulating capabilities, excellent processability, and affordability. However, these same properties, particularly its carbon backbone, make PS highly resistant to biodegradation (Hsueh et al., 2023).

To explore the possibility of PS biodegradation, the metabolic pathways involved in the degradation of petroleum hydrocarbons have been considered. These pathways are of interest because petroleum hydrocarbons have a chemical structure rich in alkanes and hydrophobic fragments, which closely resembles that of polystyrene. In this context, microorganisms could play a crucial role in the biodegradation process. Indeed, numerous studies have demonstrated the ability of certain microorganisms to bioremediate oil-polluted environments by utilizing long-chain n-alkanes as carbon source. This process occurs through the oxidation of hydrocarbons by enzymes such as alkane hydroxylases. Given the structural similarities between PS and petroleum hydrocarbons, similar metabolic pathways and enzyme systems may also support PS biodegradation (Xu et al., 2024; Ho et al., 2018; Hsueh et al., 2023; Wentzel et al., 2007). This resemblance has led to the hypothesis that polystyrene, like other hydrocarbons, could serve as a carbon source for specific microorganisms (Ho et al., 2018). Recent studies have further confirmed that some bacteria can metabolize plastic polymers, using them as an energy source and breaking them down into simpler molecules such as CO_2 and H_2O. These discoveries open up new avenues for research on harnessing microbial processes to address environmental issues caused by plastic waste (Dar et al., 2024).

A novel area of study has focused on the role of symbiotic microorganisms that colonize the gut of 'plastivorous insects', and that could play a role in the biodegradation processes of plastics (Siddiqui et al., 2024). Insects, initially identified as pests causing damage to synthetic polymers such as cable insulations, labware, plastic packaging, and plates for thermal insulation, have demonstrated a notable capability to ingest and degrade plastics, including polystyrene (Boctor et al., 2024). This ability has been particularly evident in larval instars of certain insect species belonging to the Lepidoptera and Coleoptera orders (Xu et al., 2024; Dar et al., 2024). These larvae have shown the capacity to ingest, degrade, and mineralize various plastics after passing through the intestinal tract. This process is strongly influenced by the symbiotic relationship between the larvae and their gut microbiota, which plays a crucial role in plastic biodegradation (Dar et al., 2024).

The insect gut functions as a bioreactor, where both physical and biochemical mechanisms contribute to plastic degradation. These include mastication and ingestion of plastic, interaction with intestinal contents, and microbial activity within the gut (Xu et al., 2024). More specifically, the complete mechanism of plastic biodegradation in insects can be summarized into three sequential steps (Fig. 5) (Siddiqui et al., 2024; Asiandu et al., 2021; Dar et al., 2024):

1. **Biodeterioration**: during this initial phase, the plastic is ingested by insects and mechanically broken down through chewing and grinding. This mechanical action facilitates the adhesion of gut microbiota onto the polymer surface, leading to the formation of biofilms and creating a specialized biosphere referred to as the "plastisphere." The biofilm formation, in combination with the favorable gut environment of the insect, promotes oxidation and initiates the biodegradation process, during which bacteria use the polymer as their primary carbon source.

2. **Biofragmentation**: In the second step, extracellular enzymes secreted by bacteria, such as hydrolases and monooxygenases, break down the polymers into smaller units like oligomers, dimers, or monomers. This enzymatic depolymerization reduces the molecular weight of the polymer, producing simpler compounds that can be transported into bacterial cells during the next stage (Yuan et al., 2022; Hou & Majumder, 2021).

3. **Assimilation/mineralization**: the smaller compounds produced during biofragmentation are transported into the cytoplasm of bacterial or host cells via specific membrane transport systems, where they serve as substrates for further metabolic processes. Through a cascade of enzymatic reactions, these assimilated compounds are progressively broken down into environmentally safe oxidized metabolites, including carbon dioxide (CO_2), methane (CH_4), nitrogen (N_2), and water (H_2O), effectively concluding the biodegradation process (Asiandu et al., 2021; Ho et al., 2018).

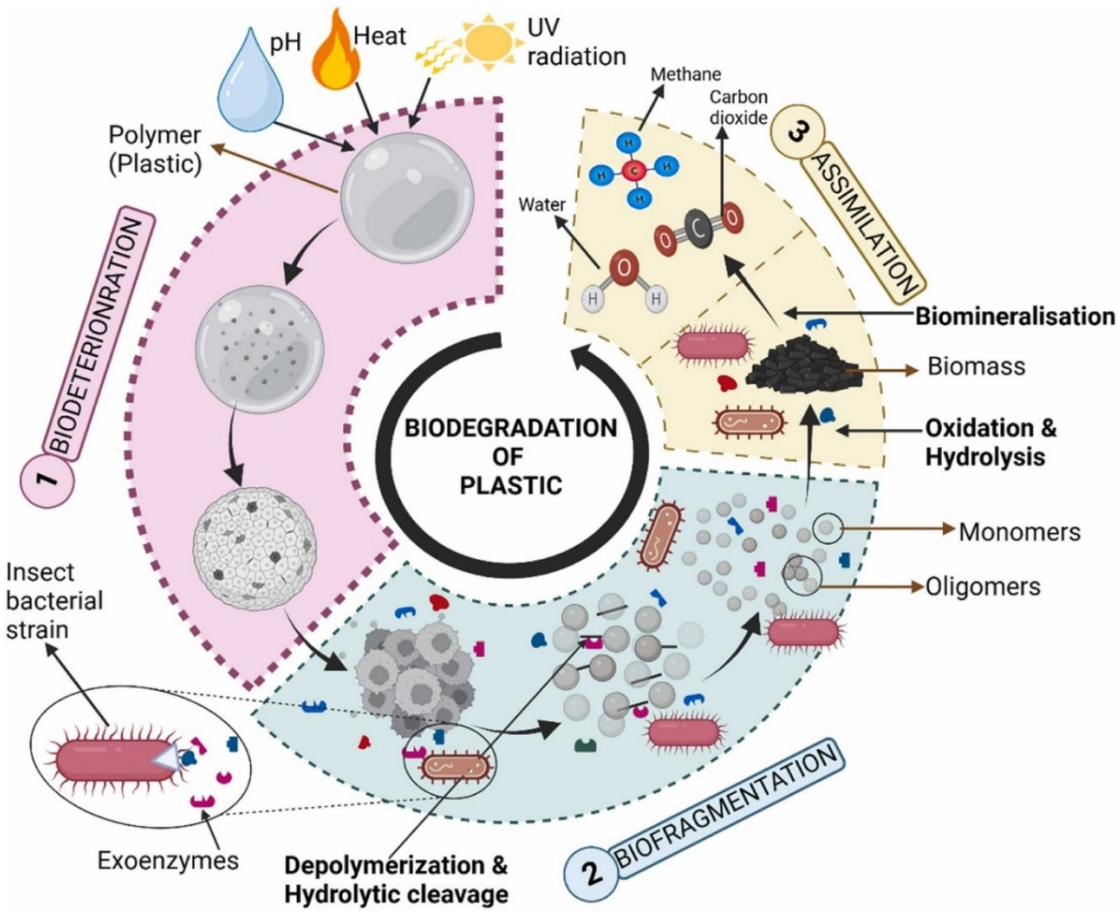

Fig. 5 - Schematic representation of the plastic biodegradation process in insect guts, illustrating the three main stages: biodeterioration, biofragmentation, and assimilation/mineralization. From study of Siddiqui et al. (2024).

Regarding polystyrene, most insect species involved in its degradation are larvae belonging to the order Coleoptera, specifically to the family of Tenebrionidae (Dar et al., 2024). These insects have demonstrated the ability to consume and degrade polystyrene, a process that has been widely investigated due to its potential environmental implications. In particular, several studies have identified symbiotic bacteria within the gut of these larvae as key contributors to the degradation process. These microorganisms can metabolize polystyrene, using it as carbon source for their growth and development.

One of the earliest significant studies on this topic, conducted in 2015, provided concrete evidence of this capability. Researchers observed that *Tenebrio molitor* (yellow mealworms) could effectively chew and consume polystyrene (Fig. 6.A). By enriching cultures derived from the guts of polystyrene-fed larvae, they successfully isolated 13 bacterial strains, among which *Exiguobacterium* sp. strain YT2 emerged as the dominant species. This strain demonstrated the

ability to form a biofilm on the surface of polystyrene and actively degrade the polymer (Yang et al., 2015).

A subsequent study in 2019 investigated another species of the same genus, *Tenebrio obscurus* (dark mealworm), and found that it exhibited a superior ability to depolymerize and biodegrade polystyrene compared to *T. molitor* (Fig. 6.B). This study further suggested that the gut microbiota, particularly bacteria from the families *Enterococcaceae*, *Spiroplasmataceae*, and *Enterobacteriaceae*, played a significant role in facilitating the degradation process and were closely associated with a polystyrene-based diet (Peng et al., 2019).

Beyond Tenebrionidae, other beetle species have also demonstrated the ability to ingest and degrade polystyrene. A 2020 study identified *Tribolium castaneum* (red flour beetle) as capable of chewing and consuming extruded polystyrene (XPS) (Fig. 6.C). Analysis of the gut microbiome of *T. castaneum* fed on plastic led to the isolation of *Acinetobacter* sp. strain AnTc-1, which exhibited significant polystyrene degradation capabilities (Wang et al., 2020).

Researchers have also identified *Zophobas atratus* (superworms) as another insect capable of ingesting and contributing to polystyrene degradation (Fig. 6.D). Like *T. molitor* and *T. obscurus*, this species belongs to the Tenebrionidae family. A 2020 study revealed that superworms not only consume Styrofoam but also ingest larger quantities compared to mealworms, likely due to their larger size. Notably, polystyrene molecules underwent chemical structural changes after passing through the gut. Specifically, the long PS chains were depolymerized into shorter fragments with a lower molecular weight, which were subsequently mineralized into CO_2. Furthermore, the administration of antibiotics significantly reduced the superworms' ability to break down polystyrene, reinforcing the crucial role of gut microbiota in this process (Yang et al., 2020). To further investigate the role of gut microbiota in *Z. atratus*, subsequent research focused on identifying specific microbial strains involved in polystyrene degradation. This led to the discovery of *Pseudomonas aeruginosa* strain DSM 50071 in the larvae's gut, marking the first time this bacterium was recognized as a potential candidate for PS degradation. It was observed that *P. aeruginosa* could attach to and proliferate on polystyrene film surfaces, indicating its ability to utilize PS as a carbon source (Kim et al., 2020).

Simultaneously, another beetle species, *Plesiophthalmus davidis*, was also found to ingest polystyrene (Fig. 6.E). Further microbial analysis identified a bacterium capable of forming biofilms on the PS surface, actively facilitating its breakdown. This microorganism was classified as *Serratia* sp. strain WSW (Woo et al., 2020).

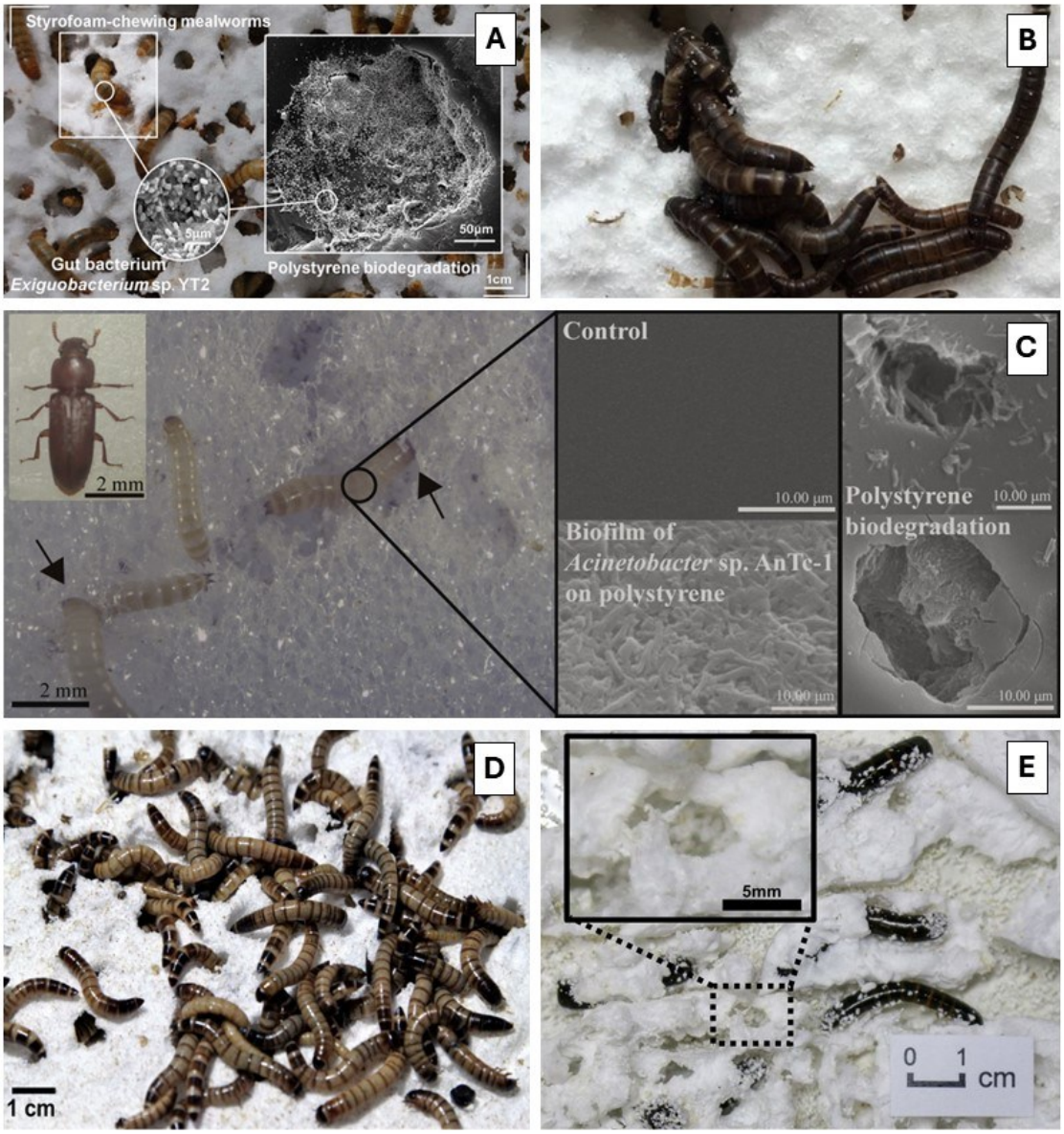

Fig. 6 – Tenebrionidae species identified as plastivorous insects in previous studies. (**A**) *Tenebrio molitor* larvae consuming polystyrene, with *Exiguobacterium* sp. strain YT2 identified as a key degrader (Yang et al., 2015). (**B**) *Tenebrio obscurus* consuming polystyrene (Peng et al., 2019). (**C**) *Tribolium castaneum* ingesting extruded polystyrene (XPS), with *Acinetobacter* sp. strain AnTc-1 isolated from its gut (Wang et al., 2020). (**D**) *Zophobas atratus* (superworms) consuming polystyrene (Yang et al., 2020). (**E**) *Plesiophthalmus davidis* feeding on polystyrene (Woo et al., 2020).

These findings demonstrate that the ability to degrade plastic is not exclusive to a single insect species but is instead widespread in nature. This highlights the need for further research, as these mechanisms could provide an eco-friendly solution to polystyrene pollution.

***Alphitobius diaperinus* (Panzer, 1797)**

Another insect model of interest in the context of polystyrene biodegradation is *Alphitobius diaperinus* (lesser mealworm), a member of Tenebrionidae family. This species, likely originated in sub-Saharan Africa, is now distributed worldwide. Morphologically, *A. diaperinus* presents distinct characteristics across its developmental stages. The adults are broadly oval, black or brownish black, with a length of approximately 6 mm (Fig. 7.A). The larvae, which exhibit an elongated and segmented body, can reach about 11 mm at full development (Fig. 7.B) (Dunford & Kaufman, 2006).

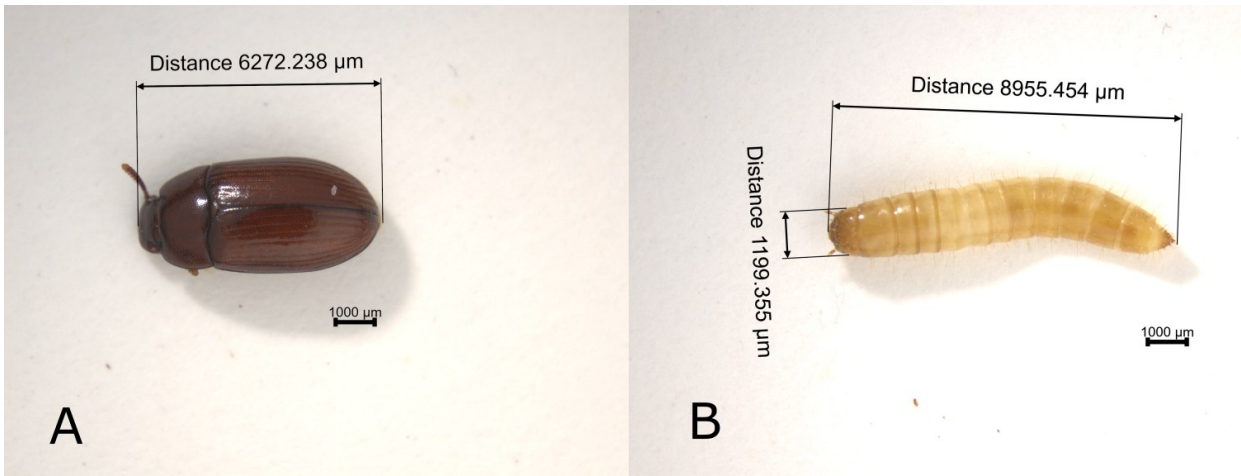

Fig. 7 - *Alphitobius diaperinus* at different developmental stages. (A) Dorsal view of an adult; (B) Larva with an elongated, segmented body.

A 2001 study provided a detailed characterization of *A. diaperinus* larval development, identifying the presence of eight distinct larval instars and establishing the average cephalic capsule size for each stage (Tab. 1) (Francisco & Do Prado, 2001).

Larval instar	Width of cephalic capsule (mm) x (± SD)
I	0.228 (± 0.0192)
II	0.288 (± 0.0225)
III	0.348 (± 0.0433)
IV	0.478 (± 0.0433)
V	0.721 (± 0.0216)
VI	1.061 (± 0.0536)
VII	1.208 (± 0.0769)
VIII	1.339 (± 0.0436)

Tab. 1 - Average width of the cephalic capsule of *Alphitobius diaperinus* larvae. Adapted from Francisco & Do Prado (2001).

A. diaperinus is particularly known as a widespread pest in stored products and the poultry industry. It acts as a vector for poultry pathogens, contributing to the spread of infectious diseases (Dunford & Kaufman, 2006). Additionally, its presence in poultry facilities causes structural damage, as larvae in their pre-pupal instar actively search for suitable pupation sites by chewing through materials such as polyurethane and polystyrene insulation panels commonly used in poultry house walls. This destructive behaviour results in increased heating costs and expensive repairs (Francisco & Do Prado, 2001).

A. diaperinus has also been investigated for its potential role in polystyrene degradation (Fig. 8). A previous study specifically examined this species' ability to degrade polystyrene, highlighting not only its capacity to ingest the plastic but also significant changes in the gut bacterial microbiome. Metabarcoding analysis revealed that larvae fed with polystyrene foam exhibited substantial differences in their gut microbiome compared to those in a control group fed a standard vegetable-based diet (Cucini et al., 2020). Subsequently, a second study conducted in 2022 analysed the gut bacterial community associated with the plastic-eating *A. diaperinus* after an enrichment phase in a medium containing PS as the sole carbon source and with limited chemical composition. After two months of enrichment, the results obtained through culture-dependent and molecular analysis indicated the predominance of three bacterial strains belonging to the genus of *Klebsiella*, *Pseudomonas*, and *Stenotrophomonas* (Cucini et al., 2022).

Fig. 8 - *Alphitobius diaperinus* larvae actively feeding on polystyrene.

These findings provided a solid scientific basis to consider *A. diaperinus* as a promising insect model for advancing research on polystyrene biodegradation, offering both ecological relevance and a concrete experimental foundation. Indeed, the present study aims to further investigate its biodegradation potential through different research approaches. In the first chapter, the research will focus on: I) optimization of rearing conditions; II) study of gut microbiota through advanced metabarcoding analysis; III) analysis of the chemical structure of the plastic polymer before and after digestion by the insect, along with the detection of polystyrene degradation by-products using different chemical techniques. In the second chapter, the genetic profile of the previously isolated bacterium *Stenotrophomonas indicatrix* strain DAI2m/c (Cucini et al., 2022) will be investigated through genome sequencing, aiming to identify enzyme-encoding genes involved in the intracellular metabolic pathways responsible for styrene monomer biodegradation. All results presented in the second chapter have been published in the journal *Scientific Reports* (Zarra et al., 2025).

CHAPTER 1

1.1 INTRODUCTION

Recent studies have increasingly focused on the role of *Alphitobius diaperinus* in polystyrene biodegradation, emphasizing its ability to ingest and degrade the polymer through the combined action of larvae and their gut microbiota (Cucini et al., 2020). However, previous research on this insect has revealed some critical challenges. In rearing systems based on a polystyrene (PS) diet, a significant reduction in larval weight was observed, along with a high mortality rate. These findings indicate that these rearing conditions are significantly stressful, creating additional challenges for planning new experiments to better understand the biodegradation process. In response to these limitations, this chapter explores three primary research lines, each aimed at overcoming these challenges and expanding the existing knowledge:

I. **Optimization of rearing conditions**:
   This first research line focuses on reducing the larval mortality rate and determining whether all larval instars have the same capacity to ingest polystyrene. This step is essential for improving the rearing condition and ensuring the planning of future experiments.

II. **Chemical analyses**:
   The second research line focuses on chemical analyses to validate and better understand the mechanisms involved in polystyrene degradation. Specifically:
   - Micro-Fourier Transform Infrared Spectroscopy (micro-FTIR) will be used to analyse frass (fecal pellet) to confirm the presence of PS residues, demonstrating its ingestion by larvae, and to evaluate structural alterations of the polymer compared to the original material provided as diet.
   - Gas Chromatography–Mass Spectrometry (GC–MS) analyses will be performed on freeze-dried larvae fed with polystyrene to detect potential by-products of polymer degradation.

III. **Metabarcoding analyses**:

The third area of research is focused on new metabarcoding analyses to provide deeper insights into the gut microbiota associated with PS degradation. These analyses will include an increased number of replicates and new experimental conditions, with a particular focus on:

- Exploring the differences in gut microbiota composition among various larval instars;
- Investigating the gut microbiota composition in the three main sections of the gastrointestinal tract (foregut, midgut, and hindgut) in last instar larvae fed with PS compared to those fed a standard vegetable-based diet (CT).

1.2 MATERIALS AND METHODS

The larvae of *A. diaperinus* used in this study were sourced from Agripet Garden (Padova, Italy; reared according to the factory protocol, see: https://www.agripetgarden.it/). Approximately 5,000 larvae were reared under controlled environmental conditions (20 ± 2 °C; 12-hour light/dark cycle; 50–70% RH) at the Department of Life Sciences of the University of Siena. The expanded polystyrene foam, commercially known as Extir® (CAS 9003-53-6), with a density of 0.01 g/cm³, was purchased from Toscoespansi s.r.l. (http://www.toscoespansi.it/). According to the supplier, the material did not contain additional additives or catalysts.

To determine the larval instar of the *A. diaperinus* larvae used in the experiments, we adopted the classification described by Francisco and Do Prado (2001). This classification is based on the measurement of cephalic capsule size, which allows for the identification of eight distinct larval instars (Tab. 1). Using these data, in the present study the larvae were grouped into three main categories for the experiments, as shown in Tab. 1.1.

GROUP	LARVAL INSTAR
L1	I, II, III
L2	IV, V, VI
L3	VII, VIII

Tab. 1.1 - Classification of *Alphitobius diaperinus* larvae into three main groups based on the cephalic capsule size and larval instar classification described in Francisco et al. (2001).

1.2.1 Optimization of rearing conditions

In this first part of the study, the goal was to monitor *A. diaperinus* larvae to optimize their rearing conditions. Specifically, the primary aim was to determine whether all larval instars exhibit the same capacity to ingest PS or if this behaviour is restricted to a specific phase of the instar larvae. To address these questions, the following protocol was applied:

a) Five identical rearing setups (replicates: A, B, C, D and E) were prepared. Each replicate contained approximately 240 larvae, with 80 individuals from each developmental group (L1, L2 and L3);
b) The larvae in each rearing setup were provided with a mixed diet consisting of carrots, bran, and a piece of polystyrene;
c) Every three days, the polystyrene pieces were removed from each setup, fragmented, and the larvae found inside were measured for cephalic capsule size using a stereomicroscope (Fig. 1.1). The rearing setups were replaced with new polystyrene pieces to continue the procedure;
d) After measurement, the larvae were transferred to secondary rearing setups (A', B', C', D', and E') without PS to monitor their progress and observe how many completed their life cycle by reaching adult stage;
e) The entire procedure was repeated five times.

Fig. 1.1 - Cephalic capsule measurement of last-instar (L3) *A. diaperinus* larvae under a stereomicroscope.

1.2.2 Chemical analyses

Chemical analyses were performed to confirm PS ingestion and evaluate its degradation by *A. diaperinus* larvae. Two techniques were used: Gas Chromatography–Mass Spectrometry (GC–MS) for detecting degradation by-products in larval tissues, and micro-Fourier Transform Infrared Spectroscopy (micro-FTIR) to confirm the ingestion of PS, its presence within the frass (fecal pellets), and to evaluate molecular changes in the polymer structure after passing through the larval gut.

1.2.2.1 Rearing setup

For both chemical analyses, only last-instar larvae (L3 group) were selected from both the polystyrene fed rearing system (PS-rearing) and the control rearing system (CT-rearing), which was maintained on a vegetable-based diet consisting of bran and carrots. Each rearing system initially included approximately 300 larvae. The colonies were maintained for about one month, ensuring regular removal of emerging adults and their replacement with new L3 larvae.

1.2.2.2 Micro-Fourier Transform Infrared Spectroscopy (micro-FTIR)

For frass collection, only larvae found inside the PS piece were selected from the PS-rearing. To maintain uniformity in the collection process, an equivalent number of larvae were randomly selected from the CT-rearing system. These larvae were cleaned of residual PS/CT powder with compressed air and placed in two clean boxes overnight to allow frass accumulation. The following day, frass was carefully collected using sterile forceps and transferred into sterile microtubes. Samples were then stored at -20°C. This procedure was repeated for approximately three weeks (Yang et al., 2018). Visual verification and chemical identification of microplastics was carried out with a micro-Fourier Transformed Infrared Spectroscope microscope (Nicolet iN10 MX Infrared Imaging Microscope, Thermo Scientific) in transmission mode. Micro-FTIR spectra of all particles were recorded in the spectral range of 4000 to 400cm^{-1} with a collection time of 45s and 128 co-scans for each measurement. The spectral resolution was 4 cm^{-1}, and the aperture size was a range of 10×10 µm to150×150 µm depending on the size of particles. For the analysis of the chemical composition of the particles, a custom spectral library (UNISI Library) was created by acquiring the chemical spectrum of the virgin material to detect direct variations in the digested particles. Additionally, built-in instrument libraries (HR Polymer Additives and Plasticizers, Wizard Library, and Thermo Electron) were used for further

verification and analysis of the obtained spectra. Components with a match ≥70% were considered acceptable.

Micro-FTIR analyses were conducted on the following sample types:

- Original feedstock materials: bran and carrots provided as part of the control diet; virgin polystyrene provided as part of the experimental diet.
- Undigested frass: frass collected from larvae in the control group (Frass CT) and the polystyrene-fed group (Frass PS) without additional chemical treatment.
- Chemically treated samples: virgin polystyrene and frass PS, both subjected to digestion with I) 10% potassium hydroxide (KOH) solution and II) 15% hydrogen peroxide (H_2O_2) solution.

For each sample type, five particles were randomly selected for analysis. On each particle, three measurements were performed.

1.2.2.3 Gas Chromatography–Mass Spectrometry (GC–MS)

The GC-MS was used to detect potential by-products resulting from the metabolic degradation of PS by *A. diaperinus* larvae. Chloroform and standards Styrene (≥98%), α-Methylstyrene (≥98.5%), Acetophenone (≥99.5%), Benzenemethanol, α,α-dimethyl- (cumyl alcohol) (97%), 2,4-di-tert-butylphenol (DTBP) (99%) were provided by Sigma-Aldrich S.r.l. (Milan, Italy). For the experiment, the larvae were selected following the same procedure previously described in the micro-FTIR analysis: only those found inside the PS piece were taken from the PS-rearing system. The larvae were collected over a period of approximately two weeks. Following collection, larvae from both PS-rearing and CT-rearing systems were lyophilized as the protocol described by Tsochatzis et al. (2020). A lyophilised sample of 200 mg of the collected insects' larvae was placed in a 2 mL vial and 500 µL of chloroform were added. The sample was homogenised with an IKA Labortechnik T25 basic (IKA Werke GmbH & Co., Staufen, Germany). The sample was vortexed and sonicated at 25°C for 30 minutes with an ultrasound bath (Bandelin Sonorex, Rangendingen, Germany) operating at a frequency of 35 kHz. After centrifugation at 2500 rpm for 5 min, supernatant and pellet were separated and the solvent was recovered. Finally, samples were filtered with PTFE 0.45 mm filters. Chromatographic analyses were performed with a Varian 3900 gas chromatograph with a CP-8400 auto-sampler coupled to Varian Saturn 2000 MS/MS ion trap mass spectrometer (Varian, Palo Alto, CA, USA). The

samples were analysed with a capillary column VF-5ms with the following dimensions: 30 m x 0.25 mm ID, 0.25 µm d.f. (FactorFour, Varian Inc., USA). The analysis was performed using a split/split-less injector at 250 °C in splitless mode, with a column flow of 1.5 mL min−1. The injection volume was 1 µl. The oven program was the following: initial temperature of 65 °C for 2 min, ramp (7 °C min−1) up to 202 °C, ramp (100 °C min−1) up to 275 °C (isothermal of 1 min). The total run time was 23 min, including a solvent delay time of 2.5 min, applying Electron Impact Ionization at 70 eV. Mass analysis and detection were performed using a scan range from 40 to 400 amu. The identification was performed using commercial standards and the NIST5 library.

1.2.3 Metabarcoding analyses

Metabarcoding analyses were conducted to investigate the gut microbiota composition of *A. diaperinus* under different experimental conditions. The aim of these analyses was to explore how the microbiota varies across larval instars and different gut sections.

1.2.3.1 Rearing setup

The findings from the experiment described in section "1.2.1 Optimization of rearing conditions" were critical for the design and planning of the metabarcoding analyses. These results offered valuable insights into larval behaviour and feeding preferences, which were essential for establishing the rearing setup used in this phase of the study. Thus, the larvae were divided into four distinct rearing groups:

- L1_CT: a group of L1 larvae fed on a diet of carrots and bran
- L2_CT: a group of L2 larvae fed on a diet of carrots and bran
- L3_CT: a group of L3 larvae fed on a diet of carrots and bran
- L3_PS: a group of L3 larvae fed exclusively with polystyrene foam.

Approximately 250 larvae were included in each rearing group. To standardize gut content before dissection and DNA extraction, the larvae were subjected to a fasting period of 12 hours.

1.2.3.2 Sample preparation

The larvae were externally sterilized by immersion in 75% ethanol for approximately 2 minutes and then rinsed five times with sterile water. Each larva was placed on a Petri dish, and the anterior and posterior ends were removed using sterile forceps. This procedure allowed the extraction of the entire gut. The extracted gut was carefully cleaned to remove fatty tissue and Malpighian tubules, following the protocol described by Wang & Zhang (2015). To perform the metabarcoding analyses, two distinct sample sets were prepared, each addressing specific research aims: the first focused on characterizing the gut microbiota across different larval instars; the second aimed at assessing microbial composition variations within specific gut sections (Fig. 1.2).

The first analysis aimed to investigate the gut microbiota composition across different larval instars (L1_CT, L2_CT, L3_CT and L3_PS).

- The entire gut was collected and placed in 1.5 ml tube.
- Each tube contained a pool of three guts.
- Samples were processed in quintuplicate, resulting in a total of 20 samples: five each for L1_CT, L2_CT, L3_CT, and L3_PS.

The second analysis focused on evaluating microbiota differences within specific sections of the gut (foregut, midgut, and hindgut) and between the two different dietary groups (*L3_CT* vs *L3_PS*).

- The gut was dissected into three sections: foregut (FG), midgut (MG), and hindgut (HG) (Fig. 1.2).
- Each section was placed in a separate 1.5 ml tube.
- Similar to the first analysis, each tube contained a pool of three gut sections.
- Samples were processed in quintuplicate, resulting in a total of 30 samples: five each for FG_CT, MG_CT, HG_CT, FG_PS, MG_PS, and HG_PS.

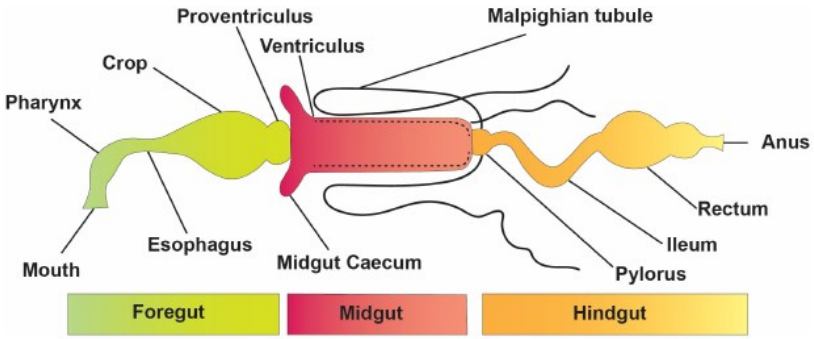

Fig. 1.2 - Schematic representation of the insect gut segmentation, showing the foregut (FG), midgut (MG), and hindgut (HG). Source: Siddiqui et al. (2022).

1.2.3.3 Extraction and sequencing of bacterial DNA

Bacterial DNA was extracted using the QIAamp® PowerFecal® Pro DNA Kit, following the manufacturer's protocol. The final DNA concentration was measured using both a NanoDrop ND1000V spectrophotometer (NanoDrop Technologies, Wilmington, DE, US) and a Qubit® fluorometer (Life Technologies Corporation, Carlsbad, CA, US). The quality of the DNA was assessed by 1% agarose gel electrophoresis to ensure its suitability for downstream analyses. The extracted DNA samples were sent to Biomarker Technologies (BMK) GmbH, located in BioZ, Johann-Krane-Weg 42, 48149 Münster, Germany, for further processing, including sample quality control (QC), library preparation, sequencing, and data quality control. A total of 50 samples underwent full-length 16S rDNA gene amplicon sequencing using the PacBio CCS mode (HiFi reads). For the amplification of the full-length 16S rDNA gene, the following primers were used:

- Forward primer (27F): 5’-AGRGTTTGATYNTGGCTCAG-3’
- Reverse primer (1492R): 5’- TASGGHTACCTTGTTASGACTT-3’

The sequencing was performed with a target of 20,000 reads per sample, ensuring high-quality data for subsequent analyses.

1.2.3.4 Data analysis

The raw reads were analysed entirely using RStudio (Posit team, 2024). To infer amplicon sequence variants (ASVs) and remove sequencing errors, the raw reads were processed using the *DADA2* package (Callahan et al., 2016). Primer sequences were removed with RemovePrimers(), and reads were filtered and trimmed (filterAndTrim()) using the following parameters: sequences with lengths between 1200 and 1450 bp were retained, while those with poor quality (*maxEE* = 10, *minLen* = 1200) or ambiguous bases (*maxN* = 0) were excluded. Dereplication (derepFastq()) and error modeling (learnErrors()) were performed to accurately identify true biological sequences and distinguish them from sequencing errors. Chimeric sequences were identified and removed using (removeBimeraDenovo()). Taxonomy assignment was conducted using the SILVA v138.1 database (Quast et al., 2012). Genus-level and species-level classifications were obtained with assignTaxonomy() and addSpecies() functions. Given the use of full-length 16S rDNA gene sequencing with PacBio HiFi technology, high-resolution amplicon sequence variants (ASVs) were inferred without applying clustering thresholds. For following sections and for consistency with common microbiome data presentation, the term "OTU" (Operational Taxonomic Unit) is used to refer to taxonomically assigned ASVs.

The relative frequencies of genera (genus frequency) were calculated to determine the distribution and proportion of each genus within the microbial communities. The visualization of genus distribution across the samples was created as bar plots using the *ggplot2* package (Wickham, 2016). For downstream analyses, the OTU tables, taxonomy tables, and sample metadata were integrated into a *phyloseq* object using the *phyloseq* package (McMurdie & Holmes, 2013). Alpha diversity indices, including Shannon and Simpson indices, were calculated using estimate_richness() from *phyloseq*. In order to assess whether alpha diversity significantly differed between experimental groups, a Kruskal-Wallis test was performed separately for each index using the kruskal.test() function in RStudio. A p-value threshold of 0.05 was used to determine statistical significance. Beta diversity was evaluated using the Bray-Curtis distance metric (distance() in *phyloseq*). The separation of microbial communities across experimental groups was visualized using Principal Coordinates Analysis (PCoA), with visual outputs specifically designed using *ggplot2*. Statistical differences in community composition were tested using *PERMANOVA* (Permutational Multivariate Analysis of Variance) via the *pairwiseAdonis* package (Martinez Arbizu, 2020). Significance was determined using 999 permutations, and p-values were adjusted for multiple testing using the Benjamini-Hochberg correction. Differential abundance analysis was conducted using *DESeq2* package (Love et al.,

2014) to identify taxa significantly enriched or depleted between experimental groups. Results were filtered to include only taxa with adjusted p-values (padj) < 0.05. Differentially abundant genera were visualized using bar plots created through *ggplot2* package (Wickham, 2016). The presence and distribution of OTUs across experimental groups were examined using Venn diagrams generated with the *VennDiagram* package (Chen, 2022). The taxonomy of shared and unique OTUs among the groups examined was extracted and saved in CSV files for further interpretation.

1.3 RESULTS

1.3.1 Optimization of rearing conditions

The measurements of cephalic capsule width revealed that the majority of larvae extracted from PS across all rearing replicates and sampling intervals belonged to the final larval instar (VIII: 1.339 mm). These results were consistent across the different experimental groups (Fig. 1.3). Following their extraction from polystyrene, larvae were transferred to secondary rearing boxes (A', B', C', D', E') to monitor their progression to adulthood. Within 15 days, 90.3% of the larvae successfully pupated and became adults, while the remaining 9.7% did not survive.

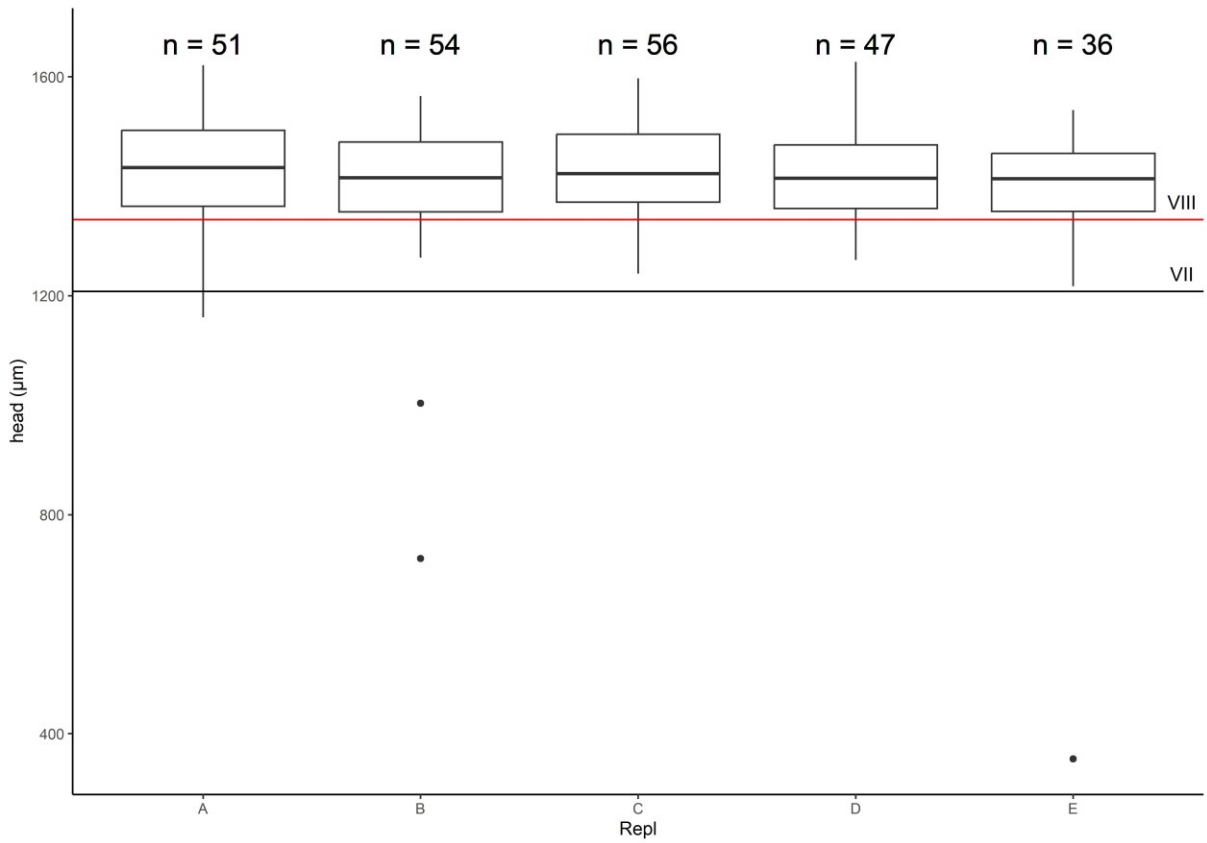

Fig. 1.3 - Boxplot showing the distribution of cephalic capsule widths for larvae extracted from polystyrene across different rearing replicates and sampling intervals. The horizontal lines represent thresholds for distinguishing larval instars based on the classification of Francisco & Do Prado (2001). In particular, the final red line corresponds to the cephalic capsule size threshold for larvae in the last larval instar. The values above each box indicate the total number of larvae extracted from PS pieces in the different sampling intervals.

1.3.2 Chemical analyses

1.3.2.1 Micro-Fourier Transform Infrared Spectroscopy (micro-FTIR)

Micro-FTIR spectroscopy was performed to assess the chemical composition of frass and evaluate potential molecular alterations in polystyrene polymer after passage through the larval gut. Several comparisons were conducted: control diet components (bran and carrots) compared with frass from larvae fed with the control diet (Frass CT) (Fig. 1.4.A); virgin polystyrene (PS) in comparison with frass from PS fed larvae (Frass PS) (Fig. 1.4.B); virgin PS contrasted with frass from PS fed larvae, both digested in H_2O_2 (Fig. 1.4.C); virgin PS compared with frass from PS fed larvae, both digested in KOH (Fig. 1.4.D). For each condition, the spectrum with the closest match to the average similarity score (calculated across all replicates and measurements) was selected for visualization. The mean match percentage and standard deviation for each comparison are reported in Tab. 1.2.

Comparison	Mean match percentage
Bran & Carrots (Feedstock) – Frass CT	78,37 ± 3,69
Virgin PS (Feedstock) – Frass PS	91,61 ± 3,91
Virgin PS (H_2O_2) – Frass PS (H_2O_2)	87,60 ± 7,9
Virgin PS (KOH) – Frass PS (KOH)	91,41 ± 5,46

Tab. 1.2 - Mean match percentage (± standard deviation) of Micro-FTIR spectra across different sample comparisons.

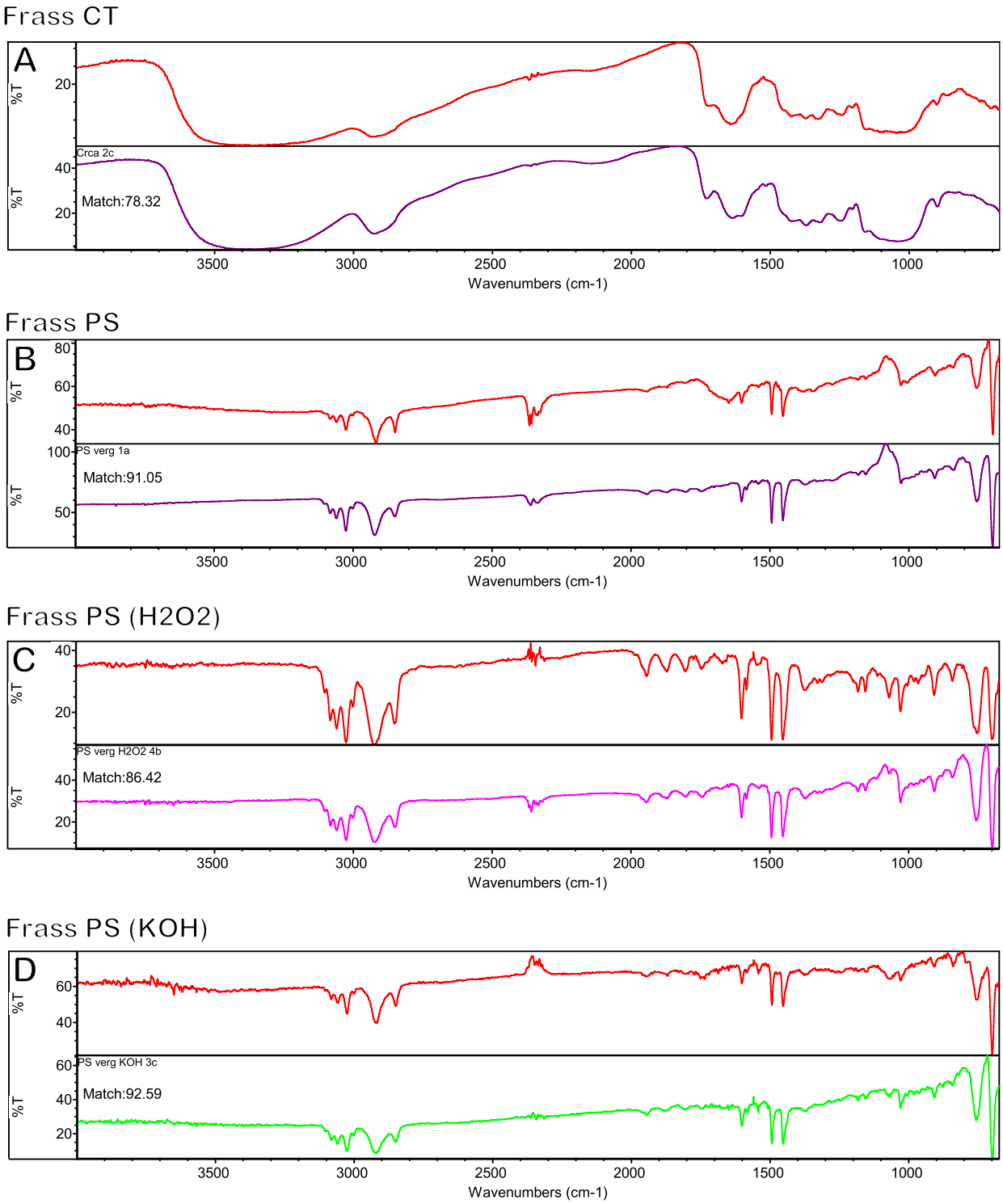

Fig. 1.4 - Micro-FTIR spectra comparing the chemical composition of frass and original feedstock materials across different conditions. The upper spectra correspond to the measured particles, while the lower spectra represent reference spectra from the UNISI Library. The match percentage indicates the similarity with the reference. (A) Control diet components vs. Frass CT. (B) Virgin polystyrene vs. Frass PS. (C) Virgin polystyrene vs. Frass PS after digestion in H_2O_2. (D) Virgin polystyrene vs. Frass PS after digestion in KOH.

1.3.2.2 Gas Chromatography–Mass Spectrometry (GC–MS)

A suitable analytical method was carried out using commercial standards to verify the presence of polystyrene-related metabolites. Metabolites were selected based on previous studies performed on *T. molitor* (Tsochatzis et al., 2020). The linearity was above 0.99 for all the analytes, and the limit of detection (LOD) ranged from 0.01 mg/kg for styrene to 0.1 mg/kg for cumyl alcohol. The recoveries from the matrix were > 93% for all the analytes.

The GC-MS analysis confirmed the presence of several compounds already identified as the main metabolites of polystyrene in *Tenebrio molitor* Coleoptera (Tsochatzis et al., 2020). Interestingly α-methylstyrene (Fig. 1.5) and cumyl alcohol (Fig. 1.6) were found in *Alphitobius diaperinus* fed with PS but not in the groups fed with CT diet. The other standards tested were not detected.

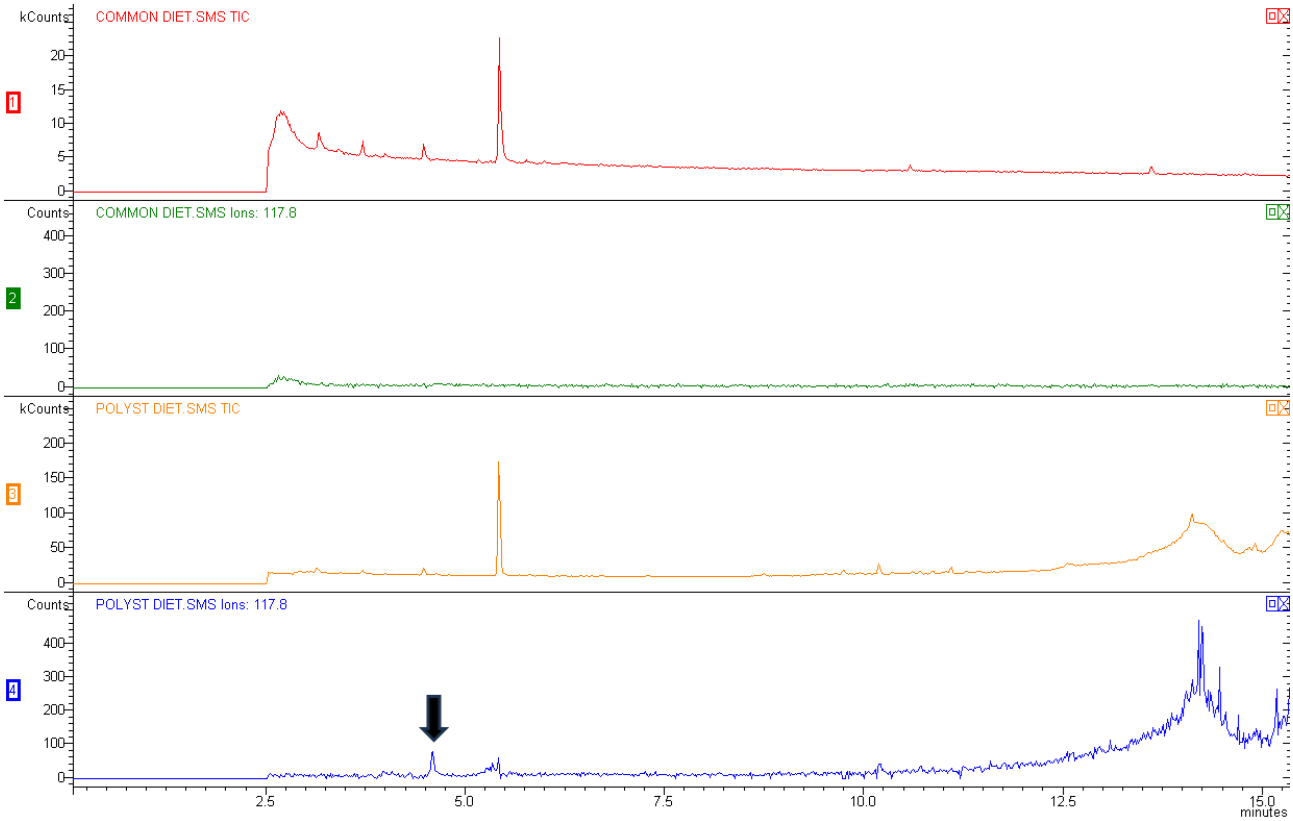

Fig. 1.5 - GC-MS extracted ion chromatogram (EIC) of plastic-related compound α-methylstyrene in *Alphitobius diaperinus* feed with a standard diet (1 GC-MS and 2 extracted ion), feed with polystyrene (3 GC-MS and 4 extracted ion).

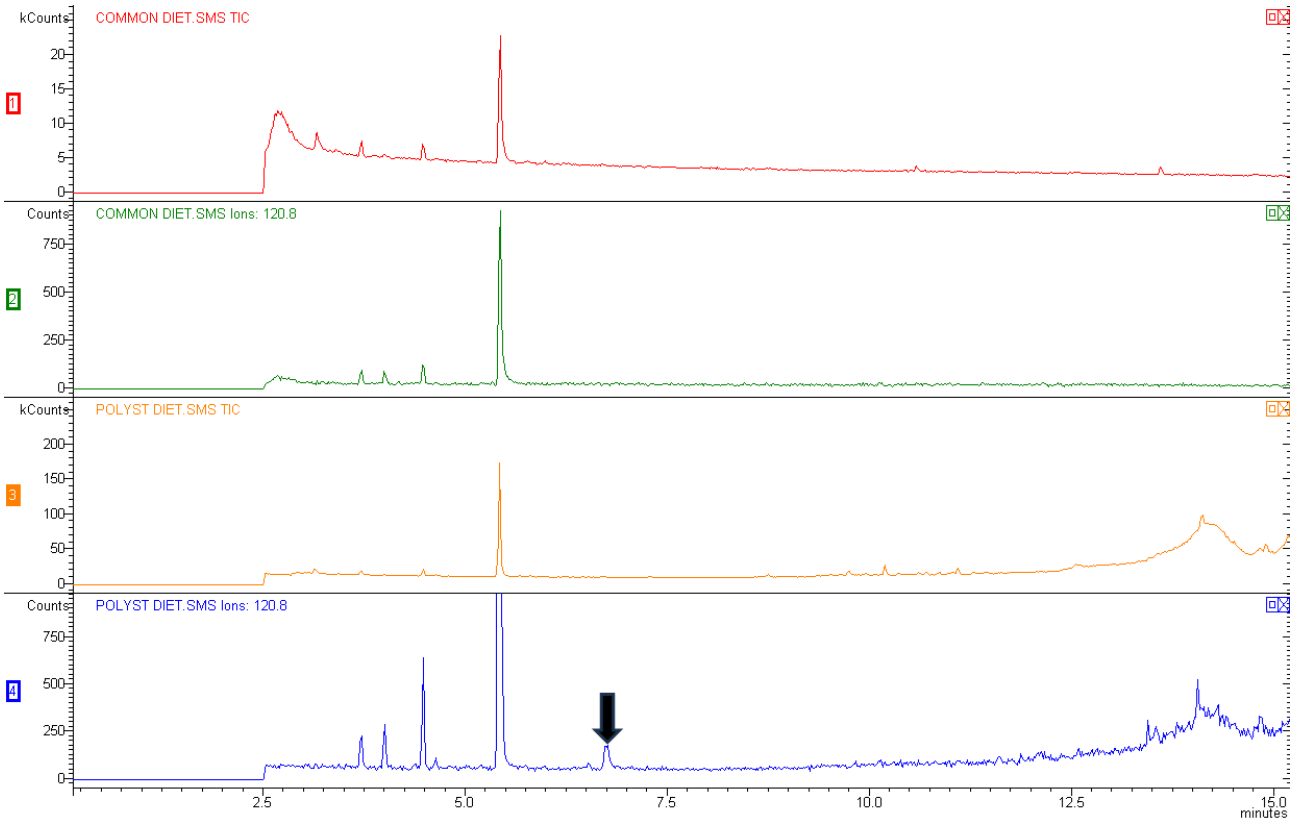

Fig. 1.6 - GC-MS extracted ion chromatogram (EIC) of plastic-related compound cumyl alcohol in *Alphitobius diaperinus* feed with a standard diet (1 GC-MS and 2 extracted ion), feed with polystyrene (3 GC-MS and 4 extracted ion).

1.3.3 Metabarcoding analyses

Metabarcoding analyses were performed to investigate the gut microbiota composition of *A. diaperinus* under different experimental conditions. The study consisted of two separate analyses: the first examined microbiota composition across different larval instars (L1_CT, L2_CT, L3_CT, L3_PS), while the second focused on microbiota differences across gut sections (foregut, midgut, hindgut) and between the two experimental groups (L3_CT vs L3_PS). For the first analysis, a total of 726,619 high-quality HiFi reads were obtained, with a per-sample range of 20,207 to 27,445. For the second analysis, 471,734 high-quality HiFi reads were obtained, showing a per-sample range of 20,434 to 27,378.

1.3.3.1 Analysis of gut microbiota across larval instars

Alpha diversity indices (Shannon and Simpson) were calculated to evaluate the microbial richness and evenness across larval instars (L1_CT, L2_CT, L3_CT, L3_PS). The results, summarized in Tab. 1.3, illustrate the differences in microbial community structure among the groups. However, no statistically significant differences were detected (Shannon: p-value = 0.901; Simpson: p-value = 0.452).

Group	Sample	Shannon index	Simpson index
CT	L1	2.53 ± 0.69	0.83 ± 0.10
CT	L2	2.51 ± 0.21	0.88 ± 0.04
CT	L3_CT	2.67 ± 0.69	0.85 ± 0.13
PS	L3_PS	2.59 ± 0.21	0.90 ± 0.02

Tab. 1.3 - Alpha diversity indices (Shannon and Simpson) across larval instars. Values are presented as mean ± standard deviation.

Beta diversity was measured using the Bray-Curtis dissimilarity metric, and the results were visualized through PCoA. Two levels of comparison were performed. The first level comparison was based on differentiation in microbial communities between control (CT) and

polystyrene-fed (PS) groups (Fig. 1.7.A). PERMANOVA results indicate that the observed differences were statistically not significant (p.adj > 0.05). The second level comparison examined the clustering of microbial communities across experimental groups, including L1-CT, L2-CT, L3-CT, and L3-PS (Fig. 1.7.B). PERMANOVA results revealed that the differences between groups were statistically not significant (p.adj > 0.05).

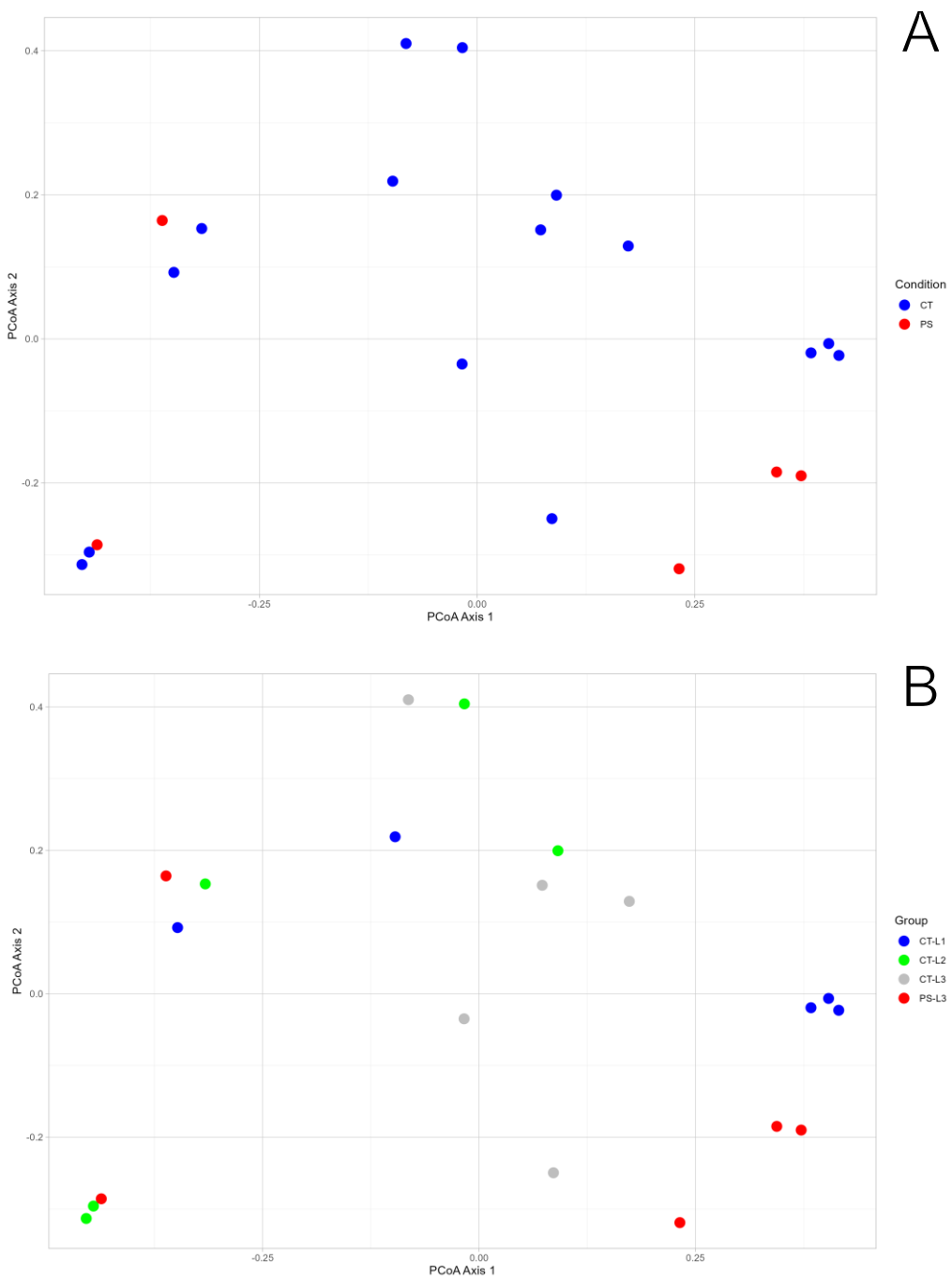

Fig. 1.7 - Principal Coordinates Analysis (PCoA) plots visualizing beta diversity among microbial communities. (A) Comparison between control (CT) and polystyrene-fed (PS) groups, highlighting the separation between the two conditions. (B) Clustering of microbial communities across experimental groups (L1-CT, L2-CT, L3-CT, and L3-PS), showing variation among different larval instars and conditions.

The genus distribution across samples is displayed in the taxa bar plot (Fig. 1.8). Each bar corresponds to one of the five replicates for each experimental group (L1-CT, L2-CT, L3-CT, and L3-PS), and the colored segments represent the relative abundance of identified genera.

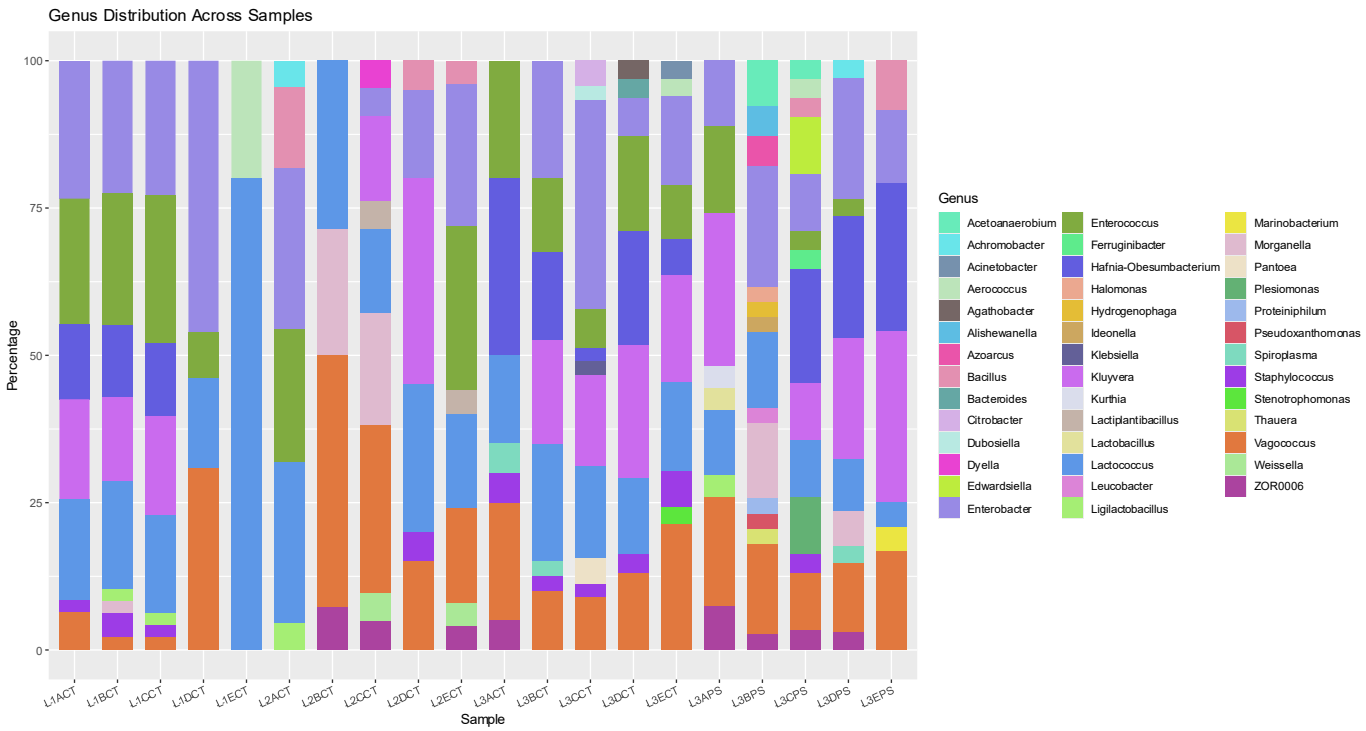

Fig. 1.8 - Taxa bar plot of genus distribution across replicates and experimental groups.

The Venn diagrams (Fig. 1.9) illustrate the distribution of OTUs across larval instars (L1CT, L2CT, L3CT and L3PS).

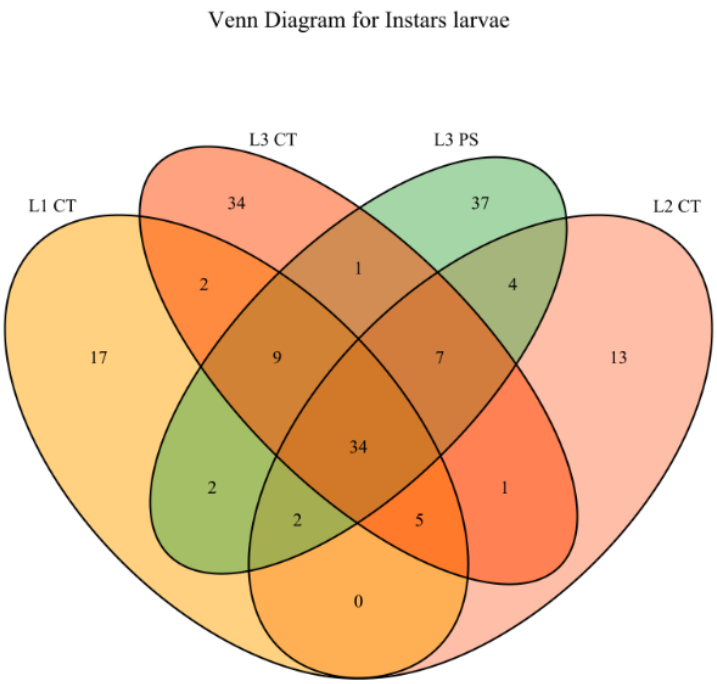

Fig. 1.9 - Venn diagrams representing OTU distribution across larval instars: L1CT, L2CT, L3CT and L3PS. Numbers indicate the OTUs that are shared between or exclusive to each instar.

To visualize bacterial genus distribution across larval instars, a heatmap was generated (Fig. 1.10). The heatmap displays the relative abundance of shared and unique bacterial genera among the different instars (L1_CT, L2_CT, L3_CT, and L3_PS), including five biological replicates per group. Only bacterial genera were considered, clustering multiple species under the same genus, which reduced the total number of taxa compared to the original dataset.

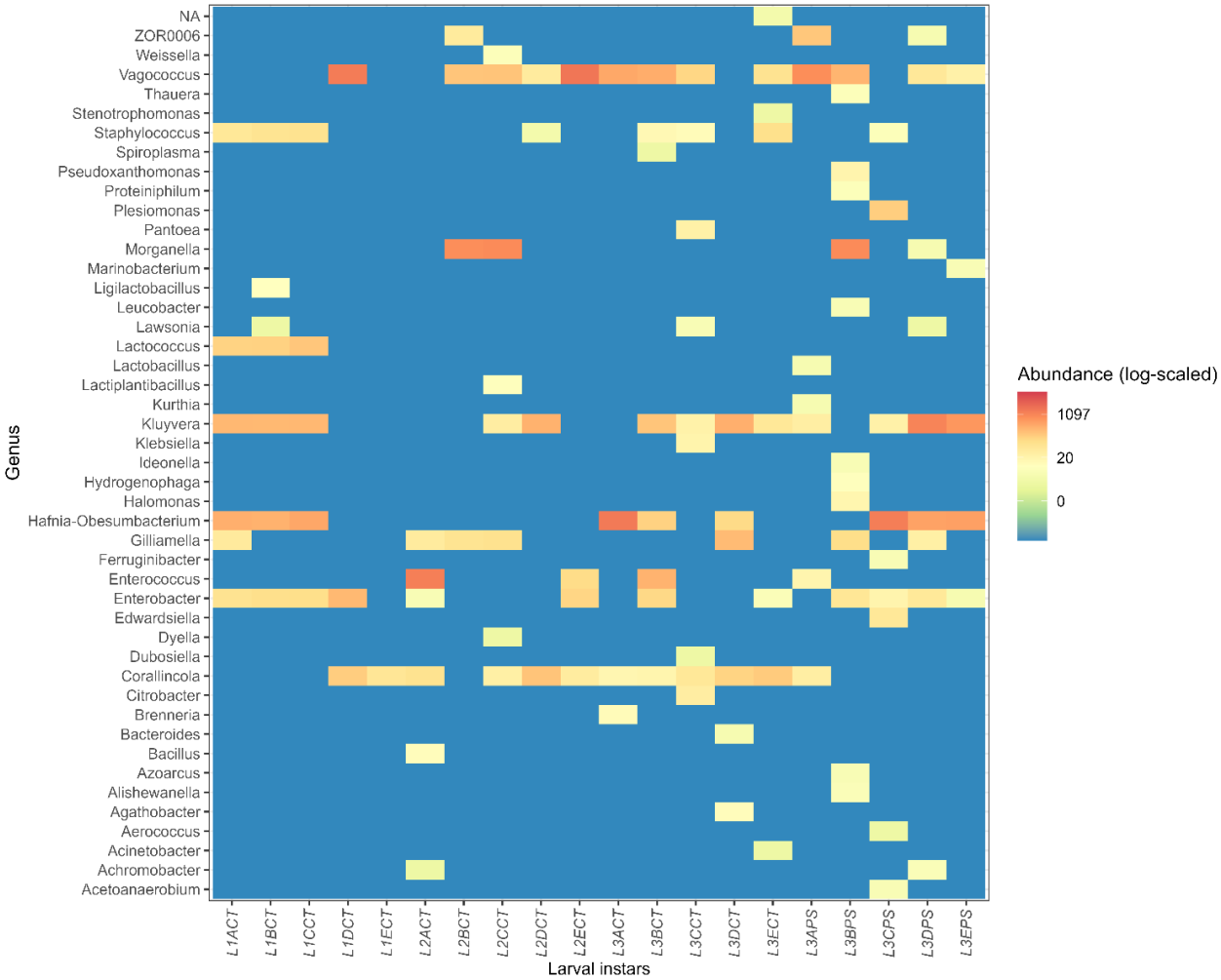

Fig. 1.10 -. Heatmap displaying the relative abundance of bacterial genera across different larval instars. The x-axis represents the 20 individual samples (five replicates per experimental group), while the y-axis lists the identified bacterial genera. The color gradient reflects the abundance levels of each genus across the samples.

Differential abundance analysis was conducted to identify differences in microbial community compositions between the experimental groups. Specifically, the analysis focused on the microbial composition among different larval instars within the CT group (L1-CT vs L2-CT; L2-CT vs L3-CT) and evaluated the impact of PS at the last larval instar (L3-CT vs L3-PS) (Fig. 1.11). The results were filtered to include only genera with adjusted p-values (p adj) < 0.05.

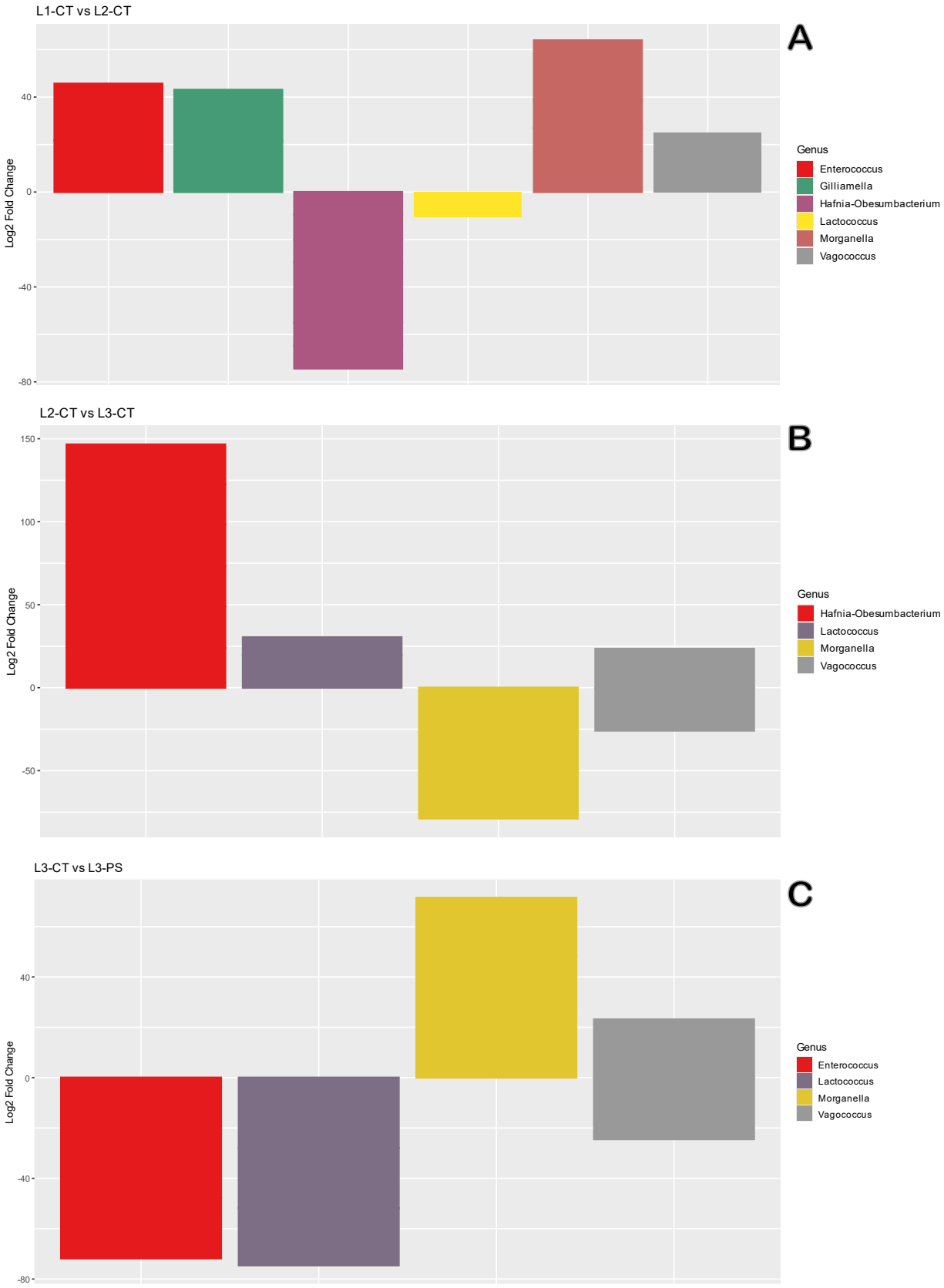

Fig. 1.11 - Bar plots showing bacterial genera differentially abundant across larval instars and between feeding conditions. (A) Differentially abundant genera between CT-L1 and CT-L2; (B) CT-L2 and CT-L3; (C) CT-L3 and PS-L3. Positive log2 fold change values indicate genera enriched in CT-L2 (A), CT-L3 (B), and PS-L3 (C), while negative values indicate genera enriched in CT-L1 (A), CT-L2 (B), and CT-L3 (C).

1.3.3.2 Analysis of gut microbiota across gut sections

Alpha diversity indices (Shannon and Simpson) were calculated to assess microbial richness and evenness across gut sections (Foregut, Midgut, Hindgut) under two dietary conditions (CT and PS). The results highlight the differences in microbial community structure between the sections and conditions (Tab. 1.4). Statistically significant differences were detected (Shannon: p-value = 0.0053; Simpson: p-value = 0.0008), indicating that internal microbial complexity varies according to anatomical location and feeding condition.

Group	Sample	Shannon index	Simpson index
CT	Foregut_CT	2.99 ± 0.61	0.92 ± 0.08
CT	Midgut_CT	2.48 ± 0.55	0.84 ± 0.05
CT	Hindgut_CT	2.85 ± 0.34	0.90 ± 0.03
PS	Foregut_PS	1.58 ± 0.02	0.66 ± 0.00
PS	Midgut_PS	2.30 ± 0.83	0.78 ± 0.10
PS	Hindgut_PS	3.11 ± 0.11	0.94 ± 0.01

Tab. 1.4 - Alpha diversity indices (Shannon and Simpson) across intestinal sections under control (CT) and polystyrene (PS) conditions. Values are presented as mean ± standard deviation.

Beta diversity was measured using the Bray-Curtis dissimilarity metric, and the results were visualized through PCoA. Two levels of comparison were conducted. The first-level comparison, focusing solely on the differentiation between CT and PS groups (Fig. 1.12.A), revealed statistically significant differences between the two groups, as indicated by PERMANOVA results (p.adj < 0.05). The second level comparison examined the clustering of microbial communities across all individual groups (FG-CT, MG-CT, HG-CT, FG-PS, MG-PS, HG-PS) (Fig. 1.12.B). Significant differences were observed between certain groups. Specifically, PERMANOVA results indicated statistically significant differences between FG-CT and FG-PS (p.adj < 0.05) and between MG-CT and MG-PS (p.adj < 0.05). No significant differences were observed between HG-CT and HG-PS (p.adj > 0.05). Intragroup comparisons revealed no statistically significant differences within the CT group. However, within the PS group, significant differences were observed between FG-PS and HG-PS (p.adj < 0.05), as well

as between MG-PS and HG-PS (p.adj < 0.05). All PERMANOVA results are summarized in Tab. 1.5. Comparisons with p.adjusted < 0.05 are considered significant.

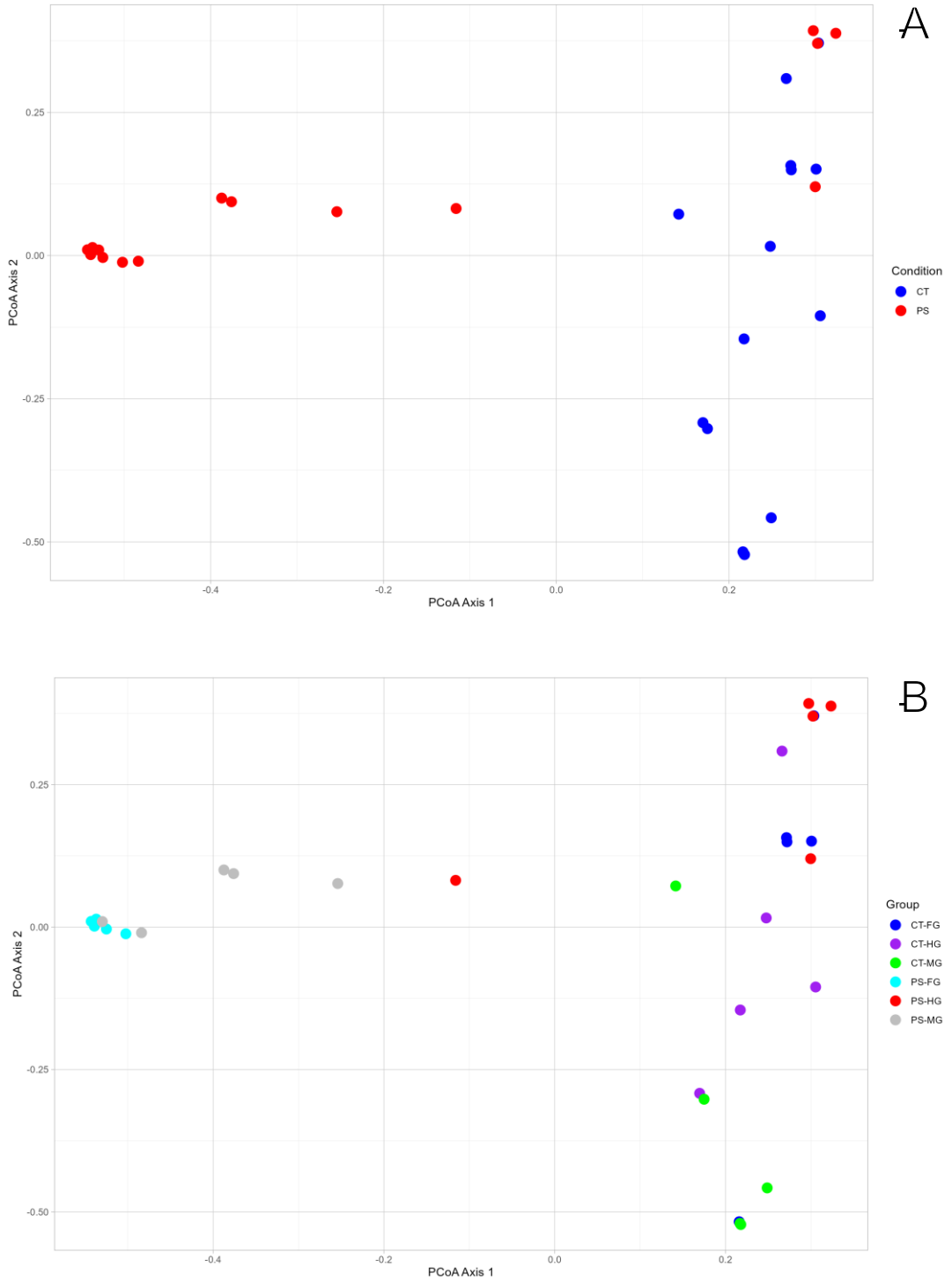

Fig. 1.12 - Principal Coordinates Analysis (PCoA) plots visualizing beta diversity among microbial communities. (A) PCoA plot illustrating the clustering of microbial communities between control (CT) and polystyrene-fed (PS) groups. (B) PCoA plot showing microbial clustering across individual groups (FG-CT, MG-CT, HG-CT, FG-PS, MG-PS, HG-PS).

Comparisons	p-value	p.adjusted
CT vs PS	**0.001**	**0.001**
FG-CT vs FG-PS	**0.012**	**0.028125**
MG-CT vs MG-PS	**0.006**	**0.028125**
HG-CT vs HG-PS	0.069	0.09375
FG-CT vs MG-CT	0.087	0.100384615384615
FG-CT vs HG-CT	0.073	0.09375
MG-CT vs HG-CT	0.075	0.09375
FG-PS vs MG-PS	0.102	0.109285714285714
FG-PS vs HG-PS	**0.008**	**0.028125**
MG-PS vs HG-PS	**0.015**	**0.028125**

Tab. 1.5 - PERMANOVA results for beta diversity comparisons between experimental groups. Both p-values and adjusted p-values (p.adjusted) are reported. Statistical significance was determined based on p.adjusted values, with a threshold of <0.05, and are highlighted in bold.

The genus distribution across samples is displayed in the taxa bar plot (Fig. 1.13). Each bar corresponds to one of the five replicates for each experimental group (FG-CT, MG-CT, HG-CT, FG-PS, MG-PS, and HG-PS), and the colored segments represent the relative abundance of identified genera.

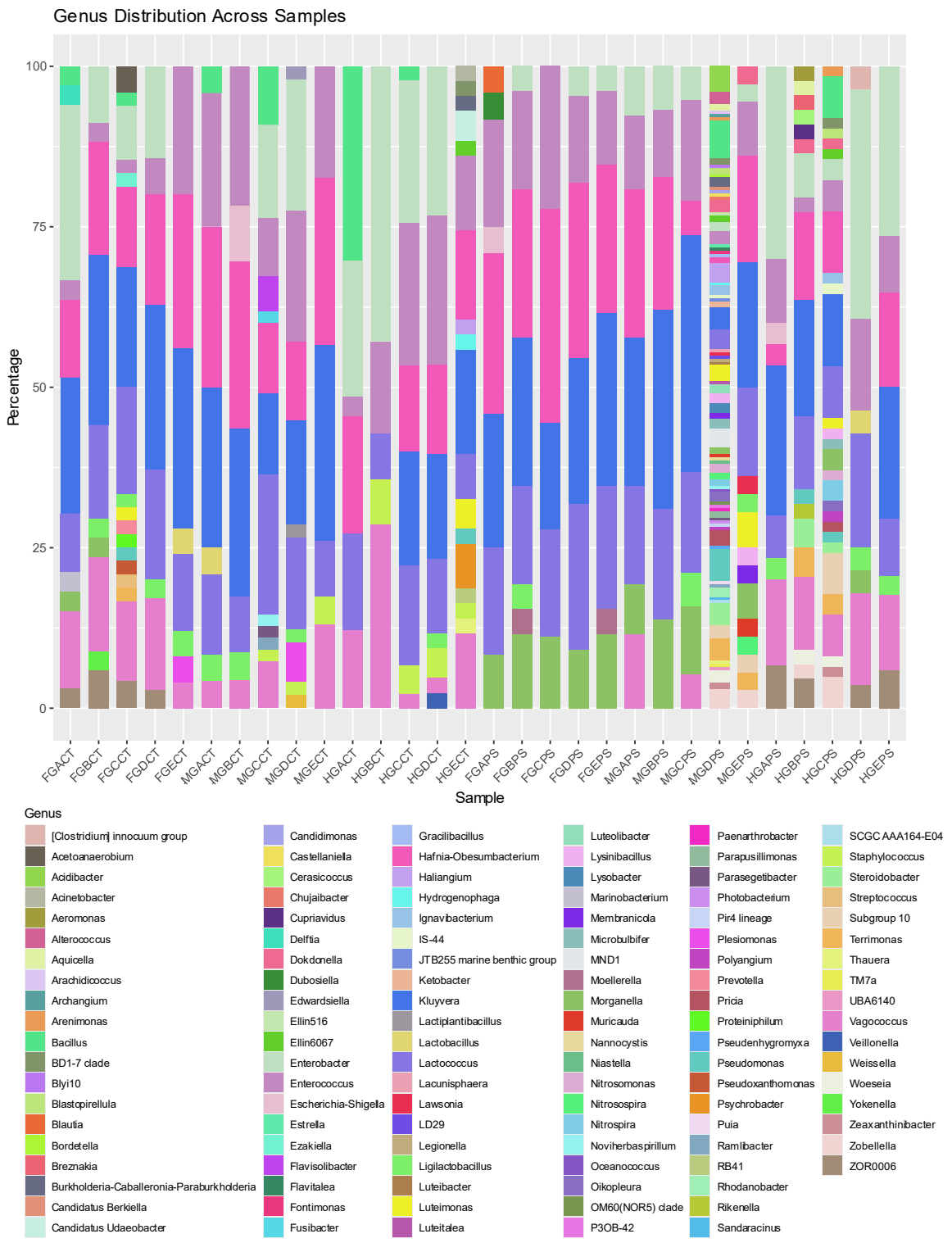

Fig. 1.13 - Taxa bar plot of genus distribution across replicates and experimental groups.

The Venn diagrams illustrate the distribution of OTUs across different gut sections within each experimental group (Fig. 1.14). The first diagram represents OTU sharing among the foregut, midgut, and hindgut in the CT group (Fig. 1.14.A), while the second diagram shows OTU distribution across the same gut sections in the PS group (Fig. 1.14.B).

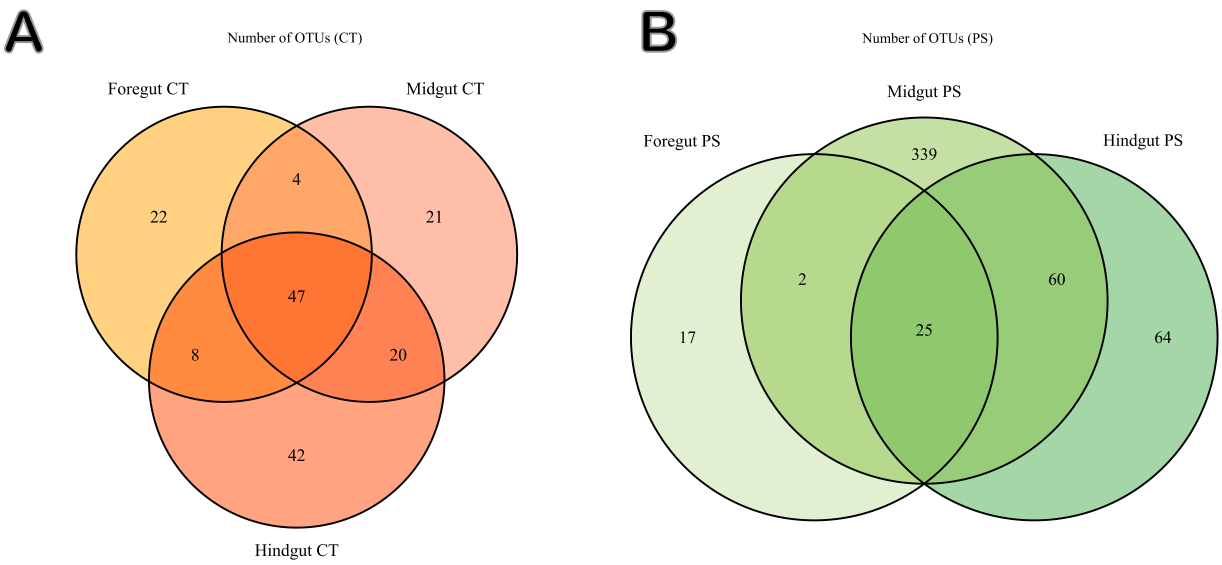

Fig. 1.14 - Venn diagrams illustrating OTU sharing among gut sections within each experimental group. (A) OTU distribution among the foregut, midgut, and hindgut in the control group (CT). (B) OTU distribution among the same gut sections in the polystyrene-fed group (PS). Numbers indicate the OTUs shared between or exclusive to each section.

To further explore the distribution of bacterial genera across gut sections, an heatmap was generated (Fig. 1.15). The heatmap visualizes the presence and relative abundance of shared and unique bacterial genera across all experimental groups (FG-CT, MG-CT, HG-CT, FG-PS, MG-PS, and HG-PS) and their respective five replicates. The dataset was filtered to genus level. Only bacterial genera were considered, clustering multiple species under the same genus, which reduced the total number of taxa compared to the original dataset.

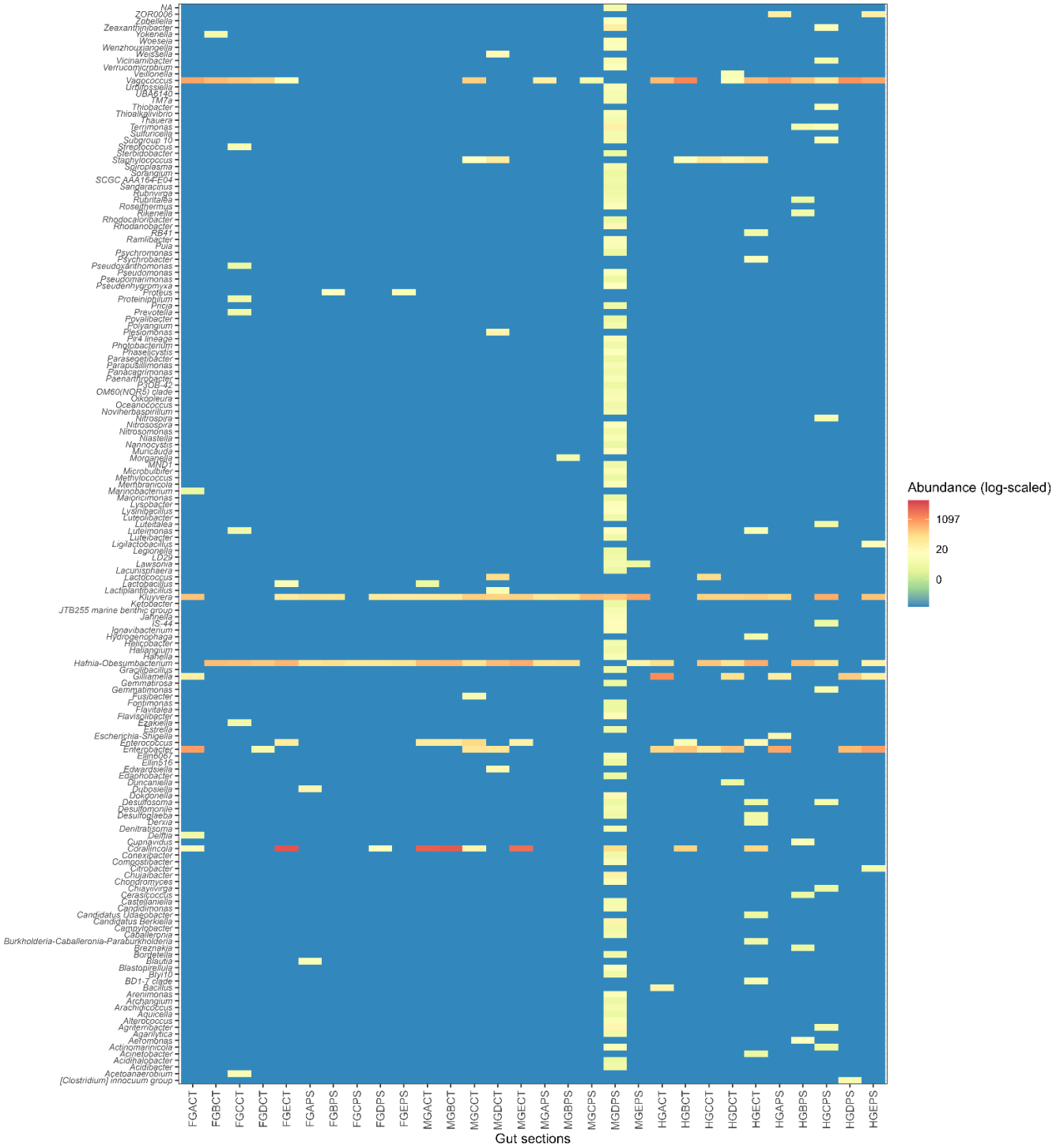

Fig. 1.15 – Heatmap illustrating the relative abundance of bacterial genera across gut sections in control (CT) and polystyrene-fed (PS) larvae. The x-axis represents the 30 individual samples (five replicates per experimental group), while the y-axis lists the identified bacterial genera. The colour gradient indicates the abundance levels of each genus within the samples.

Differential abundance analysis was conducted to identify bacterial genera significantly enriched or depleted across experimental groups. The comparisons evaluated variations in microbiota composition between the CT diet and PS diet conditions. The first comparison was focused on microbiota composition across the entire gut between CT and PS groups (Fig. 1.16). The second analysis examined microbiota differences within specific gut sections, comparing bacterial genera in the foregut (FG-CT vs. FG-PS) (Fig. 1.17.A), midgut (MG-CT vs. MG-PS) (Fig. 1.17.B), and hindgut (HG-CT vs. HG-PS) (Fig. 1.17.C). For all comparisons, only genera with adjusted p-values (p adj) < 0.05 were considered significant. The bar plots illustrate the log2 fold changes of genera between groups, with positive values indicating enrichment in the PS group and negative values representing enrichment in the CT group.

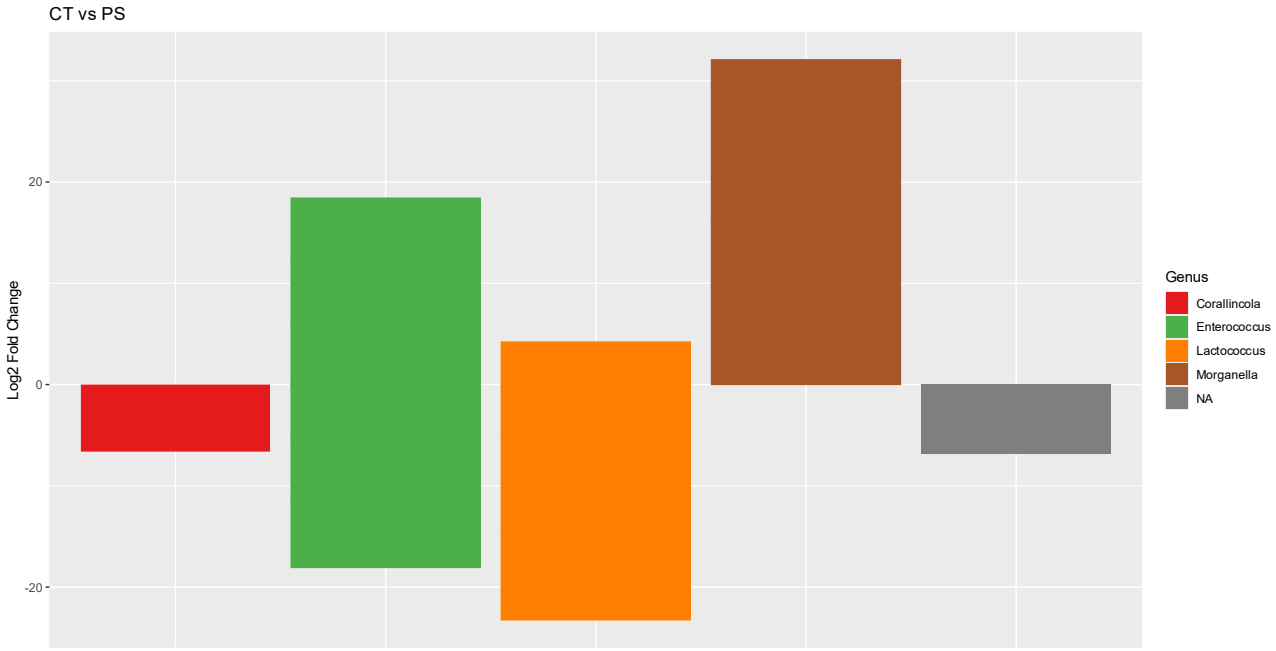

Fig. 1.16 - Bar plot representing bacterial genera differentially abundant between larvae fed with control diet (CT) and polystyrene (PS). Positive log2 fold change values indicate genera enriched in PS, while negative values indicate genera enriched in CT.

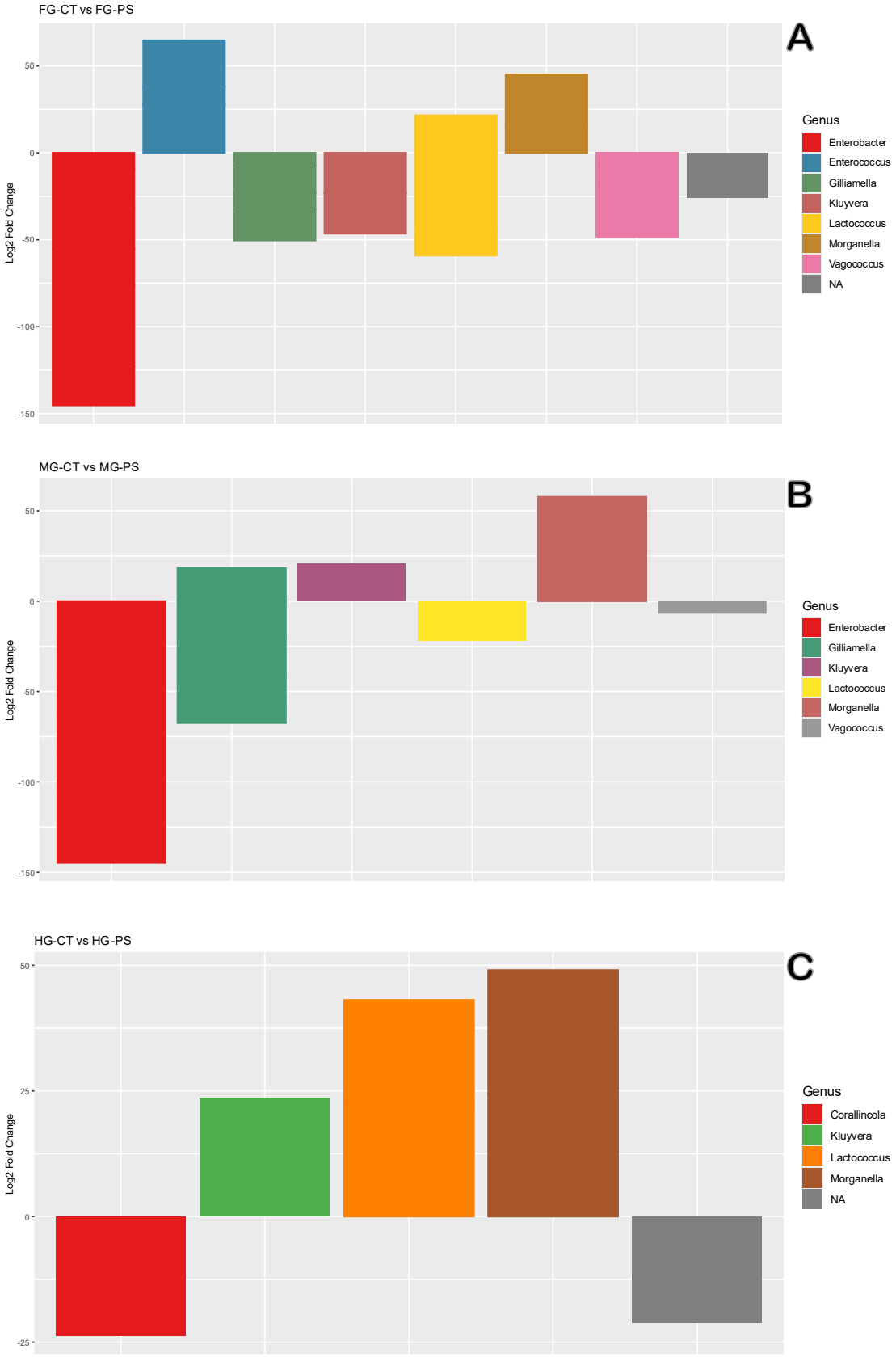

Fig. 1.17 - Bar plots representing bacterial genera differentially abundant within specific gut sections: (A) foregut (FG-CT vs. FG-PS), (B) midgut (MG-CT vs. MG-PS), and (C) hindgut (HG-CT vs. HG-PS). Positive log2 fold change values indicate genera enriched in FG-PS (A), MG-PS (B), and HG-PS (C), while negative values indicate genera enriched in FG-CT (A), MG-CT (B), and HG-CT (C).

1.4 DISCUSSION

The widespread use of plastics, combined with inadequate waste management, have contributed to plastic pollution, one of the most pressing ecological issues of the last century. The toxic effects of plastic pollution on biodiversity are well-documented, encouraging the exploration of new strategies to resolve this issue. One promising solution is biodegradation, which involves the breakdown of plastics through the combined action of plastivorous insects and their associated microbiota. In this context, *A. diaperinus* has attracted interest for its potential role in polystyrene biodegradation, as previously demonstrated in study of Cucini et al. (2020). However, expanding research is essential to enhance understanding of its degradative capabilities and to validate its role in this field. To achieve these goals, this chapter is focused on three main areas of study.

The first area of research focuses on optimizing rearing conditions, following the findings of Cucini et al. (2020), who observed high mortality rates and reduced larval weight in PS rearing systems. The results presented in Fig. 1.3 indicate that the larvae chewing and ingesting PS, whose cephalic capsules were measured, were exclusively in the last larval instar. According to the thresholds reported in Tab. 1 (Introduction), the cephalic capsule size of larvae extracted from PS exceeded the value associated with the final larval instar (VIII: 1.339 mm). To further validate these observations, larvae were transferred to secondary rearing boxes (A', B', C', D', E') after their extraction from PS. Within 15 days, 90.3% of these larvae successfully pupated and became adults, while the remaining 9.7% did not survive. This data confirms that only larvae in the last instar (VIII) exhibit a predisposition to ingest PS, likely perceiving it as a safe location for pupation and adult transition. Therefore, when designing experiments involving *A. diaperinus* in this context, it is crucial to consider the larval instar to develop effective rearing systems. These findings laid the foundation for further investigations carried out in the subsequent areas of research.

The second research line focused on chemical analyses. Micro-FTIR analyses were conducted to confirm the ingestion of PS by *A. diaperinus* and evaluate structural alterations of the polymer after passing through the larval gut. As reported in Tab. 1.2, the analyses allowed for a comparison between the original feedstock materials and frass samples, both untreated and chemically treated with two different solutions (H_2O_2 and KOH). The results highlighted partial variations across the different comparisons. Specifically, the frass from larvae fed with the CT group diet (bran and carrots) showed an average similarity of 78.37% compared to the original

feedstock (Fig. 1.4.A). In contrast, the comparisons involving frass PS (from polystyrene-fed larvae) and virgin polystyrene (Fig. 1.4.B), as well as frass PS treated with H_2O_2 (Fig. 1.4.C) and KOH (Fig. 1.4.D), showed similarity percentages of 91.61%, 87.60%, and 91.41%, respectively. These findings confirm that polystyrene is ingested by the larvae and successfully expelled, retaining approximately 90% of its original chemical structure after passing through the gut. Although partial, this slight alteration in the polymer's structure could be attributed to the action of digestive enzymes or, more likely, to the intestinal microbiota. In addition, GC-MS analyses were conducted to identify potential metabolites resulting from the degradation of polystyrene by *A. diaperinus* larvae. Two metabolites, in particular, were of significant interest: α-methylstyrene and cumyl alcohol. The chromatograms confirmed the presence of these compounds exclusively in the larvae fed with PS, while they were entirely absent in those fed with the CT diet (Fig. 1.5; Fig. 1.6). The detection of α-methylstyrene, a compound often associated with the depolymerization of PS, indicates that the larvae facilitate bond cleavage within the polymer. This observation aligns with findings in *T. molitor* reported by Tsochatzis et al. (2020), where the formation of α-methylstyrene was attributed to enzymatic or microbial activity within the gut. Similarly, the detection of cumyl alcohol, another key metabolite, suggests a gradual degradation process where oxidative or enzymatic reactions contribute to the polystyrene's transformation.

Finally, the third area of research of this study is the metabarcoding analyses, with more targeted and extensive experiments aimed at identifying microbiota variations between CT groups and PS groups under several experimental conditions. About the first metabarcoding analysis focusing on larval instars, the alpha diversity indices (Shannon and Simpson) did not reveal significant differences in microbial diversity within the entire gut across larval instars (Tab. 1.3). This was confirmed by the Kruskal–Wallis test (Shannon: p-value = 0.901; Simpson: p-value = 0.452), indicating that microbial richness and evenness remained stable throughout larval development. However, slightly higher alpha diversity values were observed in the L3-PS group, suggesting a marginally more complex microbiota under these conditions, while the lowest values were detected in the L1-CT group. The beta diversity analysis, visualized through PCoA plots, focused on microbial community differences across experimental groups and dietary conditions. In the Fig. 1.7.A, the comparison between CT and PS groups showed a partial separation of microbial community in two different clusters, suggesting a minor variation between the two dietary conditions. Although, this observation was not statistically supported by PERMANOVA. Similarly, when all experimental groups (L1-CT, L2-CT, L3-CT, and L3-PS) were compared together (Fig. 1.7.B), no clear clustering emerged based on larval

instars or diet. In fact, no statistically significant differences in microbial community composition were identified among the experimental groups based on PERMANOVA results. The taxa bar plot (Fig. 1.8), which represents microbial community composition across replicates and experimental groups, further supports these findings. The bacterial genus distribution appears relatively stable across larval instars, with a lower diversity observed in early developmental stages (L1-CT) and an increase in specific genera in the L3-PS group. This observation is also supported by the Venn diagram (Fig. 1.9). A total of 34 OTUs were shared among all groups, while the L3-PS group exhibited the highest number of unique OTUs (37), and the L1-CT group displayed only 17 unique OTUs. These findings confirm that the core microbiota remains stable among all different developmental instars and dietary conditions. Although, the polystyrene diet appears to enhance the growth of specific microbial taxa. The heatmap (Fig. 1.10) provides a more detailed visualization of bacterial abundance grouped at the genus level. Unlike OTUs, which are more specific and numerous, the genera reported here offer a general perspective of the microbial community composition. The heatmap reflects the results observed in the previous analyses, showing the presence of a core microbiota among all experimental groups, and a slight increase in bacterial abundance in the later larval instars, particularly in the L3-PS group, contrary to initial expectations. These results confirm the hypothesis that the PS diet promotes the proliferation of specific microbial taxa. Observing the heatmap, it is also possible to identify potential members of the core microbiota. These genera, in line with the 34 OTUs shared among all experimental groups as shown in the Venn diagram (Fig. 1.9), include *Corallincola, Enterobacter, Gilliamella, Kluyvera, Staphylococcus*, and *Vagococcus*. To further investigate and identify bacterial genera that are significantly more abundant in one condition compared to another, a differential abundance analysis was performed. This analysis highlights only statistically significant differences in bacterial composition. In Fig. 1.11, several comparisons were performed among all larval instars. Bacteria belonging to the genera *Enterococcus*, *Lactococcus*, and *Hafnia-Obesumbacterium* were found to be the most abundant and consistently present in the gut throughout the development of larvae in the CT group, from the early to the late instars. As also observed in the heatmap, the genus *Vagococcus* is significantly present across all experimental groups, including the PS group. Notably, in the comparison between larvae of the same instar but fed with different diets (L3-CT vs L3-PS), the bacterium *Morganella* is predominant in the PS group.

Regarding the second metabarcoding analysis focusing on gut sections, the alpha diversity indices (Shannon and Simpson) revealed clear differences among the groups analysed (Tab.

1.4). These differences were confirmed by the Kruskal-Wallis test (Shannon: p-value = 0.0053; Simpson: p-value = 0.0008), indicating a statistically significant variation in microbial richness and evenness depending on both anatomical location and diet. In the CT group, alpha diversity remained relatively constant across the three gut sections, with slightly higher values observed in the foregut (FG) (Shannon: 2.99 ± 0.61; Simpson: 0.92 ± 0.08). In contrast, the PS group showed a marked increase in diversity along the digestive tract, from the lowest values in the FG (Shannon: 1.58 ± 0.02; Simpson: 0.66 ± 0.00) to the highest in the hindgut (HG) (Shannon: 3.11 ± 0.11; Simpson: 0.94 ± 0.01). The midgut (MG) exhibits intermediate diversity values (Shannon: 2.30 ± 0.83; Simpson: 0.78 ± 0.10), with intermediate values in the midgut. These findings suggest that the effect of polystyrene on microbial diversity is spatially modulated along the gut, with a particularly enriched and complex microbiota emerging in the hindgut section. The beta diversity analysis, visualized through PCoA plots (Fig. 1.12), highlights notable differences in microbial community composition between experimental groups. The comparison between the CT and PS groups (Fig. 1.12.A) reveals a clear separation into two distinct clusters. This separation is statistically supported by the PERMANOVA analysis (Tab. 1.5), which identifies a significant difference between the CT and PS groups (p.adj = 0.001). Regarding the comparisons across all experimental groups (Fig. 1.12.B), as confirmed by PERMANOVA tests (Tab. 1.5), significant differences are observed in the FG and MG between the two dietary groups: FG-CT vs FG-PS (p.adj = 0.028) and MG-CT vs MG-PS (p.adj = 0.028). However, in the comparison of microbial composition in the HG between CT and PS groups, the PCoA plot suggests a partial separation, but this observation is not statistically supported (p.adj = 0.09). About the intragroup comparisons, no significant differences were detected among the gut sections within the CT group (p.adj > 0.05). In contrast, within the PS group, significant differences were observed, particularly between FG-PS vs HG-PS and MG-PS vs HG-PS (p.adj < 0.05), while FG-PS vs MG-PS remained non-significant (p.adj > 0.05) (Tab. 1.5). These results demonstrate that the PS diet has a significant influence on the gut microbiota composition, inducing localized changes in microbial communities, particularly in the HG section. Additionally, between the two dietary conditions, the PS diet likely promoted the development of specific microbial taxa, leading to a significant difference compared to their counterparts (FG and MG) in the CT group. The taxa bar plot (Fig. 1.13) reinforces these observations. Notably, the PS group exhibits a higher presence of microbial species compared to the CT group. This increased heterogeneity in the PS group is further supported by the Venn diagram (Fig. 1.14). Among the PS samples (Fig. 1.14.B), the MG hosts the highest number of OTUs (339), making it the most diverse section of the gut. A notable result is that in the PS

group, the core microbiota shared among all gut sections consists of only 24 OTUs, a relatively low number compared to the OTUs uniquely present in each gut section: FG-PS (17), MG-PS (339), and HG-PS (64). When compared to the Venn diagram of the CT group (Fig. 1.14.A), the differences between the two dietary conditions are further accentuated. In the CT group, the core microbiota is much larger, comprising 47 OTUs, while the unique OTUs in the individual gut sections are significantly lower: FG-CT (22), MG-CT (21), and HG-CT (42). This comparison suggests that a vegetable-based diet maintains a more uniform microbiota across the different gut sections. In contrast, the PS diet appears to induce significant microbial shifts, leading to greater heterogeneity between gut sections. This is consistent with the beta diversity results, which showed no significant differences among gut sections in the CT group, while substantial differences were observed in the PS group.

The heatmap illustrates a complete representation of bacterial distribution (genus level), not only within the same group but also between the PS and CT groups (Fig. 1.15). The core microbiota, common across all groups, is evident. Notably, some of these bacteria were also identified in the first metabarcoding analysis, confirming their role as key components of the gut microbiota in *A. diaperinus*. Among the most relevant genera are *Enterobacter*, *Kluyvera*, *Hafnia-Obesumbacterium*, *Lactococcus*, and *Vagococcus*. Of particular interest is the microbial composition observed in the midgut section of PS group, and specifically in the MGDPS sample, where several other genera were detected, such as *Arenimonas*, *Lysobacter*, and *Luteimonas*, all belonging to the Lysobacteriaceae family (Xanthomonas Group), similarly to *Stenotrophomonas* discussed in the second chapter of this study. These genera have been associated in the literature with the degradation of complex polymers (Zhang et al., 2015; Tourova et al., 2020; Gökçen et al., 2014). This observation highlights that specific gut sections may harbour microbial communities with an enhanced potential for polymer degradation. Future research could aim to establish enrichment cultures derived separately from distinct gut compartments and to apply analytical techniques such as GC-MS to detect polystyrene-derived metabolites produced during microbial degradation. However, to gain deeper insights into bacterial genera that show statistically significant differences in abundance across experimental conditions, a differential abundance analysis was carried out. In the first level of comparison between CT and PS groups (Fig. 1.16), the most significant observation is that the genus *Morganella* appears to be the most dominant in the PS group, while *Corallincola* is more prevalent in the CT group. When analysing the individual comparisons across the gut sections (Fig. 1.17), *Morganella* consistently emerges as the predominant genus in all sections of the PS group (FG, MG, and HG), while it is entirely absent in the CT group. Additionally, in the

comparisons involving the MG and HG, *Kluyvera* is also significantly more abundant in the PS samples. These findings suggest that both *Morganella* and *Kluyvera* may play crucial roles in the microbial response to PS diet.

A comparative evaluation of the two metabarcoding analyses revealed distinct patterns in the dynamics of the gut microbiota. In the first analysis, based on alpha and beta diversity metrics, no statistically significant differences were observed, suggesting that larval developmental instar has a limited impact on the overall microbial community structure. In contrast, the second analysis, focusing on gut sections, identified significant differences, indicating that anatomical compartmentalization has more influence on microbiota composition. In this context, differential abundance analyses were performed to identify bacterial taxa that consistently responded to polystyrene exposure across both experimental designs. *Morganella* and *Kluyvera* emerged as key genera enriched under PS-fed conditions. *Morganella* was found to be significantly more abundant both across different larval instars and among the gut sections, while *Kluyvera* showed a notable enrichment particularly in the midgut and hindgut of PS-fed larvae. Their presence in the gut microbiota of *A. diaperinus*, particularly in PS groups, aligns with findings reported in the literature, validating their potential roles in plastic degradation. *Morganella* was identified in both the analysis across larval instars and the analysis across gut sections. Previous studies have highlighted its significant contribution to the gut microbiota of insects exposed to polystyrene. In *Zophobas morio*, *Morganella morganii* was identified as a key component of the gut microbiota, showing a relative abundance of 12.92% in larvae fed on expanded polystyrene (EPS). Interestingly, the supplementation with microelements and vitamins further increased its prevalence, reaching 27.08% in PVC-fed larvae and 55.96% in those fed on EPS (Urbanek et al., 2024). A similar result was reached also in *Tenebrio molitor*, where the abundance of *Morganella* was found to increase when the larvae were fed polystyrene subjected to specific aging treatments, such as UV exposure combined with freezing (Ding et al., 2024). Regarding *Kluyvera*, its presence was specifically observed in the gut sections analysis, where it appeared more abundant in PS-fed larvae. In *Zophobas atratus*, *Kluyvera* has been documented as playing a significant role in plastic degradation. It was particularly abundant in larvae fed with expanded (EPS) and extruded polystyrene (XPS) compared to those fed exclusively on oatmeal (Tay et al., 2023). These findings highlight how certain bacterial genera, such as *Morganella* and *Kluyvera*, may play crucial roles in polystyrene degradation within the gut microbiota of *A. diaperinus*.

In addition to these microbial community observations, another bacterium belonging to the genus *Stenotrophomonas*, previously isolated from the gut microbiota of *A. diaperinus*, has

been associated with polystyrene degradation (Cucini et al., 2022). This isolate was later investigated to confirm its degradative capabilities, as detailed in the next chapter. However, *Stenotrophomonas* genus was not detected at statistically significant levels in the microbial community analyses conducted in this study, neither in PS-fed larvae nor in those fed a vegetable-based diet. This absence suggests that *Stenotrophomonas* may not represent a stable or dominant member of the gut microbiota of *A. diaperinus* under the experimental conditions tested, or that it was present at levels too low to be detected by metabarcoding analyses. In the first study by Cucini (2020), the *Stenotrophomonas* genus was detected in polystyrene-fed libraries but was also not statistically significant, particularly in differential abundance analysis, due to its presence in both PS and CT-fed groups (p.adj > 0.05). These observations suggest that *Stenotrophomonas* may be a transient or low abundance member of the gut microbiota of *A. diaperinus*, whose relative abundance could increase only under specific selective conditions, such as prolonged exposure to polystyrene. Supporting this hypothesis, Cucini (2022) demonstrated that a *Stenotrophomonas* strain could be isolated after a two-month enrichment culture using polystyrene as the sole carbon source. Furthermore, as will be discussed in the following chapter, a subsequent study (Zarra et al., 2025) revealed that, after one year of storage at 4°C on agar plates supplemented with polystyrene film, the same strain was able to nearly completely degrade the substrate.

Although the genus *Stenotrophomonas* was not detected through metabarcoding analyses in the present study, these findings collectively suggest that its presence, detectability, and activity within the gut microbiota are strongly influenced by specific experimental and rearing conditions. Through the application of the rearing conditions and experimental setups explored in this study, and by applying alternative culture strategies, future research may facilitate the isolation and characterization of additional bacterial taxa with metabolic capabilities relevant to polystyrene degradation.

CHAPTER 2

2.1 INTRODUCTION

The darkling beetle *Alphitobius diaperinus* has emerged as a promising model organism for investigating polystyrene (PS) biodegradation. In a first study, Cucini et al. (2020) demonstrated that larvae of *A. diaperinus* fed with PS foam exhibited significant alterations in their gut microbiota compared to a control (CT) group fed a vegetable-based diet. Metabarcoding analysis revealed important differences in microbial community composition among the two groups, suggesting that specific bacterial taxa could have a crucial role in PS digestion. A subsequent study by Cucini et al. (2022) further investigated the gut-associated bacterial communities of *A. diaperinus* larvae fed with PS by setting up an enrichment bacterial culture in a liquid carbon-free basal medium with limited chemical composition, where a PS film served as the sole carbon source. After two months of enrichment, through both culture-dependent and molecular analyses, three bacterial genera were identified: *Klebsiella*, *Pseudomonas*, and *Stenotrophomonas* (Cucini et al., 2022). Notably, bacterial isolates of each taxon demonstrated the ability to adhere to PS films and increase in viable cell numbers when cultured in a synthetic medium with PS, but statistical significance was reached only by the *Stenotrophomonas* sp. isolate. After a prolonged incubation period (1 year), this strain showed its degradative capabilities, producing a visible PS deterioration (Fig. 2.1).

This chapter focuses on the degradation potential of this bacterium, here identified as *Stenotrophomonas indicatrix* strain DAI2m/c. Through comprehensive genomic analysis, this study investigates the strain's genetic arsenal for styrene biodegradation, with particular attention to enzyme-encoding genes involved in intracellular metabolic pathways. In addition, a detailed phylogenetic analysis was performed to accurately classify the bacterial strain and explore its evolutionary relationships with related taxa.

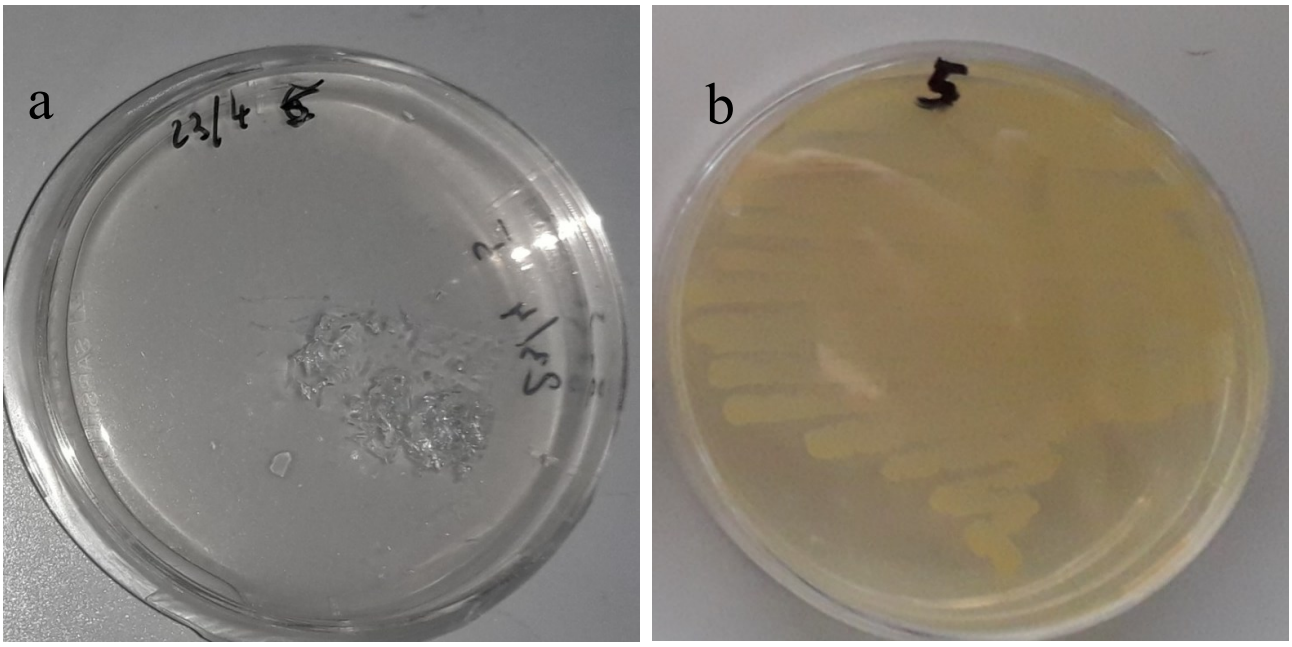

Fig. 2.1 - PS film degradation and bacterial growth on agar plates. a) PS film appearance on Liquid Carbon-Free Basal medium (LCFB) agar plates after 1 year storage at 4°C. A PS film (10 mm×10 mm; ~ 9–10 mg) was transferred from 28 days-old *Stenotrophomonas* sp. culture in LCFB at the conclusion of the experiments reported by Cucini et al. (2022). b) Growth on LB agar plate after 48 h at 27 °C of the sample collected by rubbing PS film remains with a sterile cotton swab.

2.2 MATERIALS AND METHODS

2.2.1 Bacterial strain isolation and culturing conditions

Routine bacterial cultures were maintained in Luria-Bertani (LB) broth (1% Bacto tryptone, 0.5% yeast extract, 0.5% NaCl, distilled water, pH 7.2) and LB agar (LB added with 1.5% agar) unless stated otherwise. The bacterial strain analysed in this study was originally isolated after an enrichment phase in a medium with limited chemical composition and PS as sole carbon source from PS-fed larvae of *A. diaperinus.* Based on the partial sequence of the 16S rDNA gene (474 bp), the bacterium was initially reported as *Stenotrophomona*s sp. 2m/c (Cucini et., 2022). A fortuitous observation revealed partial degradation of a PS film colonized by *Stenotrophomonas* sp. 2m/c (~9.0×10^5 attached cells) after one year of storage (Fig. 2.1.A). To recover the bacterial population, a sterile cotton swab was carefully rubbed over the entire surface of PS film remains and used to streak a LB agar plate. The resulting yellow pigmented growth (Fig. 2.1.B) likely indicated a pure culture of *Stenotrophomona*s sp. 2m/c. Yellow pigmentation was one of the characteristics previously reported for the colony morphotype shown by DAI2m/c on LB agar. In addition, phenotypic tests confirmed its classification as an aerobic/facultative anaerobic, non-glucose fermenting, non-lactose fermenting, and oxidase-negative bacterium (Cucini et al., 2022). To determine the full-length 16S rDNA sequence, a single colony *Stenotrophomona*s sp. strain 2m/c was suspended in 50 µl of sterile double-distilled water and incubated at 100°C for 5 minutes. The 16S rDNA gene was amplified using universal eubacterial primers and sequenced using the Sanger method on both strands at BMR Genomics (Padua, Italy) (Tang et al., 2006). Sequence data were analyzed via BLAST (Altschul et al., 1990), and the updated 1,497 bp sequence was deposited in the DDB/EMBL/GenBank database under the accession number OL470964.2. To further confirm its taxonomic position, the isolate was cultured on VIA (Vancomycin Imipenem Amphotericin B) selective agar medium, commonly used for the identification of *Stenotrophomonas* spp. (Kerr et al., 1996). Growth characteristics were recorded after 48 hours of incubation at 27°C.

2.2.2 Genomic DNA extraction and sequencing

Genomic DNA was extracted using the Wizard® SV Genomic DNA Purification System (Promega Corporation, Madison, WI, USA) following the manufacturer's instructions. DNA concentration was measured using a Qubit 4.0 Fluorometer (Invitrogen Ltd., Thermo Fisher Scientific, Singapore) with the Qubit 1X dsDNA HS Assay Kit (Invitrogen Ltd., Thermo Fisher

Scientific, Eugene, Oregon, USA). DNA quality was evaluated through Thermo Scientific™ NanoDrop™ One/OneC Microvolume UV-Vis Spectrophotometer (NanoDrop Technologies, Madison, WI, USA) and 1% agarose gel electrophoresis. The extracted DNA was used for whole-genome sequencing via both Illumina short-read and Oxford Nanopore Technology (ONT) long-read platforms. Illumina short-read and Oxford Nanopore Technology (ONT) long-read sequencing were performed at IGATech (Udine, Italy). For short-read sequencing, DNA libraries were prepared using Celero™ DNA-Seq kit (NuGEN, San Carlos, CA) following the manufacturer's instructions. Library quantification was conducted with a Qubit 2.0 Fluorometer (Invitrogen, Carlsbad, CA), and quality assessment was performed using an Agilent 2100 Bioanalyzer High Sensitivity DNA assay (Agilent technologies, Santa Clara, CA). DNA libraries were sequenced on a NovaSeq6000 (Illumina, Inc) in paired-end 150 bp mode. For long-read sequencing, DNA libraries were generated using the SQK-LSK114 ligation kit and sequenced on a PromethION (Oxford Nanopore) platform with a FLO-PRO114M flow cell.

2.2.3 Genome assembly and annotation

Illumina raw reads were processed for base calling, demultiplexing, and adapter masking using Illumina BCL Convert v3.9.3. Read trimming was conducted using fastp v.0.23.2 (Chen et al., 2018) under default settings. ONT reads were filtered with Filtlong v.0.2.1 (keep_percent parameter: 90%; available at: https://github.com/rrwick/Filtlong). Filtered ONT reads were employed for a *de novo* genome assembly using Flye v.2.8.1 (Kolmogorov et al., 2019) with 5 iterations and plasmid assembly rescue option. The draft genome was then reoriented to the dnaA gene using Circlator v.1.5.5 (Hunt et al., 2015). Genome polishing was performed through three iterations of Pilon v.1.24 (Walker et al., 2014), using BWA as mapper (Li & Durbin, 2009). General assembly statistics were calculated using stats.sh (available in the BBtools suite - DOE Joint Genome Institute. BBTools.), while a graphical genome representation was generated with GenoVi (Cumsille et al., 2023). Assembly completeness was assessed via BUSCO v.5.4.4 against the closest available *Xanthomonadales_odb10* database (Waterhouse et al., 2018). Annotation was conducted using the NCBI Prokaryotic Genome Annotation Pipeline (PGAP) v.2024-07-18 (Tatusova et al., 2016) and eggNOG v.5.0 (Huerta-Cepas et al., 2019). Additionally, prophage sequences were identified using the PHASTEST (PHAge Search Tool with Enhanced Sequence Translation) web server (Wishart et al., 2023), and extrachromosomal origin of replication (oriV) was detected with Ori-Finder (Gao & Zhang, 2008). BLAST algorithm (Altschul et al., 1990) was applied in order to align genome annotations with a

bacteriophage Lambda synthetic construct (KY609225) comprising the SRRz lysis gene cassette from bacteriophage Lambda that encodes holin (S, essD or ybcR), endolysin (R or ybcS), and endopeptidase (Rz or ybcT) (Campbell, 1994).

2.2.4 Identification of styrene degradation pathways

The set of orthologous enzymes associated with the canonical styrene degradation pathway (KEGG entry: map00643) was obtained from the Kyoto Encyclopedia of Genes and Genomes (KEGG) pathway database. Initially, genes annotated with a corresponding EC number in the *Stenotrophomonas* sp. 2m/c eggNOG functional dataset were extracted. A subsequent manual curation process was conducted for each enzyme in the KEGG styrene degradation pathway to validate in silico annotations and identify additional potential orthologs among non-annotated enzymes based on the presence of specific Pfam domains. Specifically, EC numbers linked to styrene degradation were cross-referenced with the UniProtKB/Swiss-Prot database, filtering results for the kingdom Bacteria and the associated Pfam domains were retrieved (Tab. 2.1). Each Pfam profile was independently pressed (hmmpress) and scanned (hmmscan) against the translated coding sequences (CDS) of *S. indicatrix* using HMMER v.3.3.2 (Eddy, 2011) with an E-value threshold of 1e-05. To gain further insights into the biological processes involved in styrene degradation and to enhance the KEGG pathway map, the same analytical approach was applied using the EAWAG Biocatalysis/Biodegradation Database (BBD) Styrene Pathway Map (Gao et al., 2010), which was originally characterized in *Rhodococcus rhodochrous* NCIMB 13259 (Warhurst et al., 1994). This integration provided a more detailed representation of the styrene degradation pathway. In parallel, a comparative genome analysis between *Stenotrophomona*s sp. 2m/c and the reference genome of *Stenotrophomonas indicatrix* (strain DAIF1, NCBI accession number: CP037883.1) (Friedrich et al., 2021) was performed using BLAST Ring Image Generator (BRIG) v.0.95 (Alikhan et al., 2011), focusing on genomic identity and genes encoding styrene-degrading enzymes.

2.2.5 Phylogenetic analysis

A total of 274 *Xanthomonadales* (also known as Lysobacteriales) RefSeq reference genomes available in the NCBI-Genome database (as of March 2024) were retrieved for phylogenetic comparison. Completeness analysis was assessed via BUSCO v.5.4.4 using the lineage *xanthomonadales_odb10* as a reference. Single-copy orthologs (scOGs; n = 1,157) from all

genomes were extracted and individually aligned with mafft v. 7.475 using the --auto parameter (Katoh &Toh, 2008). Alignments were trimmed via trimAl (Capella-Gutiérrez et al., 2009) (--automated1) and combined in a single super-matrix with catsequences (available at: https://github.com/ChrisCreevey/catsequences). A phylogenetic tree was constructed with IQ-TREE2 v.2.2.0 (Minh et al., 2020) (-B 2000 -m MFP) and visualized using the *ggtree* library v3.12.0 in the R environment (Yu et al., 2017).

2.2.6 Data availability

Code and protocols have been provided within the article and on the following link: https://github.com/ESZlab/Stenotrophomonas_indicatrix_WGS. In this repository are contained codes for genome assembly and annotation. Raw read data was uploaded to SRA: SRR29926346, SRR29926347 under the BioProject PRJNA1139115. *Stenotrophomonas indicatrix* genome was submitted to GenBank using the following accession number: CP168152.1, CP168153.1.

Pfam profiles			
Styrene degradation pathway	**Enzyme Commision (E.C.) number**	**Pfam entry**	**Protein family relative to Pfam entry**
Pathway A	1.14.14.11	PF17885	Styrene monooxygenase A putative substrate binding domain
	* 5.3.99.7	\	No Pfam available
	1.2.1.39	**PF00171**	**Aldehyde dehydrogenase family**
	* 1.14.14.54	\	No Pfam available
	1.14.13.-	**PF08028**	**Acyl-CoA dehydrogenase, C-terminal domain**
		PF02770	**Acyl-CoA dehydrogenase, middle domain**
		PF02771	**Acyl-CoA dehydrogenase, N-terminal domain**
		PF00296	**Luciferase-like monooxygenase**
		PF07883	**Cupin domain**
		PF01494	**FAD binding domain**
		PF00970	**Oxidoreductase FAD-binding domain**
		PF00111	**2Fe-2S iron-sulfur cluster binding domain**
		PF00037	**4Fe-4S binding domain**
		PF01613	**Flavin reductase like domain**
		PF00743	**Flavin-binding monooxygenase-like**
		PF14518	Iron-containing redox enzyme
		PF03241	4-hydroxyphenylacetate 3-hydroxylase C terminal
		PF11794	4-hydroxyphenylacetate 3-hydroxylase N terminal
		PF19298	3-Ketosteroid 9alpha-hydroxylase C-terminal domain
		PF19301	LigXa C-terminal domain like
		PF05834	**Lycopene cyclase protein**
		PF13434	**L-lysine 6-monooxygenase/L-ornithine 5-monooxygenase**
		PF02964	Methane monooxygenase, hydrolase gamma chain
		PF02406	MmoB/DmpM family
		PF00175	**Oxidoreductase NAD-binding domain**
		PF13450	**NAD(P)-binding Rossmann-like domain**
		PF13454	**FAD-NAD(P)-binding**
		PF03460	Nitrite/Sulfite reductase ferredoxin-like half domain
		PF01936	**NYN domain**
		PF00067	Cytochrome P450
		PF05138	Phenylacetic acid catabolic protein
		PF02332	Methane/Phenol/Toluene Hydroxylase
		PF04663	Phenol hydroxylase conserved region
		PF07976	Phenol hydroxylase, C-terminal dimerisation domain
		PF07992	**Pyridine nucleotide-disulphide oxidoreductase**
		PF14759	Reductase C-terminal
		PF00355	**Rieske [2Fe-2S] domain**
		PF00848	Ring hydroxylating alpha subunit (catalytic domain)
		PF02915	**Rubrerythrin**
		PF13577	**SnoaL-like domain**
		PF06234	Toluene-4-monooxygenase system protein B (TmoB)
		PF19112	Vanillate O-demethylase oxygenase C-terminal domain
		PF09722	Antitoxin Xre/MbcA/ParS C-terminal toxin-binding domain
		PF04945	YHS domain
	1.13.11.5	**PF04209**	**Homogentisate 1,2-dioxygenase C-terminal**
		PF20510	**Homogentisate 1,2-dioxygenase N-terminal**
	5.2.1.2	**PF02798** **PF13410** **PF13417** **PF14497**	**Glutathione S-transferase, N-terminal domain** **Glutathione S-transferase, C-terminal domain** **Glutathione S-transferase, N-terminal domain** **Glutathione S-transferase, C-terminal domain**
	** 3.7.1.2	\	no pfam available

Pathway B	1.14.12.-	PF11723	Homotrimeric ring hydroxylase
		PF00970	**Oxidoreductase FAD-binding domain**
		PF00111	**2Fe-2S iron-sulfur cluster binding domain**
		PF00042	Globin
		PF19301	LigXa C-terminal domain like
		PF00175	**Oxidoreductase NAD-binding domain**
		PF00355	**Rieske [2Fe-2S] domain**
		PF00848	Ring hydroxylating alpha subunit (catalytic domain)
		PF00866	Ring hydroxylating beta subunit
		PF13577	**SnoaL-like domain**
	1.3.1.19	**PF00106**	**short chain dehydrogenase**
	1.13.11.2	**PF00930**	**Dipeptidyl peptidase IV (DPP IV) N-terminal region**
	3.7.1.9	**PF00561**	**alpha/beta hydrolase fold**
Pathway B1	2.8.3.12	**PF01144**	**Coenzyme A transferase**
	4.2.1.54	**PF06050**	**2-hydroxyglutaryl-CoA dehydratase, D-component**
	2.8.3.1	**PF01144**	**Coenzyme A transferase**
		PF02515	**CoA-transferase family III**
		PF02550	**Acetyl-CoA hydrolase/transferase N-terminal domain**
		PF04223	**Citrate lyase, alpha subunit (CitF)**
		PF13336	**Acetyl-CoA hydrolase/transferase C-terminal domain**
Pathway B2	4.2.1.80	**PF01557**	**Fumarylacetoacetate (FAA) hydrolase family**
	4.1.3.39	**PF00682**	**HMGL-like**
		PF03328	**HpcH/HpaI aldolase/citrate lyase family**
		PF07836	DmpG-like communication domain

Tab. 2.1 - Pfam profiles (kingdom Bacteria) in the UniProtKB/Swiss-Prot database corresponding to enzymes involved in the styrene degradation pathway. Pfam profiles identified in the genome of *Stenotrophomonas indicatrix* are labelled in bold font. Pfam profiles not found in the genome of *S. indicatrix* are indicated with grey boxes. * indicates enzymes with no associated Pfam profile in the UniProtKB/Swiss-Prot database. ** indicates enzymes identified through functional annotation (eggNOG) with no associated Pfam profile in the UniProtKB/Swiss-Prot database.

2.3 RESULTS

2.3.1 Genome features

The nearly complete sequence of the *Stenotrophomonas* sp. 2m/c 16S rDNA gene (1,497 bp), obtained through Sanger sequencing and further validated via whole-genome sequencing, exhibited 100% identity with *Stenotrophomonas indicatrix* strain DAIF1 (CP037883.1) (Friedrich et al., 2021). Based on this result, the strain under study is hereafter referred to as *Stenotrophomonas indicatrix* strain DAI2m/c. To further support its taxonomic classification, the selective VIA agar medium was used with *S. indicatrix* strain DAI2m/c (Fig. 2.2). The development of dark green colonies after 48 hours of incubation at 27°C aligns with phenotypic and phylogenetic analyses, which classified it within the designated taxon (Cucini et al., 2022).

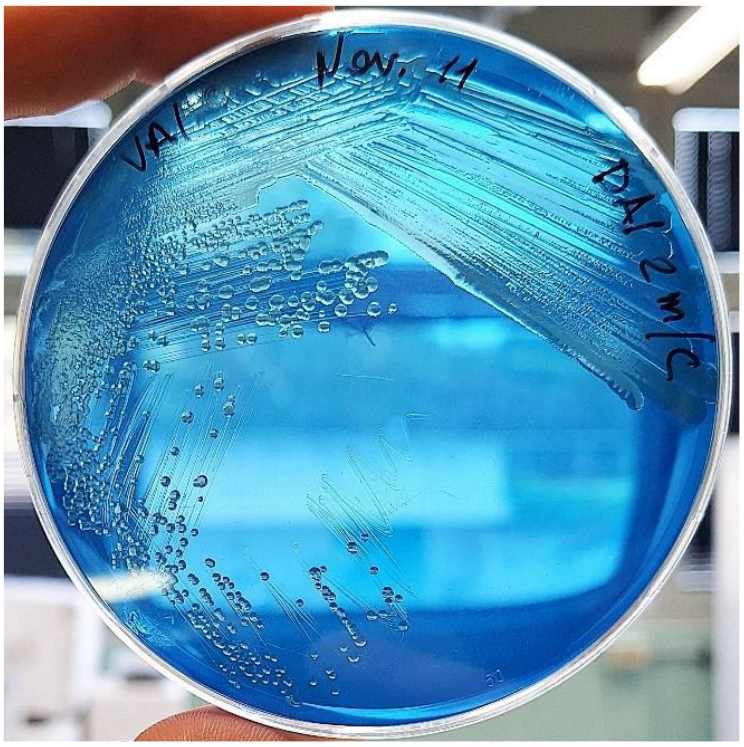

Fig. 2.2 - Growth of *Stenotrophomonas indicatrix* strain DAI2m/c on VIA selective agar. After 48 hours of incubation at 27°C, the strain developed dark green colonies.

Illumina DNA sequencing produced a total of 9.57 million read pairs, while ONT long-read sequencing generated 354.5 thousand reads, both corresponding to a coverage of 100% reads coverage. The genome assembly resulted in a single circular chromosome of 4,651,465 bp with

a GC content of 65.76%, alongside a plasmid of 7,081 bp exhibiting a GC content of 43.39% (Fig. 2.3, Tab. 2.2).

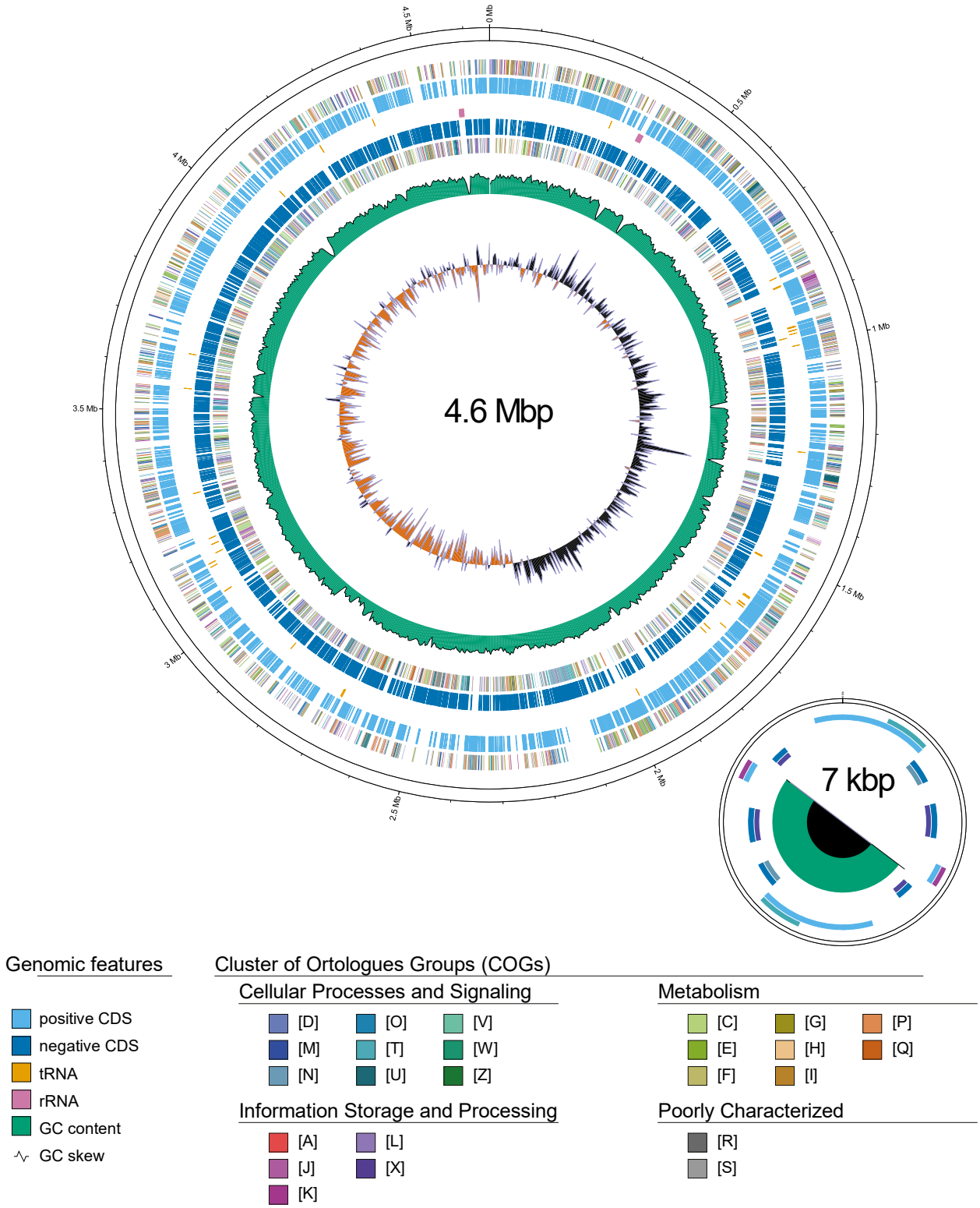

Fig. 2.3 - Circular representation of the chromosome and plasmid of *Stenotrophomonas indicatrix* strain DAI2m/c, including gene and functional regions (outer circles). GC content and skew values are displayed in the two innermost circles.

Features	Chromosome	Plasmide-like DNA
Number of circular contigs	2	
Coverage	100%	
N50/L50 (Mb)	4.651/4.651	
Single complete BUSCO	99.7%	
Single duplicated BUSCO	0.2%	
Fragmented BUSCO	0%	
Missing BUSCO	0.1%	
Total size (bp)	4,651,465	7,081
GC content	65.75%	43.39%
Genes (total)	4,245	14
CDSs (total)	4,158	14
Genes (coding)	4,123	14
CDSs (with protein)	4,123	14
Genes (RNA)	87	-
rRNAs	5, 4, 4 (5S, 16S, 23S)	-
Complete rRNAs	5, 4, 4 (5S, 16S, 23S)	-
tRNAs	70	-
ncRNAs	4	-
Pseudo Genes (total)	35	2
CDSs (without protein)	35	2
Pseudo Genes (ambiguous residues)	0 of 35	0 of 2
Pseudo Genes (frameshifted)	17 of 35	0 of 2
Pseudo Genes (incomplete)	20 of 35	0 of 2
Pseudo Genes (internal stop)	6 of 35	2
Pseudo Genes (multiple problems)	6 of 35	-

Tab. 2.2 - Genomic features of *Stenotrophomonas indicatrix* strain DAI2m/c.

The BUSCO statistics indicated a high level of completeness (99.7%), with a small fraction of duplication (0.2%) and missingness (0.1%), while no fragmentation was reported. PHASTEST analysis detected phage-related gene sequences in approximately 98% of the total length of the extrachromosomal DNA (Fig. 2.4). At the annotation level, homologous sequences were identified between the chromosome of *S. indicatrix* DAI2m/c and several phage-related genes, including holin S (pgaptmp_000287) and endolysin R (pgaptmp_000368, pgaptmp_000540, pgaptmp_001024, pgaptmp_001183, pgaptmp_001870, pgaptmp_002081, pgaptmp 002083, pgaptmp_002084, pgaptmp 002088, pgaptmp_002916, pgaptmp_003288). Additionally, the plasmid harboured sequences sharing identity with endolysin R (pgaptmp_004233, pgaptmp_004240) and endopeptidase Rz (pgaptmp_004241, pgaptmp_004234), along with two partially complete sequences homologous to holin S (pgaptmp_004232, pgaptmp_004239).

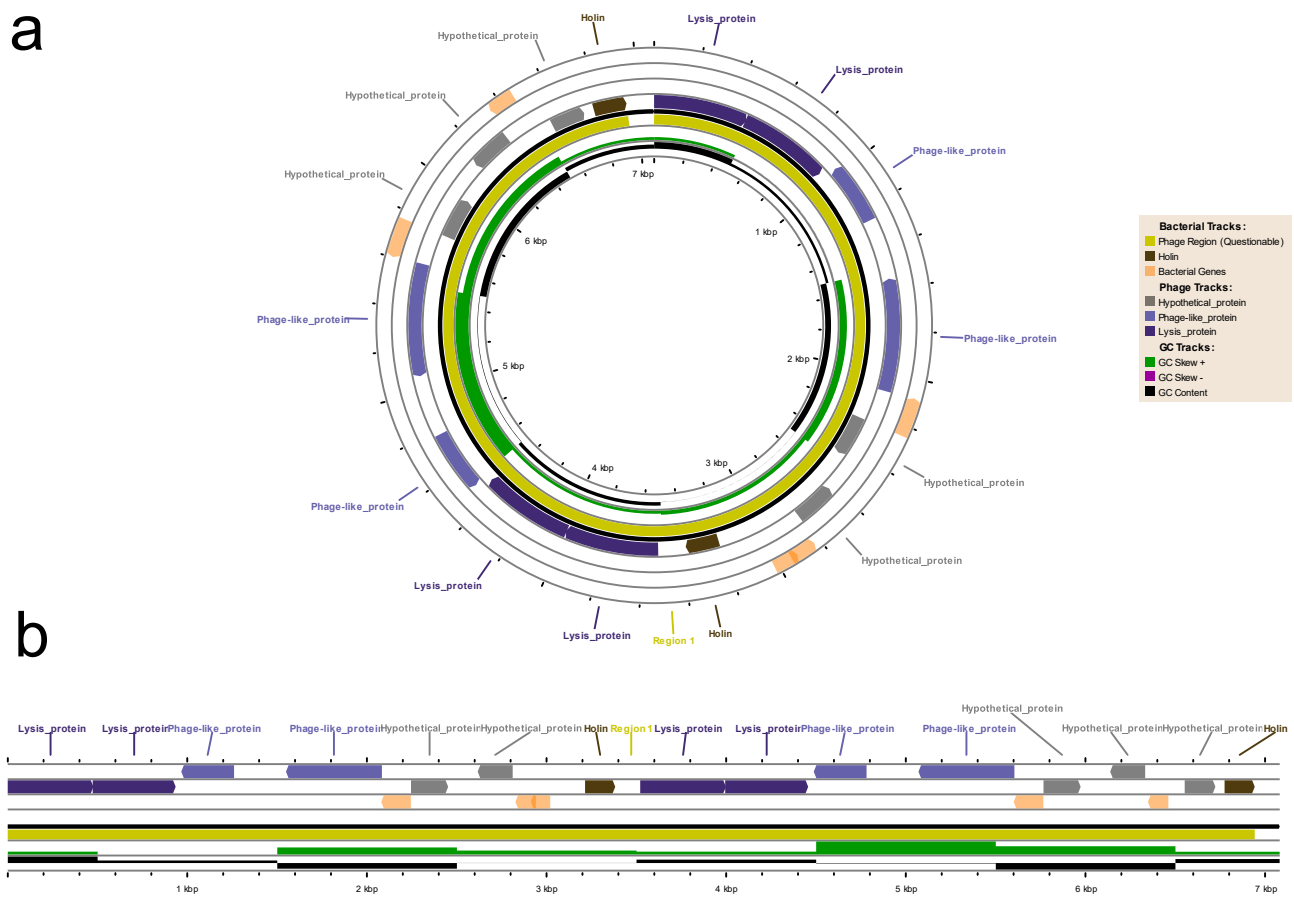

Fig. 2.4 - Prophage region in the plasmid of *Stenotrophomonas indicatrix* strain DAI2m/c spanning 6942 bp (start: 1, stop: 6943), identified through analysis with PHASTEST. The annotations include 15 phage-related proteins involved in lysis or envelope functions, as well as 5 hypothetical proteins. a) Circular representation of the plasmid. b) Linear representation of the plasmid.

2.3.2 Styrene degradation pathway

The identification of orthologous genes in the *S. indicatrix* DAI2m/c genome, based on eggNOG annotations, revealed the presence of five genes encoding enzymes involved in the styrene degradation pathway (Fig. 2.5.a): phenylacetaldehyde dehydrogenase [EC:1.2.1.39], homogentisate 1,2-dioxygenase [EC:1.13.11.5], maleylacetoacetate isomerase [EC:5.2.1.2], fumarylacetoacetase [EC:3.7.1.2], and 2-oxopent-4-enoate hydratase [EC:4.2.1.80]. Additionally, manual curation based on Pfam domain analysis identified six additional enzymes within the *S. indicatrix* DAI2m/c genome that exhibit domain compositions characteristic of styrene degradation-associated enzymes (Fig. 2.5.b): cis-1,2-dihydrobenzene-1,2-diol dehydrogenase [EC:1.3.1.19], catechol 2,3-dioxygenase [EC:1.13.11.2], 2-hydroxymuconate-semialdehyde hydrolase [EC:3.7.1.9], glutaconate CoA-transferase, subunit A [EC:2.8.3.12], lactoyl-CoA dehydratase subunit alpha [EC:4.2.1.54], and propionate CoA-transferase [EC:2.8.3.1]. However, during the manual annotation process, certain enzymes were found to be associated with multiple Pfam domains, including two oxidoreductases with incomplete classification [EC:1.14.12.-; EC:1.14.13.-] and 4-hydroxy-2-oxovalerate aldolase [EC:4.1.3.39] (Fig. 2.5.b). The search for these domains within the *S. indicatrix* DAI2m/c genome revealed only partial orthologous correspondence, identifying 5 out of 10, 21 out of 40, and 2 out of 3 domains, respectively. Although it was not possible to definitively associate these genetic elements with *S. indicatrix* DAI2m/c orthologs, a substantial number of Pfam domains were identified, suggesting that these functions might be encoded within its genome. The complete list of Pfam profiles is reported in Tab. 2.1. Conversely, styrene monooxygenase [EC:1.14.14.11], styrene-oxide isomerase [EC:5.3.99.7], and phenylacetate 2-hydroxylase [EC:1.14.14.54] were not detected, either in the automatic eggNOG annotation or through manual Pfam domain inspection.

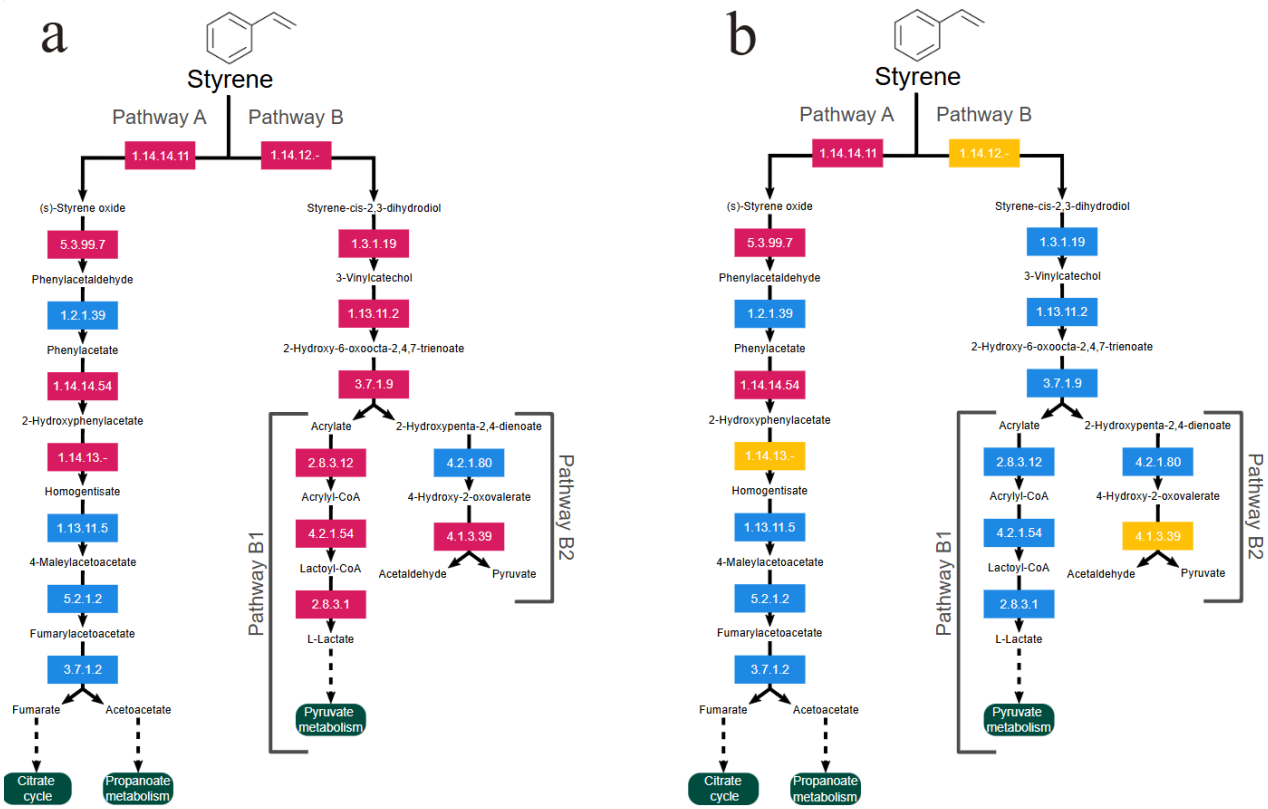

Fig. 2.5 - Representation of the styrene degradation pathway in *Stenotrophomonas indicatrix* strain DAI2m/c following the original map00634 available in the KEGG database and the Styrene Pathway Map present in BBD. a) The styrene degradation map obtained through automatic functional annotation by assigning orthologous groups via eggNOG; b) The styrene degradation map derived from manual functional annotation using Pfam domains. In both automatic and manual annotations, the presence and absence of styrene map-related enzymes are represented by blue and pink boxes, respectively. In the manual annotation, yellow boxes indicate the enzymes with partial retrieval of Pfam profiles.

All findings are consolidated in a single figure that integrates both automatic and manual annotations, providing a detailed overview of enzyme presence/absence and their specific identities (Fig. 2.6).

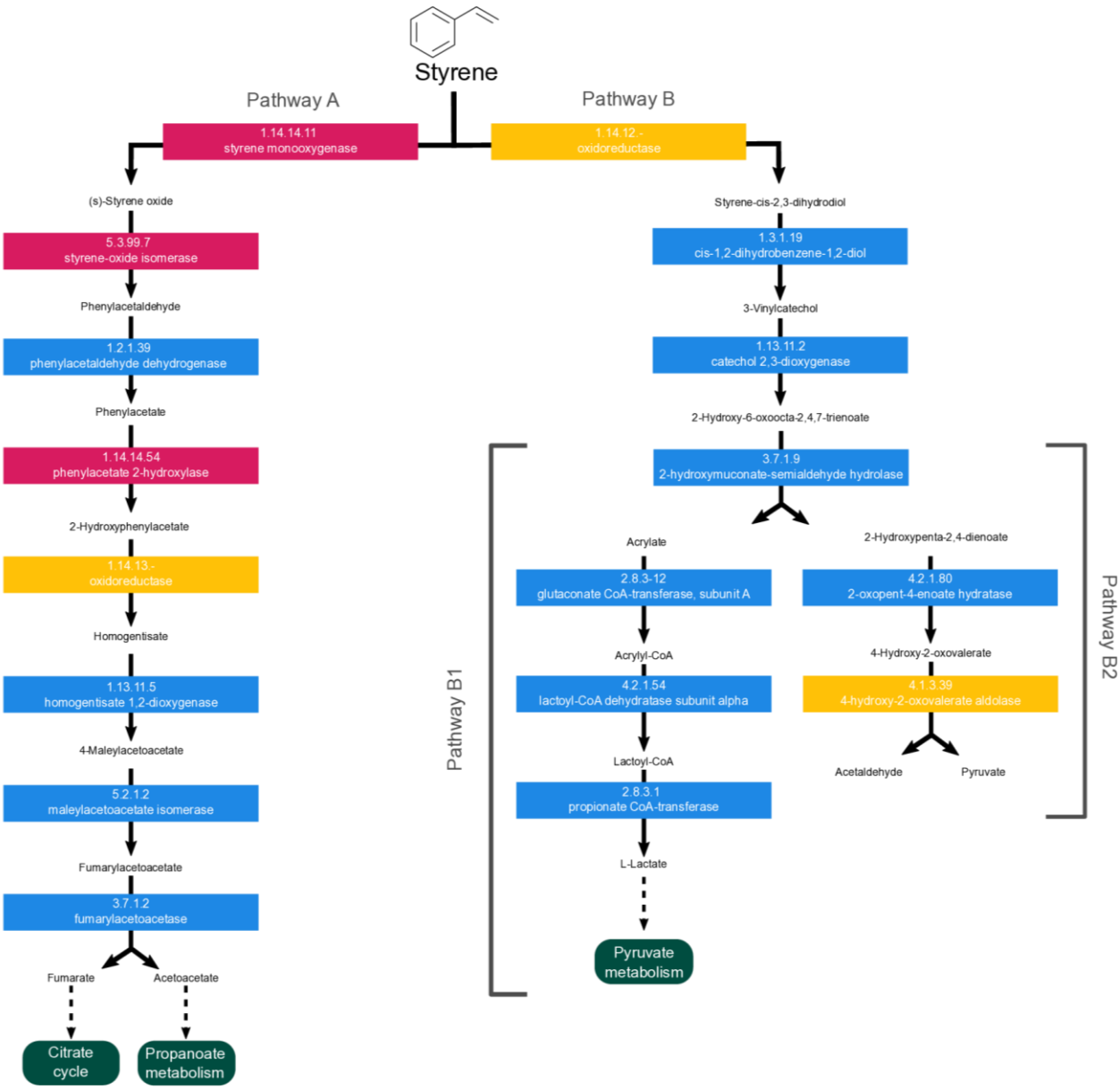

Fig. 2.6 - Representation of the styrene degradation pathway in *Stenotrophomonas indicatrix* strain DAI2m/c following the original map00634 available in the Kyoto Encyclopedia of Genes and Genomes (KEGG) pathway database, and the Styrene Pathway Map presents in the EAWAG Biocatalysis/Biodegradation Database (BBD). This styrene map reports the integration of automatic and manual annotations. The presence and absence of styrene map-related enzymes are represented by blue and pink boxes, respectively. The enzymes with partial retrieval of Pfam profiles are indicated by yellow boxes.

A comparative genomic analysis conducted using BRIG, with *S. indicatrix* strain DAIF1 as a reference, confirmed the presence of the same enzyme-encoding genes for the styrene degradation pathway in both strains. The genes identified in *S. indicatrix* DAI2m/c exhibited a

sequence identity ranging from 91% to 98% when compared to those of *S. indicatrix* DAIF1 (Fig. 2.7).

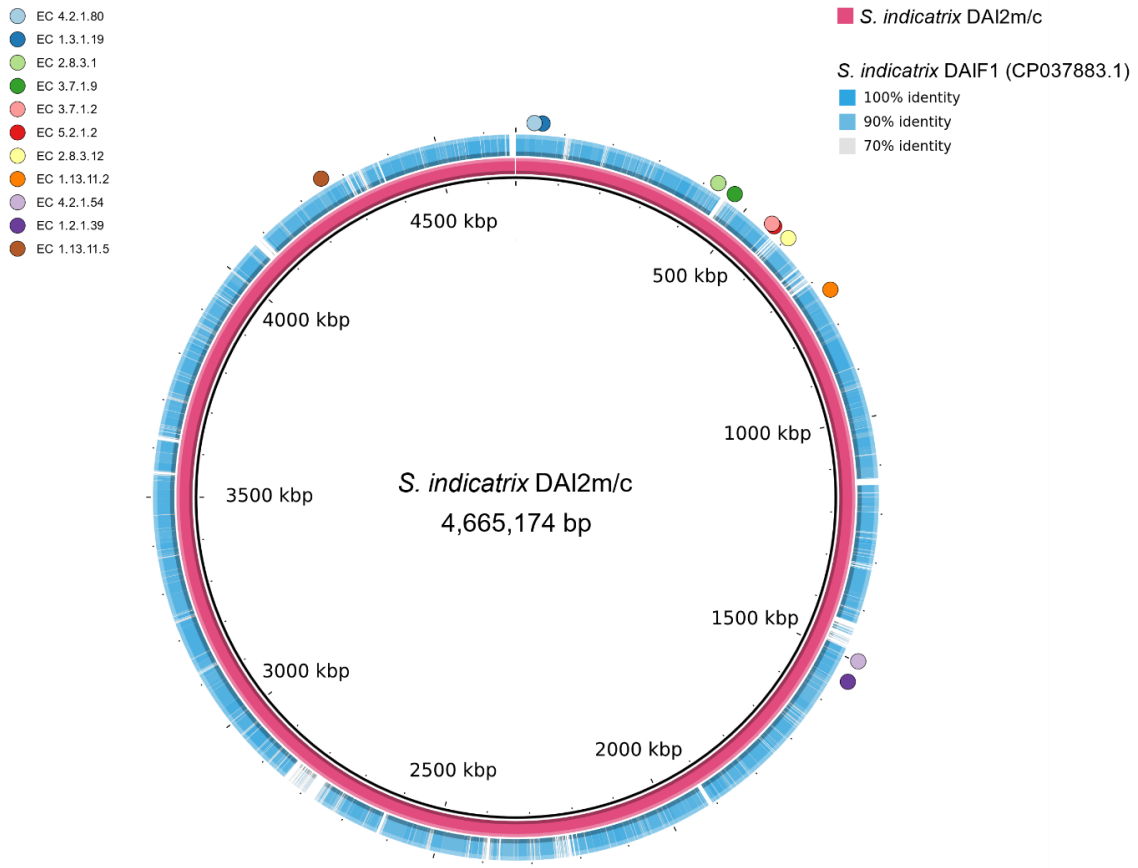

Fig. 2.7 - Circular representation of the comparative genome analysis between *Stenotrophomonas indicatrix* strain DAI2m/c and *Stenotrophomonas indicatrix* strain DAIF1. The BLAST Ring Image Generator (BRIG) was used to visualize genomic similarities and differences, with *S. indicatrix* DAIF1 serving as the reference genome. The rings represent the genomes of the two strains. The colour gradient indicates the percentage of identity of each gene in the *S. indicatrix* DAIF1, compared to those in *S. indicatrix* strain DAI2m/c. Specifically, the genes of interest involved in the styrene degradation pathway, identified through automatic and manual annotation (excluding those in the yellow boxes, see Fig. 2.5.b and Fig 2.6), are marked. The percentage identities of these enzyme-encoding genes are as follows: 4.2.1.80 (96%), 1.3.1.19 (94%), 2.8.3.1 (97%), 3.7.1.9 (91%), 3.7.1.2 (96%), 5.2.1.2 (93%), 2.8.3.12 (95%), 1.13.11.2 (96%), 4.2.1.54 (98%), 1.2.1.39 (93%), 1.13.11.5 (96%).

2.3.3 Phylogenetic analysis

The phylogenetic analysis of all the available Xanthomonadales species, based on a supermatrix of 368,075 amino acid positions, supported the monophyly of Xanthomonadaceae within a paraphyletic Rhodanobacteraceae (Fig. 2.8; Fig. 2.9). In fact, the bulk of Xanthomonadaceae is recovered as sister group to one specific group of Rhodanobacteraceae, namely *Chyayiivirga*

flava and *Aquimonas varaii*. Incidentally, two species belonging to the Xanthomonadaceae, *Pseudolysobacter antarcticus* and *Pseudomarinomonas arenosa*, were further identified as outliers (Fig 2.9). Within Xanthomonadaceae, a well-supported and relatively conserved cluster corresponding to the *Stenotrophomonas* genus was identified, encompassing 26 out of 27 recognized species. The only exception was *S. panachiumi*, which clustered within the *Xanthomonas* phylogroup, raising questions about its actual taxonomic placement. The newly sequenced *S. indicatrix* strain DAI2m/c was correctly positioned within the Xanthomonadaceae family and assigned to the *Stenotrophomonas* genus. Phylogenetic reconstruction placed it in close relation to *S. indicatrix* DAIF1 (GCF_004551575.1), with a strong association to *S. lactitubi* (GCF_900188015.1), further supporting its taxonomic classification within *Stenotrophomonas*. Although the phylogenetic reconstruction and the databases employed in this study still classify *Stenotrophomonas* within the Xanthomonadaceae family, recent studies have led to the reclassification of this family as Lysobacteriaceae (Xanthomonas group) (Yu & Wang, 2024).

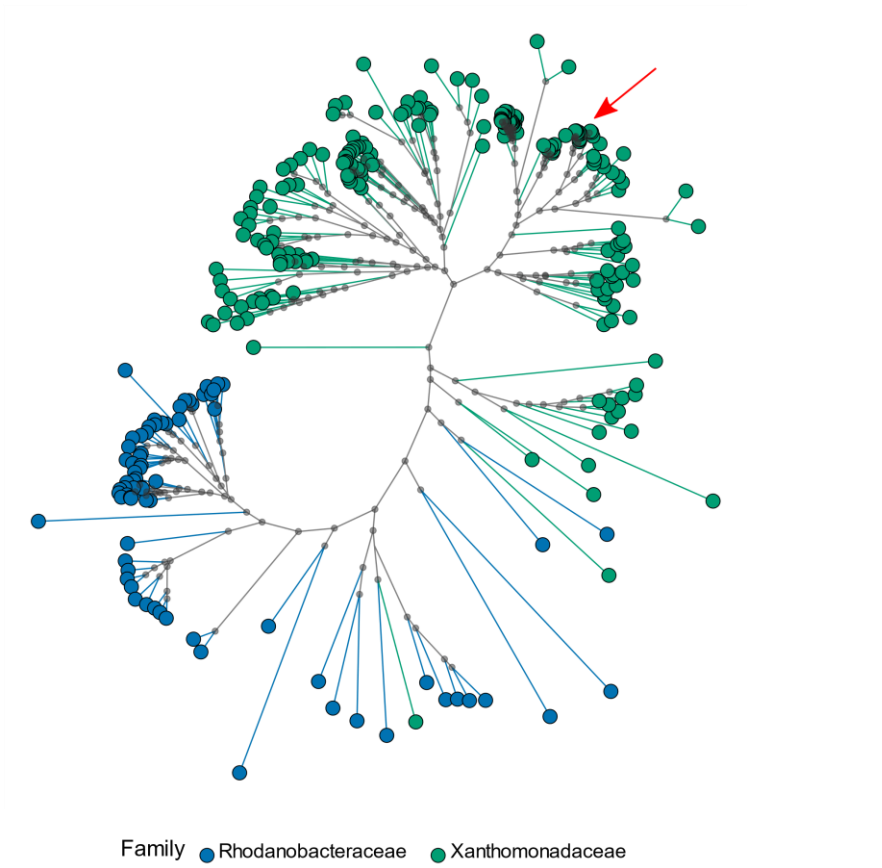

Fig. 2.8 - Unrooted phylogenetic reconstruction of the order Xanthomonadales using BUSCO scOGs. The two families are colour coded. Supported nodes (UFB > 95) are identified with a grey dot. Colours reflect family taxonomic position. The red arrow indicates the position of *S. indicatrix* strain DAI2m/c position. A more detailed representation is provided in the Fig. 2.9.

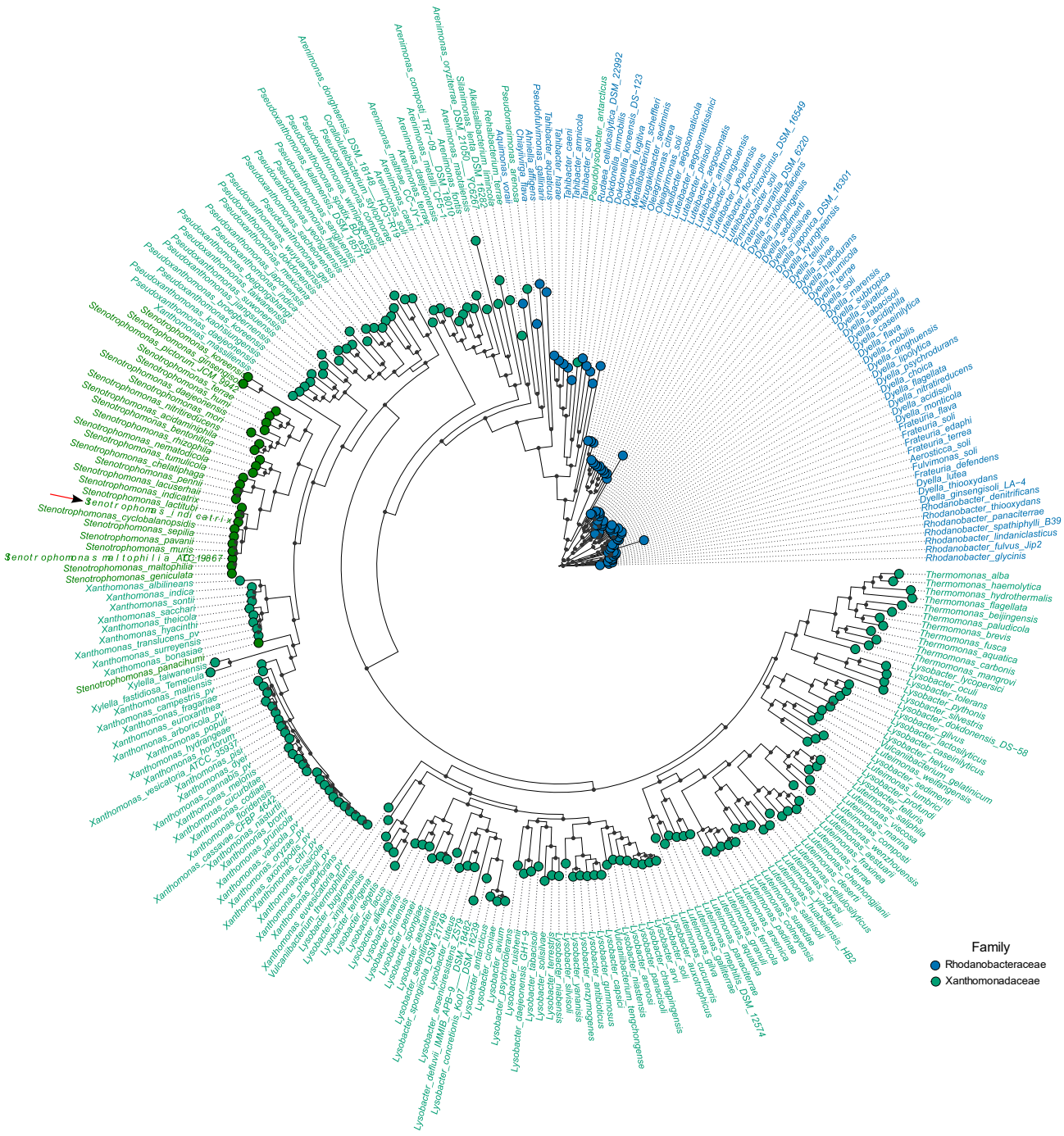

Fig 2.9 - Phylogenetic reconstruction of the order Xanthomonadales using BUSCO scOGs, rooted on the Rhodanobacter clade accordingly to Naushad et al. (2015) results. The two families are colour coded. Supported nodes (UFB > 95) are identified with a grey dot. A red arrow indicates the position of *S. indicatrix* strain DAI2m/c.

2.4 DISCUSSION

The biodegradation of polystyrene (PS) in natural environments is remarkably slow, in particular due to the chemical structure of the polymer, the intrinsic properties and the presence of various additives. Therefore, the complete degradation of PS can take decades or even centuries (Xu et al., 2024). The persistence of PS in nature contributes significantly to environmental pollution, increasing risk for human and animal health, and disrupts ecosystem (Ho et al., 2018). In this context, microorganisms play a crucial role in the breakdown of PS, in particular due to their enzymatic capabilities in degrading petroleum hydrocarbon alkanes of varying chain lengths (Xu et al., 2024; Ho et al., 2018; Hsueh et al., 2023; Wentzel et al., 2007). Given the structural similarities between petroleum hydrocarbons and PS, several bacterial enzymes of alkane metabolism (alkane 1-monooxygenase, cytochrome P450, and alkane hydroxylase) should be involved also in PS degradation process, especially facilitating the extracellular depolymerization of PS (Hou et al., 2021). While other studies have primarily focused on extracellular mechanisms driving PS degradation into oligomers and monomers (Hou et al., 2021; Juan et al., 2022), the present study investigates the intracellular pathways by which *Stenotrophomonas indicatrix* strain DAI2m/c metabolizes styrene monomers.

The genus *Stenotrophomonas* belongs to the *Xanthomonadaceae* family within the order *Xanthomonadales*, an early diverging group of *Gammaproteobacteria* (Ghosh et al., 2020). This order comprises two major families: Xanthomonadaceae (or Lysobacteriaceae) and Rhodanobacteraceae (Bansal et al., 2023). The phylogenetic analysis using BUSCO scOGs supported a paraphyletic condition for the Rhodanobacteriaceae whereas Xanthomonadaceae were identified as monophyletic, excluding the enigmatic positions of two poorly studied taxa: *P. antarcticus* and *P. arenosa*. While some authors have recently proposed reclassifying *P. antarcticus* under Rhodanobacteraceae (Bansal et al., 2023), formally belonging to the Xanthomonadaceae family (Wei et al., 2020), no systematic or phylogenetic data are currently available for *P. arenosa*. The phylogenetic reconstruction conducted in this study confirmed the correct placement of *S. indicatrix* strain DAI2m/c within the *Stenotrophomonas* genus (Fig. 2.8, Fig. 2.9).

According to metabolic pathways described in the KEGG database (entry: map00643) and the BBD Styrene Pathway Map, styrene monomers, once internalized, undergo degradation through two primary metabolic pathways, referred to here as pathway A and pathway B (Fig. 2.6). Pathway A initiates with styrene monooxygenase [EC:1.14.14.11], which catalyses the

first reaction in styrene metabolism. A sequential cascade of seven additional enzymes ultimately converts styrene into fumarate and acetoacetate, which enter as substrates in the citric acid cycle and the propanoate metabolism, respectively. Pathway B begins with an oxidoreductase [EC:1.14.12.-] that converts styrene into styrene-cis-2,3-dihydrodiol, which is subsequently processed through three enzymatic steps to yield acrylate and 2-hydroxypenta-2,4-dienoate. In sub-pathway B1, acrylate undergoes conversion to L-lactate, which then enters pyruvate metabolism. In sub-pathway B2, 2-hydroxypenta-2,4-dienoate is further degraded into acetaldehyde and pyruvate, key intermediates in various metabolic pathways. The automatic functional annotation identified five genes encoding styrene degradation enzymes, four of which belong to pathway A and one to pathway B (Fig. 2.5.a, Fig. 2.6). Manual curation using Pfam profiles confirmed these assignments and additionally identified six supplementary enzymes in pathway B (Fig. 2.5.b, Fig. 2.6). However, three enzymes, 4-hydroxy-2-oxovalerate aldolase [EC:4.1.3.39] and two oxidoreductases [EC:1.14.12.-; EC:1.14.13.-], were only partially characterized due to their non-specific protein domains. Specifically, only 66.7%, 50.0%, and 52.5% of the expected Pfam domains were retrieved in the *S. indicatrix* DAI2m/c genome. Genes encoding all enzymes in pathway B (including both sub-pathways) were fully identified on the chromosome of *S. indicatrix* DAI2m/c, suggesting that this is the primary intracellular pathway for styrene degradation. Meanwhile, only 5 out of 8 enzymes required for pathway A were detected (Fig. 2.6). Although this does not completely exclude the possibility of pathway A being functional, it suggests that alternative enzymes may recover the functionality of the 3 non-identified enzymes. Further studies are necessary to confirm this hypothesis.

Comparative genome analysis between *S. indicatrix* DAI2m/c and *S. indicatrix* DAIF1 revealed strong conservation of styrene degradation enzyme-encoding genes between the two strains, with minor identity variations (Fig. 2.7). However, a key genomic distinction was observed: unlike *S. indicatrix* DAIF1, *S. indicatrix* DAI2m/c harbours a plasmid carrying many phage-like elements (Fig. 2.4). Phage-related sequences have been extensively documented as important factors in biofilm development across multiple bacterial taxa (Wang et al., 2000; Toba et al., 2011). In particular, defective Lambda prophage DLP12 lysis genes have been shown to be essential for curli fiber production in *Escherichia coli* K-12, where curli fibers mediate cell adhesion and biofilm formation (Toba et al., 2011). The lysis genes of DLP12 show strong homology to those found in the SRRz lysis cassette of bacteriophage Lambda (Campbell, 1994). The presence of similar viral lysis sequences in various locations of the *S. indicatrix* DAI2m/c genome may play a role in biofilm development on polystyrene surfaces by facilitating the

extracellular release of DNA. Extracellular DNA is a well-known structural component of bacterial biofilms, and previous studies have demonstrated that prophage-encoded endolysins contribute to the production of bacterial membrane vesicles and biofilms in *Pseudomonas aeruginosa* (Turnbull et al., 2016). Several reports over the past decade have consistently highlighted the role of prophages in enhancing biofilm formation by promoting DNA release (Hansen et al., 2019).

CONCLUSIONS

Experimental data indicate that *Alphitobius diaperinus* larvae in the last larval instar (prepupae) are capable of ingesting polystyrene (PS). This ingestion was confirmed by micro-FTIR analyses of the frass from PS-fed larvae, which revealed an approximate 10% alteration in the polymer's chemical structure compared to the original feedstock. Moreover, the presence of this slight variation, confirmed by the detection of two specific degradation by-products (α-methylstyrene and cumyl alcohol) through GC-MS, supports the conclusion that the PS polymer can be partially metabolized.

Metabarcoding analyses further demonstrated that a PS-based diet promotes the proliferation of specific bacterial taxa. In particular, genera such as *Morganella* and *Kluyvera* were significantly expressed in the PS-fed larvae, while they remained undetectable in larvae fed a vegetable-based diet. These differences were observed both across larval instars, where the overall microbiota remains stable, and among different gut sections (foregut, midgut, and hindgut) of larvae at last larval instar. The increased microbial diversity in the PS-fed samples suggests that the PS substrate enables the expansion of certain microbial species. Although *Morganella* and *Kluyvera* were found to be significantly enriched in PS-fed larvae, their specific role in polystyrene degradation remains to be elucidated. Future studies should focus on isolating these strains, validating their degradation capabilities through in vitro assays, and exploring their genetic profiles through genomic analysis.

Among the challenges encountered in this first part of the study, one of the most significant was the optimization of the rearing setup for *A. diaperinus* larvae. In the initial phase, larvae were reared based solely on diet (CT vs PS) without considering their developmental stage, which led to limited ingestion of PS and high mortality rates. Only after identifying that PS ingestion was predominantly carried out by mature larvae, the experimental design was revised to separate individuals by larval instar. This adjustment improved both PS consumption and larval survival, highlighting the importance of developmental instar as a critical factor in biodegradation experiments. An additional difficulty was also related to the complexity and variability of the gut microbiota itself, a highly dynamic ecosystem that is influenced by multiple factors and difficult to standardize across biological replicates. Working with such a complex microbial community requires careful experimental design and interpretation across different experimental conditions. Overall, these results confirm the role of *A. diaperinus* as a plastivorous insect, effectively functioning as a natural bioreactor.

Further attention was directed toward the characterization of individual bacterial taxa with potential degradative capabilities, focusing particularly on isolates associated with PS-fed larvae. The specific microenvironments inside the gut of *A. diaperinus* seem to promote the development and proliferation of bacterial taxa involved in the degradation processes of PS. An example is the study on *Stenotrophomonas indicatrix* strain DAI2m/c, isolated from the gut of PS fed larvae, which integrated genomic and bioinformatic analyses to characterize its genome and identify previously undescribed intracellular pathways, providing deeper insight into the mechanisms underlying PS degradation. The analysis conducted on *S. indicatrix* strain DAI2m/c not only highlighted its potential for styrene biodegradation but also demonstrated that the methodological approach based on styrene degradation pathways is applicable to other bacterial taxa isolated from the microbiomes of plastivorous insects. Although the genomic annotation revealed two potential pathways for styrene degradation, only one appeared to be complete based on the identified genes. In particular, only 5 out of 8 enzymes associated with the other pathway were detected, leaving some steps potentially incomplete or not fully characterized. Therefore, further experimental validation would be necessary to confirm the actual expression and functionality of the enzymes involved, particularly those belonging to the complete pathway. This represents an important direction for future studies aiming to better define the contribution of each metabolic pathway under polystyrene degradation conditions. Taken together, in line with the recent scientific trends shifting from solely investigating the degradation capabilities of plastivorous insects to analyzing the diversity and richness of their associated microbiomes, these findings indicate that *S. indicatrix* strain DAI2m/c possesses the necessary features to be integrated into synthetic microbial communities designed for polystyrene biodegradation.

The biotechnological relevance of this research stems from its interdisciplinary approach, which integrates entomology, microbiology, genomics, and analytical chemistry, and from its contribution to the emerging field of insect mediated bioremediation. Beyond the fundamental insights into polystyrene ingestion and partial biodegradation by *Alphitobius diaperinus* and *Stenotrophomonas indicatrix*, the results of this study open new avenues for applied research. The observed microbial activities could serve as a foundation for the development of eco-sustainable strategies for plastic waste management. One promising direction involves the design of natural or synthetic bioreactors, integrating selected insect larvae and bacterial consortia under controlled conditions to enhance PS degradation rates. Nevertheless, several challenges must be addressed to fill the gap between laboratory findings and real-world applications. These include the optimization of microbial efficiency, the scalability of

degradation processes, the precise quantification of degradation rates under controlled experimental conditions, and the safe management of metabolic byproducts. Future research should also focus on developing targeted enrichment cultures under diverse rearing and experimental conditions to isolate the most effective microbial components, exploring extracellular enzymatic activities directed at polystyrene polymers, designing large scale degradation systems, and assessing the environmental safety and industrial feasibility of the proposed biological solutions, thereby providing a deeper understanding of the complete biodegradation process.

ACKNOWLEDGEMENTS

Firstly, I would like to express my sincere gratitude to my supervisor, Prof. Antonio Carapelli, as well as Prof. Francesco Nardi and Prof. Francesco Frati, for their scientific support, valuable insights, and expertise. I am also deeply thankful to the members of the ESZlab group for the projects, ideas, and collaborations we have shared. In particular, I would like to extend my profound gratitude to Dr. Claudio Cucini and Dr. Rebecca Funari, my colleagues and friends, for their constant support, continuous collaboration, and for the many moments we shared. I also wish to express my gratitude to Prof. Laura Marri for her scientific guidance and constructive feedback. Additionally, I would like to acknowledge Prof. Cristina Panti and Prof. Elena Dreassi, with whom I had the pleasure of collaborating. Finally, I extend my sincere thanks to the reviewers and the members of dissertation committee for their time and contributions.

Borsa finanziata nell'ambito della borsa di dottorato del Programma Operativo Nazionale Ricerca e Innovazione 2014-2020 (CCI 2014IT16M2OP005), risorse FSE REACT-EU, Azione IV.4 “Dottorati e contratti di ricerca su tematiche dell’innovazione” e Azione IV.5 “Dottorati su tematiche Green”

Titolo Progetto: Il microbioma intestinale dei coleotteri e la sua capacità di decomporre in maniera eco-sostenibile i rifiuti di polistirene.

REFERENCES

Alikhan, N. F., Petty, N. K., Ben Zakour, N. L., & Beatson, S. A. (2011). BLAST Ring Image Generator (BRIG): simple prokaryote genome comparisons. BMC genomics, 12, 1-10.

Altschul, S. F., Gish, W., Miller, W., Myers, E. W., & Lipman, D. J. (1990). Basic local alignment search tool. Journal of molecular biology, 215(3), 403-410.

Asiandu, A. P., Wahyudi, A., & Sari, S. W. (2021). A review: plastics waste biodegradation using plastics-degrading bacteria. Journal of Environmental Treatment Techniques, 9(1), 148-157.

Bansal, K., Kumar, S., Singh, A., Chaudhary, A., & Patil, P. B. (2023). Redefining the taxonomic boundaries of genus *Xanthomonas*. Taxonomy, 3(4), 452-465.

Boctor, J., Pandey, G., Xu, W., Murphy, D. V., & Hoyle, F. C. (2024). Nature's Plastic Predators: A Comprehensive and Bibliometric Review of Plastivore Insects. Polymers, 16(12), 1671.

Brandon, A. M., Gao, S. H., Tian, R., Ning, D., Yang, S. S., Zhou, J., ... & Criddle, C. S. (2018). Biodegradation of polyethylene and plastic mixtures in mealworms (larvae of *Tenebrio molitor*) and effects on the gut microbiome. Environmental science & technology, 52(11), 6526-6533.

Bucci, K., Tulio, M., & Rochman, C. M. (2020). What is known and unknown about the effects of plastic pollution: A meta-analysis and systematic review. Ecological Applications, *30*(2), e02044.

Callahan, B. J., McMurdie, P. J., Rosen, M. J., Han, A. W., Johnson, A. J. A., & Holmes, S. P. (2016). DADA2: High-resolution sample inference from Illumina amplicon data. Nature methods, 13(7), 581-583.

Campbell, A. (1994). Comparative molecular biology of lambdoid phages. Annual review of microbiology, 48, 193-223.

Capella-Gutiérrez, S., Silla-Martínez, J. M., & Gabaldón, T. (2009). trimAl: a tool for automated alignment trimming in large-scale phylogenetic analyses. Bioinformatics, 25(15), 1972-1973.

Chaukura, N., Gwenzi, W., Bunhu, T., Ruziwa, D. T., & Pumure, I. (2016). Potential uses and value-added products derived from waste polystyrene in developing countries: A review. Resources, Conservation and Recycling, 107, 157-165.

Chen, H. (2022). VennDiagram: generate high-resolution venn and euler plots.(2018). R package version 1.6. 20.

Chen, S., Zhou, Y., Chen, Y., & Gu, J. (2018). fastp: an ultra-fast all-in-one FASTQ preprocessor. Bioinformatics, 34(17), i884-i890.

Cucini, C., Funari, R., Mercati, D., Nardi, F., Carapelli, A., & Marri, L. (2022). Polystyrene shaping effect on the enriched bacterial community from the plastic-eating *Alphitobius diaperinus* (Insecta: Coleoptera). Symbiosis, 86(3), 305-313.

Cucini, C., Leo, C., Vitale, M., Frati, F., Carapelli, A., & Nardi, F. (2020). Bacterial and fungal diversity in the gut of polystyrene-fed *Alphitobius diaperinus* (Insecta: Coleoptera). Animal Gene, 17, 200109.

Cumsille, A., Durán, R. E., Rodríguez-Delherbe, A., Saona-Urmeneta, V., Cámara, B., Seeger, M., ... & Buil-Aranda, C. (2023). GenoVi, an open-source automated circular genome visualizer for bacteria and archaea. PLoS Computational Biology, 19(4), e1010998.

Dar, M. A., Xie, R., Zabed, H. M., Pawar, K. D., Dhole, N. P., & Sun, J. (2024). Current paradigms and future challenges in harnessing gut bacterial symbionts of insects for biodegradation of plastic wastes. Insect Science. Advance online publication. https://doi.org/10.1111/1744-7917.13417.

Ding, M. Q., Ding, J., Yang, S. S., Ren, X. R., Shi, S. N., Zhang, L. Y., ... & Wu, W. M. (2024). Effects of plastic aging on biodegradation of polystyrene by *Tenebrio molitor* larvae: Insights into gut microbiome and bacterial metabolism. Science of The Total Environment, 953, 176130.

DOE Joint Genome Institute. BBTools. Accessed July 21, 2024. https://jgi.doe.gov/data-and-tools/software-tools/bbtools/.

Dunford, J. C., & Kaufman, P. E. (2006). Lesser mealworm, litter beetle, *Alphitobius diaperinus* (Panzer)(Insecta: Coleoptera: Tenebrionidae): EENY-367/IN662, rev. 6/2006. EDIS, 2006.

Eddy, S. R. (2011). Accelerated profile HMM searches. PLoS computational biology, 7(10), e1002195.

Evode, N., Qamar, S. A., Bilal, M., Barceló, D., & Iqbal, H. M. (2021). Plastic waste and its management strategies for environmental sustainability. Case Studies in Chemical and Environmental Engineering, 4, 100142.

Francisco, O., & Do Prado, A. P. (2001). Characterization of the larval stages of *Alphitobius diaperinus* (Panzer)(Coleoptera: Tenebrionidae) using head capsule width. Revista Brasileira de Biologia, 61, 125-131.

Friedrich, I., Hollensteiner, J., Scherf, J., Weyergraf, J., Klassen, A., Poehlein, A., ... & Daniel, R. (2021). Complete genome sequence of *Stenotrophomonas indicatrix* DAIF1. Microbiology Resource Announcements, 10(6), 10-1128.

Gallo, F., Fossi, C., Weber, R., Santillo, D., Sousa, J., Ingram, I., ... & Romano, D. (2018). Marine litter plastics and microplastics and their toxic chemicals components: the need for urgent preventive measures. Environmental Sciences Europe, 30, 1-14.

Gao, F., & Zhang, C. T. (2008). Ori-Finder: a web-based system for finding oriC s in unannotated bacterial genomes. BMC bioinformatics, 9, 1-6.

Germanov, E. S., Marshall, A. D., Bejder, L., Fossi, M. C., & Loneragan, N. R. (2018). Microplastics: no small problem for filter-feeding megafauna. Trends in ecology & evolution, 33(4), 227-232.

Ghosh, R., Chatterjee, S., & Mandal, N. C. (2020). *Stenotrophomonas*. In Beneficial microbes in agro-ecology Academic Press, 427-442.

Gökçen, A., Vilcinskas, A., & Wiesner, J. (2014). Biofilm-degrading enzymes from Lysobacter gummosus. Virulence, 5(3), 378-387.

Hansen, M. F., Svenningsen, S. L., Røder, H. L., Middelboe, M., & Burmølle, M. (2019). Big impact of the tiny: bacteriophage–bacteria interactions in biofilms. Trends in microbiology, 27(9), 739-752.

Ho, B. T., Roberts, T. K., & Lucas, S. (2018). An overview on biodegradation of polystyrene and modified polystyrene: the microbial approach. Critical reviews in biotechnology, 38(2), 308-320.

Hou, L., & Majumder, E. L. W. (2021). Potential for and distribution of enzymatic biodegradation of polystyrene by environmental microorganisms. Materials, 14(3), 503.

Hsueh, S. W., Jian, Y. H., Fugmann, S. D., & Yang, S. Y. (2023). Polystyrene-colonizing bacteria are enriched for long-chain alkane degradation pathways. Plos one, 18(10), e0292137.

Huang, S., Wang, H., Ahmad, W., Ahmad, A., Ivanovich Vatin, N., Mohamed, A. M., ... & Mehmood, I. (2022). Plastic waste management strategies and their environmental aspects: A scientometric analysis and comprehensive review. International Journal of Environmental Research and Public Health, 19(8), 4556.

Huerta-Cepas, J., Szklarczyk, D., Heller, D., Hernández-Plaza, A., Forslund, S. K., Cook, H., ... & Bork, P. (2019). eggNOG 5.0: a hierarchical, functionally and phylogenetically annotated orthology resource based on 5090 organisms and 2502 viruses. Nucleic acids research, 47(D1), D309-D314.

Hunt, M., Silva, N. D., Otto, T. D., Parkhill, J., Keane, J. A., & Harris, S. R. (2015). Circlator: automated circularization of genome assemblies using long sequencing reads. Genome biology, 16, 1-10.

Katoh, K., & Toh, H. (2008). Recent developments in the MAFFT multiple sequence alignment program. Briefings in bioinformatics, 9(4), 286-298.

Kerr, K. G., Denton, M., Todd, N., Corps, C. M., Kumari, P., & Hawkey, P. M. (1996). A new selective differential medium for isolation of *Stenotrophomonas maltophilia*. European Journal of Clinical Microbiology and Infectious Diseases, 15, 607-610.

Kim, H. R., Lee, H. M., Yu, H. C., Jeon, E., Lee, S., Li, J., & Kim, D. H. (2020). Biodegradation of polystyrene by Pseudomonas sp. isolated from the gut of superworms (larvae of *Zophobas atratus*). Environmental science & technology, 54(11), 6987-6996.

Kolmogorov, M., Yuan, J., Lin, Y., & Pevzner, P. A. (2019). Assembly of long, error-prone reads using repeat graphs. Nature Biotechnology, 37(5), 540-546.

Lamba, P., Kaur, D. P., Raj, S., & Sorout, J. (2022). Recycling/reuse of plastic waste as construction material for sustainable development: a review. Environmental Science and Pollution Research, 29(57), 86156-86179.

Li, H., & Durbin, R. (2009). Fast and accurate short read alignment with Burrows–Wheeler transform. bioinformatics, 25(14), 1754-1760.

Li, P., Wang, X., Su, M., Zou, X., Duan, L., & Zhang, H. (2021). Characteristics of plastic pollution in the environment: a review. Bulletin of environmental contamination and toxicology, 107, 577-584.

Love, M., Anders, S., & Huber, W. (2014). Differential analysis of count data–the DESeq2 package. Genome Biol, 15(550), 10-1186.

Martinez Arbizu, P. (2020). pairwiseAdonis: Pairwise multilevel comparison using adonis. R package. Version 0.4. Available on URL: https://github. com/pmartinezarbizu/pairwiseAdonis.

McMurdie, P. J., & Holmes, S. (2013). phyloseq: an R package for reproducible interactive analysis and graphics of microbiome census data. PloS one, 8(4), e61217.

Minh, B. Q., Schmidt, H. A., Chernomor, O., Schrempf, D., Woodhams, M. D., Von Haeseler, A., & Lanfear, R. (2020). IQ-TREE 2: new models and efficient methods for phylogenetic inference in the genomic era. Molecular biology and evolution, 37(5), 1530-1534.

Naushad, S., Adeolu, M., Wong, S., Sohail, M., Schellhorn, H. E., & Gupta, R. S. (2015). A phylogenomic and molecular marker based taxonomic framework for the order Xanthomonadales: proposal to transfer the families Algiphilaceae and Solimonadaceae to the order Nevskiales ord. nov. and to create a new family within the order Xanthomonadales, the family Rhodanobacteraceae fam. nov., containing the genus *Rhodanobacter* and its closest relatives. Antonie van Leeuwenhoek, 107, 467-485.

Okan, M., Aydin, H. M., & Barsbay, M. (2019). Current approaches to waste polymer utilization and minimization: a review. Journal of Chemical Technology & Biotechnology, 94(1), 8-21.

Peng, B. Y., Su, Y., Chen, Z., Chen, J., Zhou, X., Benbow, M. E., ... & Zhang, Y. (2019). Biodegradation of polystyrene by dark (*Tenebrio obscurus*) and yellow (*Tenebrio molitor*) mealworms (Coleoptera: Tenebrionidae). Environmental science & technology, 53(9), 5256-5265.

Pivato, A. F., Miranda, G. M., Prichula, J., Lima, J. E., Ligabue, R. A., Seixas, A., & Trentin, D. S. (2022). Hydrocarbon-based plastics: Progress and perspectives on consumption and biodegradation by insect larvae. Chemosphere, 293, 133600.

Plastics Europe. Plastics – the Fast Facts 2023 • Plastics Europe. Accessed July 21, 2024. 335 https://plasticseurope.org/knowledge-hub/plastics-the-fast-facts-2023/.

Posit team (2024). Rstudio: Integrated Development Environment for R. Posit Software, PBC, Boston, MA. URL http://www.posit.co/.

Quast, C., Pruesse, E., Yilmaz, P., Gerken, J., Schweer, T., Yarza, P., ... & Glöckner, F. O. (2012). The SILVA ribosomal RNA gene database project: improved data processing and web-based tools. Nucleic acids research, 41(D1), D590-D596.

Schellenberg, J., & Leder, H. J. (2006). Syndiotactic polystyrene: Process and applications. Advances in Polymer Technology: Journal of the Polymer Processing Institute, 25(3), 141-151.

Sharma, H., & Neelam, D. K. (2023). Understanding challenges associated with plastic and bacterial approach toward plastic degradation. Journal of Basic Microbiology, 63(3-4), 292-307.

Siddiqui, J. A., Khan, M. M., Bamisile, B. S., Hafeez, M., Qasim, M., Rasheed, M. T., ... & Xu, Y. (2022). Role of insect gut microbiota in pesticide degradation: a review. Frontiers in microbiology, 13, 870462.

Siddiqui, S. A., Abd Manap, A. S., Kolobe, S. D., Monnye, M., Yudhistira, B., & Fernando, I. (2024). Insects for plastic biodegradation–A review. Process Safety and Environmental Protection, 186, 833-849.

Tang, Y. W., Stratton, C. W., & Han, X. Y. (2006). Bacterial identification based on 16S ribosomal RNA gene sequence analysis. Advanced techniques in diagnostic microbiology, 323-332.

Tatusova, T., DiCuccio, M., Badretdin, A., Chetvernin, V., Nawrocki, E. P., Zaslavsky, L., ... & Ostell, J. (2016). NCBI prokaryotic genome annotation pipeline. Nucleic acids research, 44(14), 6614-6624.

Tay, J. H., Asib, N., Aziz, N. A. A., & Tan, G. H. (2023). Biodegradation of expanded and extruded polystyrene with different diets by using *Zophobas atratus* larvae (Coleoptera: Tenebrionidae). Pertanika Journal of Tropical Agricultural Science, 46(2).

Toba, F. A., Thompson, M. G., Campbell, B. R., Junker, L. M., Rueggeberg, K. G., & Hay, A. G. (2011). Role of DLP12 lysis genes in *Escherichia coli* biofilm formation. Microbiology, 157(6), 1640-1650.

Tourova, T., Sokolova, D., Nazina, T., Grouzdev, D., Kurshev, E., & Laptev, A. (2020). Biodiversity of microorganisms colonizing the surface of polystyrene samples exposed to different aqueous environments. Sustainability, 12(9), 3624.

Tsochatzis, E., Lopes, J. A., Gika, H., & Theodoridis, G. (2020). Polystyrene biodegradation by *Tenebrio molito*r larvae: identification of generated substances using a GC-MS untargeted screening method. Polymers, 13(1), 17.

Turnbull, L., Toyofuku, M., Hynen, A. L., Kurosawa, M., Pessi, G., Petty, N. K., ... & Whitchurch, C. B. (2016). Explosive cell lysis as a mechanism for the biogenesis of bacterial membrane vesicles and biofilms. Nature communications, 7(1), 11220.

Urbanek, A. K., Rybak, J., Hanus-Lorenz, B., Komisarczyk, D. A., & Mirończuk, A. M. (2024). *Zophobas morio* versus *Tenebrio molitor*: Diversity in gut microbiota of larvae fed with polymers. Science of the Total Environment, 952, 176005.

Vo, C. V., Bunge, F., Duffy, J., & Hood, L. (2011). Advances in thermal insulation of extruded polystyrene foams. Cellular Polymers, 30(3), 137-156.

Walker, B. J., Abeel, T., Shea, T., Priest, M., Abouelliel, A., Sakthikumar, S., ... & Earl, A. M. (2014). Pilon: an integrated tool for comprehensive microbial variant detection and genome assembly improvement. PloS one, 9(11), e112963.

Wang, I. N., Smith, D. L., & Young, R. (2000). Holins: the protein clocks of bacteriophage infections. Annual Reviews in Microbiology, 54(1), 799-825.

Wang, Y., & Zhang, Y. (2015). Investigation of gut-associated bacteria in *Tenebrio molitor* (Coleoptera: Tenebrionidae) larvae using culture-dependent and DGGE methods. Annals of the Entomological Society of America, 108(5), 941-949.

Wang, Z., Xin, X., Shi, X., & Zhang, Y. (2020). A polystyrene-degrading *Acinetobacter* bacterium isolated from the larvae of *Tribolium castaneum*. Science of the Total Environment, 726, 138564.

Warhurst, A. M., Clarke, K. F., Hill, R. A., Holt, R. A., & Fewson, C. A. (1994). Metabolism of styrene by *Rhodococcus rhodochrous* NCIMB 13259. Applied and Environmental Microbiology, 60(4), 1137-1145.

Waterhouse, R. M., Seppey, M., Simão, F. A., Manni, M., Ioannidis, P., Klioutchnikov, G., ... & Zdobnov, E. M. (2018). BUSCO applications from quality assessments to gene prediction and phylogenomics. Molecular biology and evolution, 35(3), 543-548.

Wei, Z., Wu, T., Huang, Y., Zhu, G., Zhang, Y., Geng, Y., & Peng, F. (2020). *Pseudolysobacter antarcticus* gen. nov., sp. nov., isolated from soil in Fildes Peninsula, Antarctica. International Journal of Systematic and Evolutionary Microbiology, 70(3), 1861-1867.

Wentzel, A., Ellingsen, T. E., Kotlar, H. K., Zotchev, S. B., & Throne-Holst, M. (2007). Bacterial metabolism of long-chain n-alkanes. Applied microbiology and biotechnology, 76, 1209-1221.

Wickham, H., ggplot2: Elegant Graphics for Data Analysis. Springer-Verlag New York. (2016)

Wishart, D. S., Han, S., Saha, S., Oler, E., Peters, H., Grant, J. R., ... & Gautam, V. (2023). PHASTEST: faster than PHASTER, better than PHAST. Nucleic Acids Research, 51(W1), W443-W450.

Wojnowska-Baryła, I., Bernat, K., & Zaborowska, M. (2022). Plastic waste degradation in landfill conditions: the problem with microplastics, and their direct and indirect environmental effects. International Journal of Environmental Research and Public Health, 19(20), 13223.

Woo, S., Song, I., & Cha, H. J. (2020). Fast and facile biodegradation of polystyrene by the gut microbial flora of *Plesiophthalmus davidis* larvae. Applied and Environmental Microbiology, 86(18), e01361-20.

Xu, L., Li, Z., Wang, L., Xu, Z., Zhang, S., & Zhang, Q. (2024). Progress in polystyrene biodegradation by insect gut microbiota. World Journal of Microbiology and Biotechnology, 40(5), 143.

Yang, S. S., Brandon, A. M., Flanagan, J. C. A., Yang, J., Ning, D., Cai, S. Y., ... & Wu, W. M. (2018). Biodegradation of polystyrene wastes in yellow mealworms (larvae of *Tenebrio molitor* Linnaeus): factors affecting biodegradation rates and the ability of polystyrene-fed larvae to complete their life cycle. Chemosphere, 191, 979-989.

Yang, Y., Wang, J., & Xia, M. (2020). Biodegradation and mineralization of polystyrene by plastic-eating superworms *Zophobas atratus*. Science of the total environment, 708, 135233.

Yang, Y., Yang, J., Wu, W. M., Zhao, J., Song, Y., Gao, L., ... & Jiang, L. (2015). Biodegradation and mineralization of polystyrene by plastic-eating mealworms: part 2. Role of gut microorganisms. Environmental science & technology, 49(20), 12087-12093.

Yu, G., Smith, D. K., Zhu, H., Guan, Y., & Lam, T. T. Y. (2017). ggtree: an R package for visualization and annotation of phylogenetic trees with their covariates and other associated data. Methods in Ecology and Evolution, 8(1), 28-36.

Yu, Z. L., & Wang, R. B. (2024). Revised taxonomic classification of the *Stenotrophomonas* genomes, providing new insights into the genus *Stenotrophomonas*. *Frontiers in Microbiology*, *15*, 1488674.

Yuan, J., Cao, J., Yu, F., & Ma, J. (2022). Microbial degradation of polystyrene microplastics by a novel isolated bacterium in aquatic ecosystem. Sustainable Chemistry and Pharmacy, 30, 100873.

Zarra, F., Funari, R., Cucini, C., Nardi, F., Carapelli, A., Marri, L., & Frati, F. (2025). Novel insights into insect mediated polystyrene biodegradation through bacterial genome analyses. Scientific Reports, 15(1), 1047.

Zhang, F., Zhao, Y., Wang, D., Yan, M., Zhang, J., Zhang, P., ... & Chen, C. (2021). Current technologies for plastic waste treatment: A review. Journal of Cleaner Production, 282, 124523.

Zhang, L., Wang, X., Yu, M., Qiao, Y., & Zhang, X. H. (2015). Genomic analysis of Luteimonas abyssi XH031 T: insights into its adaption to the subseafloor environment of South Pacific Gyre and ecological role in biogeochemical cycle. BMC genomics, 16, 1-14.